Chem Soc Rev

REVIEW ARTICLE

View Article Online
View Journal

Cite this: DOI: 10.1039/d4cs01237b

Recent advances in thermocatalytic acetylene selective hydrogenation

Xiaocheng Lan,[a] Jingguang G. Chen *[b] and Tiefeng Wang *[a]

Selective acetylene hydrogenation is a crucial reaction for purifying ethylene in the petroleum industry and presents a promising non-oil route for producing ethylene by integrating acetylene production from natural gas and coal. Despite significant advancements in catalyst development, achieving both high catalytic activity and ethylene selectivity remains challenging due to competing side reactions, including over-hydrogenation to ethane, C–C coupling leading to oligomers, and C–C bond cleavage resulting in coke formation. This review provides a comprehensive overview of recent progress in the development of catalysts and understanding of reaction mechanism for acetylene hydrogenation to ethylene. Firstly, benchmarks for conversion and selectivity calculation are critically discussed. Then, research on active site design is categorized into monometallic sites, disordered alloy sites, intermetallic compound (IMC) sites, and single-atom (SA) sites, with a distinction between Pd-based and non-Pd-based catalysts. This categorization highlights the active site design strategies and summarizes state-of-the-art performance metrics. Emphasis is placed on the structure–performance relationships and the role of different active metals in enhancing ethylene selectivity and catalytic activity. In addition, the roles of catalyst support and modifiers are reviewed. Finally, we discuss challenges and future research directions in mechanistic understanding and catalyst design, aiming to guide further innovations in this important field.

Received 30th April 2025

DOI: 10.1039/d4cs01237b

rsc.li/chem-soc-rev

1. Introduction

The selective hydrogenation of acetylene to ethylene is a catalytic reaction with both significant industrial value and academic interest. In industrial applications, this reaction serves as a crucial ethylene purification technology in the petrochemical industry, selectively removing trace amounts of acetylene impurities from ethylene feedstock to ensure the stability of downstream polymerization processes.[1–3] Moreover, its integration with acetylene production from natural gas or coal-based processes offers an alternative route for ethylene production beyond petroleum dependence.[4–6] From an academic

[a] Department of Chemical Engineering, Tsinghua University, Beijing 100084, China. E-mail: wangtf@tsinghua.edu.cn
[b] Department of Chemical Engineering, Columbia University, New York, NY 10027, USA. E-mail: jgchen@columbia.edu

Xiaocheng Lan

Dr Xiaocheng Lan is an Assistant Researcher in the Department of Chemical Engineering at Tsinghua University. He received his bachelor's and doctoral degrees in Chemical Engineering from Tsinghua University in 2014 and 2019, respectively. He worked as a postdoctoral researcher at Tsinghua University from 2019 to 2021. His research focuses on heterogeneous catalysis and slurry bed reactors for fine chemistry and renewable energy.

Jingguang G. Chen

Dr Jingguang G. Chen is the Thayer Lindsley Professor of Chemical Engineering at Columbia University, with a joint appointment at Brookhaven National Laboratory. His research interests include fundamental understanding of carbides, nitrides and bimetallic catalysts for applications in thermocatalysis and electrocatalysis. His research group utilizes a combination of experimental studies, in situ characterization and density functional theory calculations.

perspective, this reaction is widely regarded as a model system for selective hydrogenation, providing valuable insights into the structure–activity relationship between active site configurations, surface adsorption behaviors, and reaction selectivity.[7–9]

The primary target product of acetylene hydrogenation is ethylene, while undesired side reactions mainly include the over-hydrogenation to ethane, C–C coupling reactions forming oligomers, and C–C bond cleavage leading to coke formation. Suppressing these side reactions to enhance ethylene selectivity remains a key challenge in catalyst design. Palladium has long been recognized as an outstanding active metal due to its superior activity and ethylene selectivity. In 2006 and 2008, Borodziński and Bond reviewed Pd catalysts for acetylene hydrogenation in ethylene-rich streams, addressing critical aspects such as Pd phase evolution (PdC_x and PdH_x formation), hydrogenation mechanisms over Pd sites, reaction kinetics, and the effects of Pd particle size, carbon monoxide, and promoters.[1,2] However, monometallic Pd catalysts alone fail to fully meet the stringent industrial requirements for acetylene selective hydrogenation, necessitating continuous efforts to develop more advanced catalysts. The early introduction of the ''site isolation'' concept, which minimizes neighboring Pd active sites by incorporating a secondary metal, significantly improved the catalytic performance. The most commonly studied bimetallic catalyst, PdAg alloy, remains widely used in modern petrochemical industries for removing trace acetylene from ethylene-rich streams.[2] To further enhance catalytic performance, researchers have explored various active site configurations, including disordered alloy sites, ordered intermetallic compound (IMC) phases, and single-atom (SA) sites. Additionally, to reduce the catalyst costs, the development of non-Pd-based catalysts incorporating more abundant and cost-effective elements has become an important research direction. Furthermore, the influence of supports and modifiers on the overall catalytic performance has also been extensively investigated.

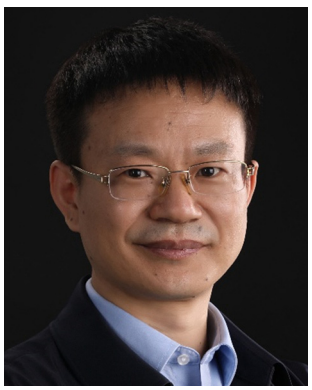

Tiefeng Wang

Dr Tiefeng Wang is a Professor and former Chair of the Department of Chemical Engineering at Tsinghua University. He received his PhD from Tsinghua University in 2004 and was a visiting professor at the University of Delaware from 2010 to 2011. His research focuses on heterogeneous catalysis, multiphase flow reactors, and clean energy chemical engineering. He has published over 280 papers and holds more than 40 patents. He has developed several industrialized technologies, including a partial oxidation reactor for natural gas and a slurry reactor for methyl methacrylate (MMA) synthesis, which have been successfully implemented in industry.

Since 2008, significant efforts have been devoted to developing highly efficient catalysts for acetylene hydrogenation. Previous reviews have summarized progress by categorizing catalysts into Pd-based, Ni-based, IB metal-based, bimetallic/trimetallic, and other types, with some focusing exclusively on non-noble metal-based catalysts.[3,10] However, a review based on active site types—monometallic sites, disordered alloy sites, IMC phases, and SA sites—would provide more depth in mechanistic understanding and guide further catalyst design. In addition, the roles of supports and modifiers are also crucial for achieving superior catalytic performance, yet a systematic review of these aspects is still lacking. Furthermore, the use of inconsistent calculation methods to report selectivity in the literature renders direct comparisons of catalytic performance across studies difficult. Therefore, it is timely to establish a comprehensive framework that not only systematically addresses recent advancements in acetylene selective hydrogenation but also defines standardized benchmarks for performance evaluation.

This review classifies various active sites and elucidates their roles in acetylene hydrogenation. Additionally, the effects of catalyst support and modifiers are thoroughly examined to guide rational catalyst design (Fig. 1). Section 2 provides an overview of industrial processes and reaction pathways, with a particular focus on defining benchmark for selectivity calculations to establish a standardized basis for comparing catalytic performance reported in the literature. In Section 3, the active sites are structurally categorized into monometallic sites, disordered alloy sites, IMC phases, and SA sites, further distinguishing between Pd-based and non-Pd-based catalysts to analyze the influence of different active metals on acetylene hydrogenation performance. This section presents the overall development trends and the state-of-the-art in active site design, emphasizing the structure–performance relationship and key research directions for enhancing ethylene selectivity and activity. Density functional theory (DFT) calculations on acetylene hydrogenation over different active sites are discussed in Section 4 to provide mechanistic insights and guide the rational design of active sites. Sections 5 and 6 summarize the role of catalyst supports and modifiers in improving catalytic performance, with an emphasis on their effects on selectivity and activity. Section 7 discusses the varying catalyst design requirements across different industrial processes for acetylene hydrogenation, highlighting the challenges and future perspectives in mechanistic understanding and catalyst development to anticipate future trends in this field. In addition, this section discusses the extension of catalytic strategies to the selective hydrogenation of other alkynes and dienes, as well as the emerging alternatives to thermocatalysis, including electrocatalytic and photocatalytic acetylene hydrogenation, highlighting their opportunities and limitations.

2. Overview of acetylene hydrogenation reaction

2.1 Industrial processes for acetylene hydrogenation

The primary application of acetylene selective hydrogenation is in the modern petrochemical industry, where trace amounts of

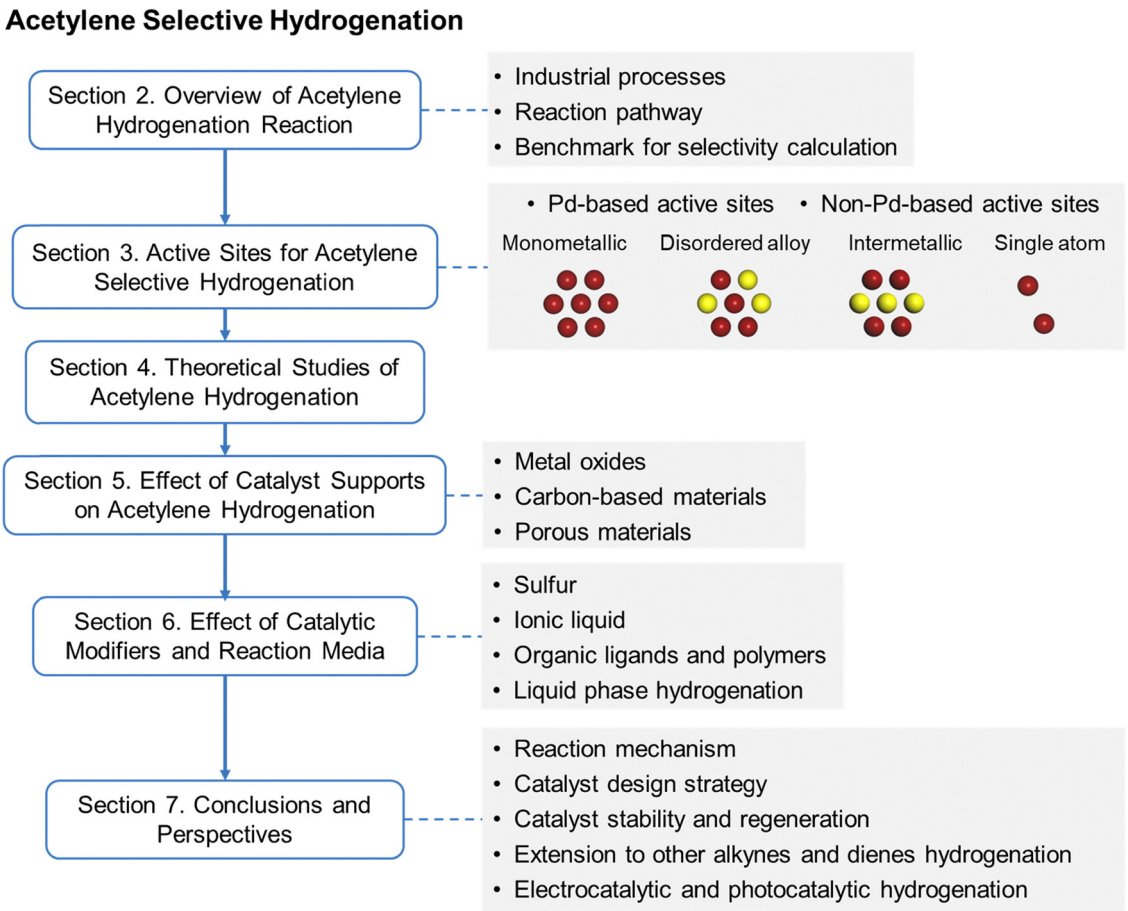

Fig. 1 Overview of the scope of the review.

acetylene need to be effectively removed from ethylene-rich streams. To meet the requirement of acetylene content (<10 ppm or even lower) in polymer-grade ethylene, an extremely high conversion of acetylene (>99.5% based on 0.2% acetylene feed concentration) must be achieved while limiting ethylene loss to no more than 1%. There are two main processes for acetylene hydrogenation in ethylene-rich streams, namely the tail-end and the front-end processes. The characteristics, advantages, and disadvantages of these two processes have been well summarized by Borodziński and Bond.[1] The primary difference between these processes lies in the feed composition (Table 1). The tail-end process typically operates with a H_2/C_2H_2 ratio of 1.2, while the front-end process exhibits a H_2/C_2H_2 ratio of 110.

Another potential industrial application of acetylene hydrogenation is the increased utilization of non-oil alternative resources to produce ethylene, such as coal and natural gas. This potential route for producing ethylene involves first producing acetylene, followed by its hydrogenation to ethylene. Several commercial processes have been developed to produce acetylene from these resources, including partial oxidation of natural gas (POX), thermal plasma pyrolysis of coal (PPY), and the calcium carbide process. The typical product concentrations for these processes are summarized in Table 1. For the gas products of POX and PPY, the concentrations of both acetylene and CO are several times higher than those from naphtha cracking. Similar to conventional acetylene hydrogenation in the petrochemical route, the tail-end process can be used by initially separating the large amounts of CO and H_2. However, this process incurs higher costs due to the separation and operational complexities, as the conventional solvent extraction process for separating C_2H_2 from CO is both costly

Table 1 Typical composition of acetylene containing gas in industrial processes

Feedstock	Process	C_2H_2	CO	H_2	C_2H_4	Ref
Oil	Naphtha cracking (tail-end)	2%	40 ppm	2.4%	71%	1
Oil	Naphtha cracking (front-end)	0.2%	2800 ppm	22%	37%	1
Natural gas	Partial oxidation	8%	20–25%	~50%	~0.2%	11
Coal	Pyrolysis in thermal plasma	6–8%	~10%	70–80%	~1%	12

and energy-intensive. On the other hand, direct hydrogenation of acetylene under high concentrations of CO and H_2, similar to the front-end process, simplifies the overall process. This approach is particularly beneficial when the downstream process involves CO, such as in hydroformylation of ethylene, as it eliminates the need to reintroduce CO. Nevertheless, designing highly efficient catalysts for acetylene hydrogenation under these harsh feed conditions remains a challenge. The large amounts of CO present can poison the metal active sites and accelerate the formation of oligomers, complicating the catalytic process.

2.2 Reaction pathway of acetylene hydrogenation

The reaction pathways for acetylene hydrogenation are illustrated in Fig. 2. Acetylene and atomic hydrogen adsorb onto the catalyst surface, where subsequent reactions at the active sites lead to the formation of ethylene, representing the primary reaction pathway. However, three main side reactions may occur during the hydrogenation process. The first one involves over-hydrogenation, where adsorbed ethylene or other C_2 unsaturated intermediates further react with active hydrogen to form ethane. The second side reaction consists of coupling, where adsorbed acetylene and ethylene species undergo C–C coupling, leading to chain growth and the generation of C_{4+} products such as 1,3-butadiene and butene. These coupling by-products typically exhibit strong polymerization tendencies on the catalyst surface, often resulting in the formation of polymeric deposits (referred to as green oil, GO), which can block the active sites and lead to catalyst deactivation. The third side reaction involves C–C bond cleavage, leading to coke deposition that typically modifies the active phase, including the formation of PdC_x on Pd-based catalysts under reaction conditions.

The hydrogenation of unsaturated carbon–carbon bonds is an exothermic reaction. The standard molar enthalpy changes (ΔH) of the main and side reactions in acetylene selective hydrogenation are shown in eqn (1)–(5):

$$C_2H_2 + H_2 \rightarrow C_2H_4 \quad \Delta H^{\theta}_{298} = -172\ \text{kJ mol}^{-1} \qquad (1)$$

$$C_2H_4 + H_2 \rightarrow C_2H_6 \quad \Delta H^{\theta}_{298} = -136\ \text{kJ mol}^{-1} \qquad (2)$$

$$2C_2H_2 + H_2 \rightarrow C_4H_6 \quad \Delta H^{\theta}_{298} = -343\ \text{J mol}^{-1} \qquad (3)$$

$$C_2H_2 \rightarrow 2C_2 + H_2 \quad \Delta H^{\theta}_{298} = -433\ \text{kJ mol}^{-1} \qquad (4)$$

$$C_2H_2 \rightarrow C + CH_4 \quad \Delta H^{\theta}_{298} = -125\ \text{kJ mol}^{-1} \qquad (5)$$

In petrochemical processes, ethylene purification reactions are typically carried out using gas-phase hydrogenation in fixed-bed reactors. However, this process is susceptible to a phenomenon known as "thermal runaway", which can lead to sintering of the active metal and catalyst deactivation. Furthermore, high temperatures can accelerate the hydrogenation of ethylene to ethane and promote the formation of green oil. In acetylene hydrogenation for petrochemical processes, reactors generally operate at low temperatures, with inlet temperatures around 50–60 °C and outlet temperatures ranging in 70–100 °C. In the industrial route for producing ethylene from coal and natural gas, the exothermic heat generated is much higher compared to petrochemical processes (under the same gas space velocity), due to the significantly higher concentration of acetylene. This necessitates more rigorous catalyst specifications and imposes stricter demands on both reactor engineering and process design to effectively manage the high heat transfer requirements.

2.3 Benchmark for calculating acetylene conversion and ethylene selectivity

Research on acetylene hydrogenation is generally carried out in a fixed-bed or stirred reactor under continuous flow conditions. The inlet and outlet gases are typically analysed by gas chromatography (GC) equipped with a gas sample loop. The GC provides the peak areas of each product in the gas sample, which can be used to further calculate molar concentrations. However, it should be noted that the peak area ratio from chromatogram should not be directly used as the molar concentration. The accurate formulas for calculating the conversion (X) and selectivity (S) are as follows:

$$X = \frac{F_{C_2H_2,in} - F_{C_2H_2,out}}{F_{C_2H_2,in}} = \frac{v_{in}C_{C_2H_2,in} - v_{out}C_{C_2H_2,out}}{v_{in}C_{C_2H_2,in}} = \frac{C_{C_2H_2,in} - \varepsilon C_{C_2H_2,out}}{C_{C_2H_2,in}} \qquad (6)$$

$$S_i = \frac{F_{i,out} - F_{i,in}}{F_{C_2H_2,in} - F_{C_2H_2,out}} = \frac{\varepsilon C_{i,out} - C_{i,in}}{C_{C_2H_2,in} - \varepsilon C_{C_2H_2,out}} \qquad (7)$$

where $F_{i,in}$ and $F_{i,out}$ represent the molar flow rates of component i, $C_{i,in}$ and $C_{i,out}$ denote the molar concentrations of component i, v_{in} and v_{out} are the volumetric flow rates, ε is

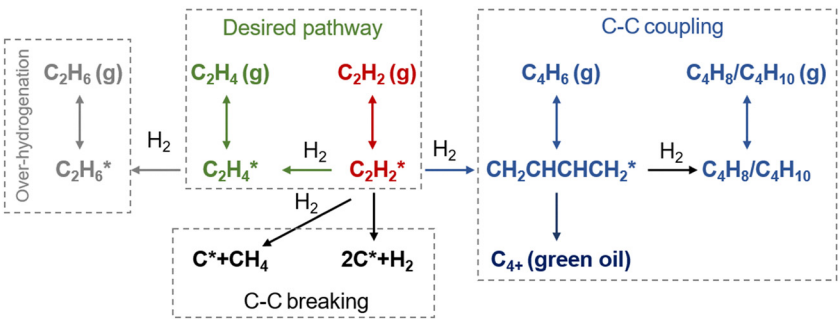

Fig. 2 Reaction pathways for acetylene hydrogenation.

the volume ratio of the outlet to inlet gases, and the subscript "in" and "out" refer to the inlet and outlet of the reactor, respectively.

Ethylene selectivity is one of the most important indicators for evaluating catalyst performance. In the feed conditions of the petrochemical industry, the concentration of acetylene is usually below 0.5%, therefore the volume change after the reaction can be neglected ($\varepsilon \approx 1$) when excess ethylene in the feed does not undergo over-hydrogenation. Therefore, ethylene selectivity can be expressed as:

$$S_{C_2H_4} = \frac{\varepsilon C_{C_2H_4,out} - C_{C_2H_4,in}}{C_{C_2H_2,in} - \varepsilon C_{C_2H_2,out}} = \frac{C_{C_2H_4,out} - C_{C_2H_4,in}}{C_{C_2H_2,in} - C_{C_2H_2,out}} \quad (8)$$

Theoretically, ethylene selectivity can be calculated using eqn (8). However, in acetylene hydrogenation within an ethylene-rich stream, the concentration of ethylene is nearly 30-fold higher or more than that of acetylene. Considering systematic errors from flow meter control, and GC sampling and analysis, even a fluctuation of ±1% in ethylene concentration can result in more than ±30% variation in $S_{C_2H_4}$ directly calculated using eqn (8). Therefore, several studies have cautioned against directly measuring changes in ethylene concentration for calculating $S_{C_2H_4}$ due to the inherent limitations in measurement accuracy.

Over the past decade, several alternative methods have been proposed for the indirect calculation of ethylene selectivity under feed conditions involving ethylene-rich streams, as summarized in Table 2. Methods A, B, C, and D estimate ethylene selectivity indirectly by measuring ethane and C_4 components, since these species can be accurately quantified due to their absence in the feed. However, acetylene hydrogenation is often accompanied by oligomerization, leading to the formation of GO, which consists of deposited long-chain hydrocarbons. GC used for quantitative analysis primarily detects light hydrocarbons such as acetylene, ethylene, ethane, and C_4, while GO components remain undetected. The omission of GO in Methods A, B, C, and D may result in an overestimation of the intrinsic selectivity toward ethylene. Notably, Methods D consider only ethylene and ethane as products, disregarding C_4 by-products and GO formation, which can further overestimate the intrinsic ethylene selectivity. Another strategy to estimate the ethylene selectivity in ethylene-rich stream is to carried out isotope labeling experiments, where Method E was used to determine $S_{C_2H_4}$ by using two different isotopes, ^{13}C and ^{12}C, for ethylene and acetylene, respectively.[13]

For acetylene hydrogenation in an ethylene-free feed stream, the change in ethylene concentration can be accurately measured, enabling direct calculation of $S_{C_2H_4}$ using Method E. Additionally, Methods F and G have been proposed as simplified approaches for calculating ethylene selectivity. However, Method F neglects the formation of GO, while Method G excludes both C_4 and GO by-products, potentially leading to an overestimation of ethylene selectivity.

Based on the above discussion, the following recommendations are proposed for calculating ethylene selectivity:

(i) When comparing state-of-the-art catalyst performance, a standardized ethylene selectivity calculation method should be adopted.

(ii) For testing new catalysts for industrial processes involving ethylene-rich feed streams, the primary objective is to reduce trace acetylene to the ppm level while minimizing ethylene loss. Therefore, the residual acetylene concentration and the absolute ethylene concentration in the reaction effluent are key performance indicators. To evaluate both catalytic activity and selectivity, it is recommended to follow the strategy proposed by Borodziński and Bond,[2] as illustrated in Fig. 3.

(iii) To investigate the acetylene hydrogenation mechanism over specific active sites, using an ethylene-free feed stream can provide a more accurate determination of the intrinsic selectivity of the products.

(iv) For testing new catalysts for the production of ethylene from coal and natural gas, the volume change after the reaction cannot be neglected due to the high acetylene concentration. Therefore, ε must be taken into account when calculating the conversion and selectivity.

Table 2 Methods for ethylene selectivity calculation reported in the literature

Method	Formula of $S_{C_2H_4}$	Advantages or limitations
Indirect method (in ethylene-rich feed stream)		
A	$S_{C_2H_4} = \frac{C_{C_2H_2,in} - C_{C_2H_2,out}}{C_{C_2H_2,in} - C_{C_2H_2,out} + C_{C_2H_6,out}}$	• Selectivity definition differs from the conventional approach • Overestimate the selectivity due to the neglect of C_4 and GO
B	$S_{C_2H_4} = \frac{C_{C_2H_2,in} - C_{C_2H_2,out}}{C_{C_2H_2,in} - C_{C_2H_2,out} + C_{C_2H_6,out} + 2C_{C_4,out}}$	• Selectivity definition differs from the conventional approach • Overestimate the selectivity due to the neglect of GO
C	$S_{C_2H_4} = 1 - \frac{C_{C_2H_6,out} - C_{C_2H_6,in} + 2(C_{C_4,out} - C_{C_4,in})}{C_{C_2H_2,in} - C_{C_2H_2,out}}$	• Overestimate the selectivity due to the neglect of GO
D	$S_{C_2H_4} = 1 - \frac{C_{C_2H_6,out} - C_{C_2H_6,in}}{C_{C_2H_2,in} - C_{C_2H_2,out}}$	• Overestimate the selectivity due to the neglect of C_4 and GO • Direct method (in ethylene-free feed stream)
E	$S_{C_2H_4} = \frac{C_{C_2H_4,out}}{C_{C_2H_2,in} - C_{C_2H_2,out}}$	• Not suitable for ethylene-rich feed streams • Accurately defines selectivity for ethylene-free feed streams
F	$S_{C_2H_4} = \frac{C_{C_2H_4,out}}{C_{C_2H_4,out} + C_{C_2H_6,out} + 2C_{C_4,out}}$	• Overestimate the selectivity due to the neglect of GO
G	$S_{C_2H_4} = \frac{C_{C_2H_4,out}}{C_{C_2H_4,out} + C_{C_2H_6,out}}$	• Overestimate the selectivity due to the neglect of C_4 and GO

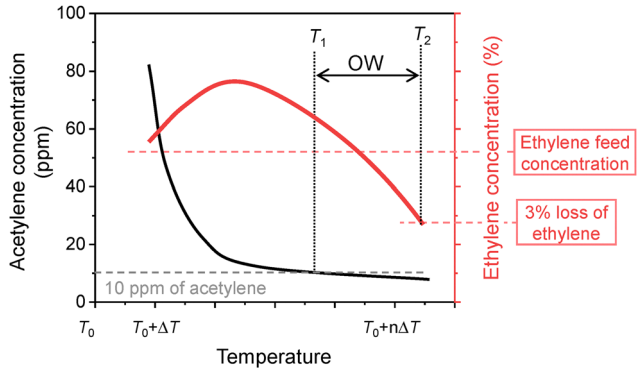

Fig. 3 Acetylene hydrogenation test for catalysts in ethylene-rich streams. Reprinted with permission from ref. 2. Copyright 2008 Taylor & Francis. The difference between T_1 and T_2 is called the operating window (OW). Catalyst with a large OW is more thermally stable at the temperature necessary to remove acetylene from the feed.

3. Active sites for acetylene selective hydrogenation

In acetylene selective hydrogenation, the active metal sites are typically hydrogenation-active transition metals, such as Pd, Au, Ni, and Cu. Based on their structural characteristics, active sites for acetylene hydrogenation can be classified into monometallic, disordered alloy, IMC, and SA sites. This section provides a comprehensive summary and discussion of research progress based on active site structures. Section 3.1 presents the development trends and the current advances in active site design. Given that Pd is the most extensively studied active metal for acetylene hydrogenation, Sections 3.2 and 3.3 further distinguish between Pd-based and non-Pd-based active sites, respectively.

3.1 Overview and state-of-the-art of active site design

Acetylene selective hydrogenation requires the conversion of C≡C bonds to C=C while simultaneously suppressing both over-hydrogenation to ethane and C–C coupling reactions that lead to oligomerization. The key challenge in this reaction lies in the design of active sites with high performance. It has been reported that active sites composed of neighbouring active metal ensembles preferentially stabilize di-σ-bonded acetylene and adsorbed ethylene, thereby promoting both ethylene over-hydrogenation and C–C coupling reactions.[2,14] Despite its relatively high ethylene selectivity among monometallic catalysts, Pd nanoparticles (NPs) inherently feature adjacent active sites that facilitate side reactions and thus compromise ethylene selectivity.

An effective strategy to enhance ethylene selectivity is the incorporation of a secondary metal to construct selective hydrogenation active sites (Fig. 4a). The electronic interaction between the secondary metal and the active metal modulates the adsorption strength of C≡C and C=C bonds, thereby enhancing ethylene selectivity. In addition, site isolation by the secondary metal or a single-atom structure spatially separates the active metal sites, preventing C–C coupling reactions and ethylene over-hydrogenation. Guided by these active site design principles, research over the past decade has focused on enhancing catalyst performance. Beyond monometallic sites, the active sites in acetylene hydrogenation catalysts can be classified into three distinct types (Fig. 4b):

(1) Multi-metallic sites with disordered alloy structures. A representative class of multi-metallic catalysts consists of disordered alloy phases. In such disordered alloys, the surface atomic arrangement is unpredictable, leading to the presence of adjacent active metal sites.

(2) IMC sites with well-defined structures. IMCs possess precisely defined atomic compositions and ordered structures, in which metal atoms are arranged in a highly specific manner.

(3) SA sites. By maximizing the spatial separation of metal centers, SA structures completely eliminate neighboring active metal sites.

Fig. 4c and d illustrate the number of annual publications (since 2008) related to these active site categories for both Pd-based and non-Pd-based catalysts, respectively. For Pd-based catalysts, secondary metal modification has been widely explored to enhance selectivity and stability. Additionally, since the emergence of the SA concept, there has been a growing interest in developing high-performance Pd SA catalysts, particularly in the past five years. Researchers have also increasingly focused on replacing Pd with alternative metal sites, particularly non-precious metals. Over the past five years, efforts have primarily centered on the development of multi-metallic alloy and IMC active sites.

Tables 3–10 summarize the state-of-the-art catalytic performance for acetylene selective hydrogenation, categorized according to the active site classifications discussed above. In Section 2.3, we highlighted the importance of using benchmark methods for calculating ethylene selectivity. Correspondingly, we also include the specific calculation methods used in each study in Tables 3–10. To ensure a fair comparison, the performance of different catalysts is analyzed based on results obtained using the same calculation method.

Fig. 5a and d illustrate the ethylene selectivity of Pd-based and non-Pd-based catalysts under ethylene-free feed conditions, with $S_{C_2H_4}$ calculated using Method E. A monometallic Pd active site typically achieves ~60% ethylene selectivity (E) due to ethane formation and C_{4+} byproducts. Incorporating a secondary metal, forming either a disordered alloy or an IMC phase, typically enhances ethylene selectivity to 70–80% (E). For Ni-based catalysts, monometallic Ni generally exhibits poor ethylene selectivity due to the formation of C_4 species and GO. Ni alloys and Ni-based IMC structures can improve ethylene selectivity to some extent.

Under ethylene-rich feed conditions, ethylene selectivity is predominantly calculated using Methods C and D (Fig. 5b, c, e and f). Method D provides insights into the ability to suppress the ethylene over-hydrogenation pathway. Notably, Pd SA sites exhibit exceptional resistance to ethane formation even at nearly 100% acetylene conversion (Fig. 5c). Similarly, Cu single-atom catalysts effectively suppress both ethane and C_4 formation, achieving $S_{C_2H_4}$ above 90% (C) (Fig. 5e).

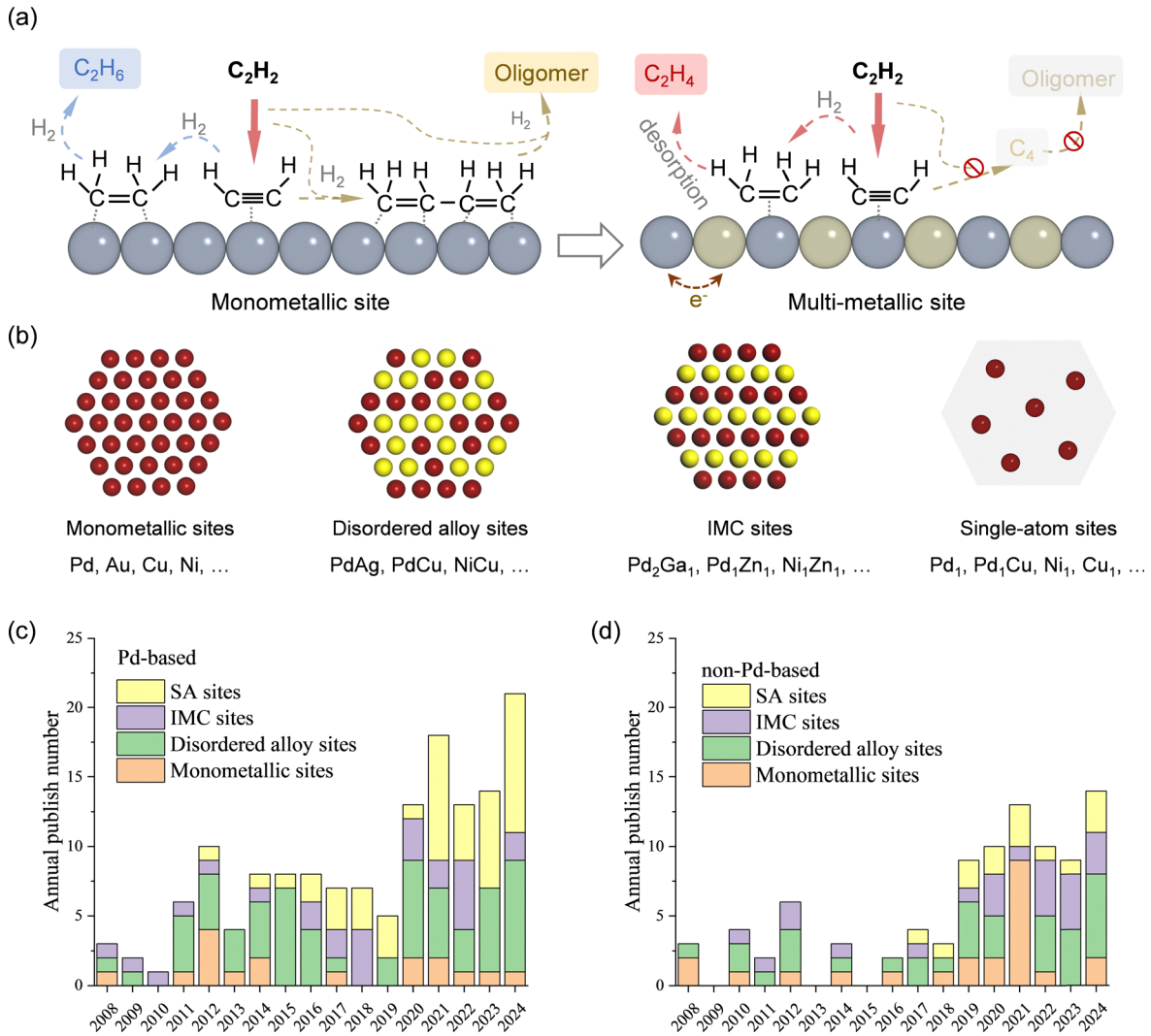

Fig. 4 (a) Schematic illustration of the active sites design strategy. (b) Four distinct types of active sites for acetylene hydrogenation. Annual published papers for the corresponding active sties of (c) Pd-based catalyst and (d) non-Pd-based catalysts.

The catalytic activity is defined as the moles of acetylene converted per hour per active metal site. It should be noted that the activity is strongly influenced by reaction temperature and acetylene concentration. These factors must be taken into account when comparing catalytic performance from different studies. Fig. 6 presents a comparative analysis of the hydrogenation activity of different types of active sites under an acetylene feed concentration of ~1%. Pd-based active sites generally demonstrate significantly higher activity compared to non-Pd-based active sites. For instance, Pd SA sites exhibit an activity that is more than two orders of magnitude higher than that of Cu SA sites.

3.2 Pd-based active sites

Pd-based active sites are the most extensively studied catalysts for acetylene selective hydrogenation and are the primary catalysts currently used in industrial acetylene hydrogenation processes. Compared to non-Pd-based catalysts, Pd-based catalysts exhibit a significant advantage in catalytic activity. The evolution of Pd-based active sites has progressed from monometallic Pd to Pd-based disordered alloys, followed by Pd IMC sites and Pd SA sites. In addition, Pd-based active sites coated with carbon or metal oxide layer are reported as an efficient strategy to enhance the catalytic performance. In this section, we summarize the catalytic performance and research progress of Pd-based active sites across the different structural categories.

3.2.1 Monometallic Pd active site. Monometallic Pd active sites represent one of the earliest investigated catalysts for acetylene hydrogenation. Their catalytic mechanisms and performance have been reviewed by Borodziński and Bond.[2] A key conclusion from reported studies is that the turnover frequency (TOF) of surface-exposed Pd active sites is approximately proportional to particle size. This relationship arises due to geometric effects induced by the carbonaceous layer deposited on the Pd surface. In contrast, selectivity toward ethylene and activation energy are almost independent of particle size.

Table 3 Monometallic Pd catalysts for acetylene hydrogenation

Catalyst	Description	T, °C	Feed[a], %	X, %	S, %	Activity[b]	Method[c]	Ref
Pd/CNF	8 nm Pd	150	2/4/0	36	1	4434.2	E	15
Pd/CNF	11 nm Pd	150	2/4/0	47	59	5789.1	E	
Pd/CNF	13 nm Pd	150	2/4/0	43	62	5296.4	E	
Pd/TiO_2		31	1.1/3.3/95.6	43	50	204.1	D	16
Pd/TiO_2	H RF plasma treat	31	1.1/3.3/95.6	37	74	175.6	D	
Pd/TiO_2	O RF plasma treat	31	1.1/3.3/95.6	30	90	142.4	D	
Pd/TiO_2	Ar RF plasma treat	31	1.1/3.3/95.6	27	94	128.1	D	
Pd/LDH	Spherical Pd	50	0.3/0.6/32.9	20	85	53.1	E*	17
Pd/MgAl-LDH	Tetra Pd	50	0.3/0.6/32.9	48	97	127.4	E*	
Pd/MgAl-LDH	Octa Pd	50	0.3/0.6/32.9	47	89	129.5	E*	
Pd/MgAl-LDH	L-Wires Pd	40	0.3/0.6/32.9	50	82	76.2	E*	18
Pd/MgAl-LDH	S-Wires Pd	40	0.3/0.6/32.9	45	84	68.3	E*	
Pd/MgAl-LDH	Cuboctahedral Pd	40	0.3/0.6/32.9	45	84	68.0	E*	
Pd/CNF	Cubic Pd	120	1.5/20/0	13	62	—	E	19
Pd/CNF	Cuboctahedral Pd	120	1.5/20/0	13	64	—	E	
Pd/CNF	Octahedral Pd	120	1.5/20/0	13	65	—	E	
Pd/Al_2O_3	Cubic Pd	60	0.6/1.2/49.3	75	32	133.1	E*	20
Pd/Al_2O_3	Spherical Pd	60	0.6/1.2/49.3	75	−5	51.2	E*	
Pd/ZnO	Octahedra Pd	100	2/4/0	25	90	6681.6	—	21
Pd/ZnO	Cubes Pd	100	2/4/0	30	80	6472.8	—	
Pd/SiO_2	Octahedra Pd	100	2/4/0	25	90	4554.0	—	
Pd/SiO_2	Cubes Pd	100	2/4/0	20	80	2070.0	—	
Pd/Al_2O_3		140	2/20/0	60	62	3420.6	E	22
Pd/C		75	1/1/0	92	50	—	—	23
Pd–B/C	Subsurface B atom	75	1/1/0	81	78	—	—	
Pd–Li/C	Subsurface Li atom	75	1/1/0	83	79	—	—	
Pd/msAC	2 nm Pd	260	—	100	~90	—	—	24
Pd/CNTs	PdC_x	200	0.9/8.8/88.2	82	40	—	B	25
Pd-ac/Al_2O_3	PdC_x	70	0.3/0.7/33	95	60	—	E*	26
PdAl-120	PdC_x	80	2/2.2/80	90	93	—	D	27

[a] The feed composition listed in the table corresponds to $C_2H_2/H_2/C_2H_4$. [b] Activity is calculated as the number of moles of acetylene converted per hour per total molar Pd active metal ($mol_{C_2H_2}$ mol_{Pd}^{-1} h^{-1}). [c] Method refers to the calculation method specified in Table 2. E* indicates that Method E was applied under ethylene-rich feed conditions.

The formation of β-PdH_x and PdC_x phases has also been reviewed.[1,2] The formation of both β-PdH_x and PdC_x contributes to enhanced activity in acetylene hydrogenation, while the β-PdH_x phase reduces ethylene selectivity. Since 2008, researchers have continued to investigate the effect of PdC_x. It has been reported that the PdC_x phase promotes higher ethylene selectivity. Compared to Pd/α-Al_2O_3 catalysts, Pd/α-Al_2O_3-AAS catalysts containing the PdC_x phase showed improved ethylene selectivity, increasing from approximately 70% to 85% (calculated using Method E).[200] Furthermore, researchers have identified that metal precursors, additives, and carbonization conditions significantly influence the formation of a stable PdC_x phase. The introduction of silane coupling agents and the use of $Pd(acac)_2$ as the metal precursor have been identified as effective strategies for promoting the formation of the PdC_x phase.[26,201]

Advancements in nanocrystal synthesis have led researchers to investigate the influence of the Pd crystal structure on catalytic performance. By synthesizing Pd NPs in various shapes, including cubic (exposing only (100) faces), octahedral (exposing only (111) faces), cuboctahedral (exposing both (100) and (111) faces), and spherical Pd (primarily exposing (111) faces), researchers have investigated how the exposed Pd crystal facets affect acetylene hydrogenation activity and selectivity. For instance, Kim *et al.*[20] synthesized cubic and spherical Pd NPs supported on alumina. Their results demonstrated that Pd sites on the (100) face of cubic NPs exhibited a TOF more than twice that of Pd sites on the (111) face of spherical NPs. Additionally, cubic Pd NPs displayed higher ethylene selectivity. However, other studies have drawn contrasting conclusions. It is commonly believed that the Pd(111) facet exhibits higher hydrogenation activity and selectivity.[17,21] Yarulin *et al.*[19] demonstrated that atoms on the (111) face are approximately 1.5 times more active than those on the (100) face. Recently, Xing *et al.*[202] combined experimental results with computational methods, including the atomic pair distribution function and reverse Monte Carlo method. Their work revealed the presence of surface Pd sites with compressive strain in spherical Pd NPs (Fig. 7). This strain downshifts the local d-band and weakens the strength of ethylene adsorption, leading to an enhanced ethylene selectivity.

3.2.2 Multi-metallic sites with disordered alloy structure

3.2.2.1 PdAg alloy. The PdAg alloy is the most commonly studied bimetallic catalyst for acetylene hydrogenation and remains widely used in the modern petrochemical industry. The incorporation of Ag enhances the ethylene selectivity of Pd-based catalysts through both electronic and geometric effects. Electronically, the interaction between Ag and Pd weakens ethylene adsorption on the surface, thereby suppressing its further hydrogenation to ethane.[203] Geometrically, the presence of Ag reduces the number of neighboring Pd surface atoms, which in turn lowers the formation of oligomers.

Table 4 Pd-based alloy catalysts for acetylene hydrogenation

Catalyst	Description	T, °C	Feed[a], %	X, %	S, %	Activity[b]	Method[c]	Ref
PdAg								
$PdAg/Al_2O_3$		35	1/1.4/30	70	~67		C	28
$PdAg/Al_2O_3$		60	0.9/1.8/97.2	90	20	316.1	—	29
$NiPdAg/Al_2O_3$		60	1.1/2.2/96.8	87	25	355.9	—	30
$Pd@Ag/TiO_2$		60	0.73/1.46/52.6	82	79	215.5	C	31
$PdAg/SiO_2$		65	1/5/20	18	79	116.6	B	32
$PdAg/Al_2O_3$	Egg-shell	30	1/1/30	44	75	325.7	—	33
PdAg/MgAl-LDH	Mesocrystal	77	0.35/0.6/32.8	90	82	1.8	E*	34
Ag@PdAg/LDHs	Core–shell	100	0.31/0.6/32	99.5	97	7.6	E*	35
PdAg/carbon material		45	4/excess/0	35	76	15963.0	E	36
$100Pd_0Ag/Al_2O_3$		50	1.47/6.95/29.5	~70	50	1400.0	B	37
$90Pd_{10}Ag/Al_2O_3$		50	1.47/6.95/29.5	~70	60		B	
$75Pd_{25}Ag/Al_2O_3$		50	1.47/6.95/29.5	~70	70		B	
$50Pd_{50}Ag/Al_2O_3$		50	1.47/6.95/29.5	~70	75		B	
$PdAg/Al_2O_3$		150	14.3/71.4/14.3	95	62	5416.0	E*	38
Pd/K^+-*b*-zeolite		30	2.5/10/2.5		−5		E	39
$PdAg/K^+$-*b*-zeolite		75	2.5/10/2.5		70		E	
PdCu								
$PdCu/Al_2O_3$		60	0.9/1.8/97.2	100	5	351.2	—	40
$PdCu/Al_2O_3$		90	0.6/1.8/0	70	62		E	41
$PdCu/Al_2O_3$		80	0.59/1.76/0	100	72		E	42
$CuPd/Al_2O_3$	Copper rich	50	0.59/1.76/0	35.3	63.4		E	43
PdCu/MgAl-cHT		100	0.3/0.6/32.9	100	84	367.3	E*	44
$AgPd_{0.64}/TiO_2$		40	1/25/25	<3	99	54.3	D	45
$CuPd_{0.08}/TiO_2$		40	1/25/25	<3	100	92.6	D	
$CuPd_{0.02}/TiO_2$		40	1/25/25	<3	98.5	108.5	D	
Pd/TiO_2		40	1/25/25	<3	95	47.9	D	
Pd/oCNTs		200	0.5/5/20.1	97.1	39	237.5	C	46
Pd_3Cu/oCNT		200	0.5/5/20.1	98.5	55	228.0	C	
Pd_2Cu/oCNT		200	0.5/5/20.1	99.2	68	205.6	C	
PdCu/oCNT		200	0.5/5/20.1	98.8	72	152.0	C	
$PdCu_3$/oCNT		200	0.5/5/20.1	98.5	71	106.0	C	
Pd/BF-500/250	Pd–Cu–Zn	80	0.625/6.25/31.25	25	85		C	47
PdCu/C	FCC phase	100	0.33/0.66/33	100	61	502.4	E*	48
PdCu/C	BCC phase	100	0.33/0.66/33	100	86	460.9	E*	
Pd_1Cu_2/C	Pd : Cu = 48 : 51	96	0.33/0.66/33	88	82	163.4	E*	49
Pd_1Cu_3/C	Pd : Cu = 38 : 62	116	0.33/0.66/33	85	87	180.4	E*	
Pd_1Cu_4/C	Pd : Cu = 34 : 66	135	0.33/0.66/33	80	98	145.7	E*	
PdCu/siloxene		200	1/10/0	91	93	4323.3	E	50
$Pd_{40}Cu_{60}$	Disorder phase	200	0.5/5/50	90	74		B	51
$Pd_{40}Cu_{60}$	Order phase	200	0.5/5/50	90	92		B	
$PdCu/SiO_2$	B2 phase	25	1/2/1	43	78		—	52
$PdCu/SiO_2$	FCC phase	25	1/2/1	13	71		—	
$CuPd\text{-}2/Al_2O_3$	B2 phase	90	0.5/3/0	100	95		E	53
Pd/SiO_2(NS)		70	12.5/37.5/0	55	47		E	54
Pd_1Cu_1/SiO_2(NS)		70	12.5/37.5/0	40	55		E	
Pd_1Cu_3/SiO_2		70	12.5/37.5/0	42	47		E	
Au@PdCu/C		122	0.33/0.66/32.98	100	92	210.0	E*	55
PdAu								
$PdAu/MgAlO_x$	Nanoflowers	100	0.3/0.3/31.7	94	53	376.0	E*	56
$AuPd/TiO_2$		250	0.97/2.91/96.1	50	93	3632.4	D	57
$Au@Pd/TiO_2$	Core–shell	90	1.2/2.2/0	100	53		E	58
m-$PdAuAg_2$/HT		140	0.33/0.6/32.8	99.5	76.2	391.9	E*	59
TiO_x/Au_8Pd@SBA			0.5/5/10	92	75		C	60
PdZn								
$Pd/\gamma\text{-}Al_2O_3$		60	1.2/2.5/96.3	47.2	31.3	118.8	A	61
$Pd–Zn/\gamma\text{-}Al_2O_3$		60	1.2/2.5/96.3	56.1	74.4	140.4	A	
$Pd/\alpha\text{-}Al_2O_3$		60	1.2/2.5/96.3	64.9	21.2	21.2	A	
$PdZn/\alpha\text{-}Al_2O_3$		60	1.2/2.5/96.3	67.1	88.6	23.0	A	
PdZn/carbon material		45	4/excess/0	40	73	18243.4	E	62
Pd/ZnO/SMFs	PdZn	140	1.5/20/0	15	82		E	63
Pd/CNFs/SMFs		140	1.5/20/0	15	70		E	
PdCo								
CoPd/MgO		110	0.5/1/70	78	59	334.9	C	64
Pd/MgO		110	0.5/1/70	80	5	316.7	C	
$PdCo/Al_2O_3$		85	0.33/0.66/33	99.5	88	522.6	E*	65

Table 4 (*continued*)

Catalyst	Description	*T*, °C	Feed[a], %	*X*, %	*S*, %	Activity[b]	Method[c]	Ref
Pd/C		45	4/96/0	72	60	10946.1	E	66
PdCo(1 : 0.5)/C		45	4/96/0	65	63	9881.9	E	
PdCo(1 : 1)/C		45	4/96/0	50	66	7601.4	E	
PdCo(1 : 2)/C		45	4/96/0	30	67	4560.9	E	
PdCo(1 : 4)/C		45	4/96/0	7	67	1064.2	E	
PdX								
SnPd/MWNTs		160	10/20/0	100	93		E	67
Pd/MWNTs		160	10/20/0	100	87		E	
PdTi/SiO_2-T		110	1/4/0	100	89		E	68
Pd/SiO_2		110	1/4/0	100	64		E	
PdGa/MgO–Al_2O_3		45	0.3/0.6/32.9	85.9	87.2	518.4	E*	69
Pd/MgO–Al_2O_3		45	0.3/0.6/32.9	89.5	54.7		E*	
PdNi/MgAlO		70	0.3/0.6/32.9	92	70		E*	70
PdIn/Al_2O_3		60	0.6/1.8/0	95	70	779.9	C	71
PdMn-2-300/Al_2O_3		40	1.05/1.94/5.01	87	81	449.1	E*	72
Pd NPs@$Bi_{0.5}$/Al_2O_3		120	1/20/20	70	99	1995.4	D	73
$Pd_{0.25}La_{0.25}$/N-pgBC		70	1/2/0	94	53		E	74

[a] The feed composition listed in the table corresponds to $C_2H_2/H_2/C_2H_4$. [b] Activity is calculated as the number of moles of acetylene converted per hour per total molar Pd active metal ($mol_{C_2H_2}$ mol_{Pd}^{-1} h^{-1}). [c] Method refers to the calculation method specified in Table 2. E* indicates that Method E was applied under ethylene-rich feed conditions.

An optimal Ag/Pd ratio was observed in the catalytic performance of PdAg catalysts. An excessive amount of Ag can significantly decrease hydrogenation activity, due to the poor H_2 dissociation ability of metallic Ag. Delgado *et al.*[37] reported that PdAg catalysts prepared by one-pot synthesis exhibited the best catalytic performance in terms of ethylene selectivity and stability at a Pd/Ag atomic ratio of 1.0. However, other studies have reported that Pd/Ag atomic ratios either below or above 1.0 also achieve optimal performance.[28,38] This discrepancy can be attributed to differences in catalyst preparation methods, which significantly affect the microscopic mixing and structural configuration of PdAg NPs. PdAg bimetallic alloys exist as solid solutions, where the Pd and Ag atom randomly distributed within the NPs. Identical overall composition may produce a mixture of monometallic and bimetallic NPs with ill-defined compositions. Surface segregation of Pd during reactions further complicates the structure–property relationships. Williams *et al.*[32] reported an enhanced ethylene selectivity of ~80% (E) by synthesizing PdAg/SiO_2 catalysts *via* a galvanic displacement method, which achieved near-atomic dispersion of Pd on Ag surfaces. Thermal treatment under H_2 flow at 400–500 °C enabled Ag intercalation into Pd lattices, generating a $Pd_{0.6}Ag_{0.4}$ solid solution with ~76% (E) ethylene selectivity.[36]

The surface atomic composition and arrangement of NPs play a crucial role in catalytic performance. The incorporation of Ag effectively isolates neighboring Pd active sites. To investigate the geometric effect of Ag, researchers have directly deposited Ag atoms onto Pd NP surfaces using electroless deposition (ED) or surface redox (SR) methods.[29,204,205] Their results showed that both TOF and ethylene selectivity increased with Ag coverage. Higher Ag coverage leads to the formation of smaller Pd ensembles, which causes acetylene to adsorb as a π-bonded species, favoring selective hydrogenation to ethylene. Additionally, Pd@Ag core–shell catalysts have been proposed to enhance catalytic performance.[31,33,35] Compared with PdAg/TiO_2 catalysts prepared by co-impregnation, Pd@Ag catalysts synthesized *via* sequential photodeposition increased ethylene selectivity from ~20% to ~80% (C).[31]

3.2.2.2 PdCu alloy. Different from Ag, which primarily acts as a promoter, metallic Cu exhibits intrinsic activity for acetylene hydrogenation. However, its hydrogen dissociation capability is relatively weak compared to the Pd active sites. The activation energy for H_2 dissociation on a Cu(111) surface has been calculated to be 0.46 eV, significantly higher than that on Pd(111) (0.20 eV).[206]

To enhance the catalytic activity, Pd has been incorporated into Cu-based catalysts at Cu/Pd atomic ratios ranging from 10 to 50.[41–45,50] The PdCu catalyst with a Cu/Pd ratio of 43.6 exhibited a TOF that was an order of magnitude higher than that of monometallic Cu.[44] At high Cu/Pd ratios, Pd atoms can be isolated within Cu particles, where hydrogen dissociation occurs on Pd sites, followed by hydrogen spillover to adjacent Cu sites, thereby enhancing the overall hydrogenation activity.[41] The Cu/Pd ratio also plays a crucial role in determining ethylene selectivity. A PdCu catalyst with a Cu/Pd ratio of 50 exhibited an ethylene selectivity of 70–80% (E), while further decreasing the Cu/Pd ratio to 10 led to excessive hydrogenation of ethylene to ethane.[41,42]

PdCu catalysts with lower Cu/Pd atomic ratios (~1.0) have also been investigated for acetylene hydrogenation.[40,46,49,54] In these cases, Pd and Cu form a bimetallic alloy phase with a solid-solution structure, where Pd and Cu atoms are randomly distributed. Similar to PdAg catalysts, an optimal balance between catalytic activity and selectivity is closely related to the PdCu ratio. At low Cu/Pd ratios (*e.g.*, Pd_3Cu), the catalyst exhibited large Pd ensembles with minimal Pd isolation, which promoted the over-hydrogenation of ethylene to ethane. Conversely, at high Cu/Pd ratios (*e.g.*, $PdCu_3$), the catalysts were limited by H_2 activation and thus showed higher selectivity

Table 5 Pd-based IMC catalysts for acetylene hydrogenation

Catalyst	Description	T, °C	Feed[a], %	X, %	S, %	Activity[b]	Method[c]	Ref.
PdGa								
PdGa etched	Bulk	200	0.5/5/50	91	56	—	B	75
Pd_3Ga_7 etched	Bulk	200	0.5/5/50	65	48	—	B	
Pd/Al_2O_3	Pd	200	0.5/5/50	43	17	—	B	
Pd_2Ga/Al_2O_3	Pd_2Ga	200	0.5/5/50	88	67	6615.1	B	76
Pd/Al_2O_3	Pd	200	0.5/5/50	42	49	2451.9	B	
$Pd_2Ga/MgGa_2O_4$	Pd_2Ga	200	0.5/5/50	98	70	28600.4	B	77
$GaPd/Al_2O_3$	Nano-PdGa	200	0.5/5/50	83.9	82	4140.0	B	78
$GaPd_2/Al_2O_3$	Nano-Pd_2Ga	200	0.5/5/50	87.6	66	7120.0	B	
Pd/Al_2O_3	Pd	200	0.5/5/50	44.9	20	2450.0	B	
$GaPd_2/a\text{-}Al_2O_3$	Pd_2Ga	200	0.5/5/50	92	76	480.0	B	79
Sputtered $GaPd_2$	Pd_2Ga	200	0.5/5/50	41.1	72	3930.0	B	80
$Pd–Ga_2O_3$	$Pd_2Ga–Pd_1$	200	0.5/10/20	88	80	—	C	81
$Pd–Ga_2O_3$	$Pd_2Ga–Pd_3$	140	0.5/10/20	97	60	—	C	
PdIn								
$InPd_2$ powder	$InPd_2$	200	0.5/5/50	90	80	—	B	82
$PdIn/MgAl_2O_4$	PdIn	90	0.5/5/50	95	90	325.0	B	83
$Pd_3In/MgAl_2O_4$	Pd_3In	90	0.5/5/50	100	20	342.1		
PdIn/CNT	Pd_3In	50	0.5/2.5/30	90	10	256.5	C	84
PdIn/CNT	PdIn	50	0.5/2.5/30	50	90	142.5	C	
PdIn/CNT	Pd_2In_3	50	0.5/2.5/30	18	80	51.3	C	
$Pd/In_2O_3/SiO_2$	PdIn	100	1/10/0	80	68	—	E	85
PdZn								
Pd/ZnO	Pd_1Zn_1	60	2/20/0	98	70	1676.1	E	86
Pd/ZnO	Pd_1Zn_1	80	2/20/40	92	89	—	D	
Pd_8Zn_{44}	Pd_8Zn_{44}	100	1/31/18	100	82	—	E	13
Pd_9Zn_{43}	Pd_9Zn_{43}	100	1/31/18	100	70	—	E	
Pd_8AuZn_{43}	Pd_8AuZn_{43}	100	1/31/18	100	63	—	E	
$Pd_{3.9}Zn_{6.1}/CNS$	$Pd_{3.9}Zn_{6.1}$	60	1/20/19	40	90	—	D	87
PdZn	PdZn	60	1/20/19	15	45	—	D	
Pd_3ZnC_x	Pd_3ZnC_x	120	2/2.2/80	89	92	528.5	D	88
Others								
Bulk-$Pd_{11}Bi_2Se_2$		200	0.5/5/50	75	93	—	B	89
PdBi/Calcite	Pd_1Bi_1	120	1/20/20	60	>99	380.1	D	90
$PdBi/SiO_2$	Pd_3Bi	40	1/4/0	78	80	277.9	G	91
Sn–Pd/MWNTs	Pd_2Sn	160	10/20/0	100	93	—	E	67
Pd_2Sn/C	Pd_2Sn	160	0.33/0.66/32.8	100	92	17.3	E*	92
Pd_3P/TiO_2	Pd_3P	225	1.2/2.4/0	100	78	—	E	93
PdP_2/TiO_2	PdP_2	225	1.2/2.4/0	100	84	—	E	
$Ga_{1-x}Sn_xPd_2$	Bulk-Ga_1Pd_2	200	0.5/5/50	91	83	5.5	B	94
$Ga_{1-x}Sn_xPd_2$	Bulk-$Ga_{0.7}Sn_{0.3}Pd_2$	200	0.5/5/50	91	83	9.5	B	
$CaPdH_2$		100	1/10/0	85	81	—	E	95

[a] The feed composition listed in the table corresponds to $C_2H_2/H_2/C_2H_4$. [b] Activity is calculated as the number of moles of acetylene converted per hour per total molar Pd active metal ($mol_{C_2H_2}$ mol_{Pd}^{-1} h^{-1}). [c] Method refers to the calculation method specified in Table 2. E* indicates that Method E was applied under ethylene-rich feed conditions.

to polymerization byproducts.[46] The crystal structure of PdCu significantly influences acetylene hydrogenation performance.[48,52,53,207] It has been reported that modifying the $Cu_{60}Pd_{40}$ structure from a disordered phase to a partially ordered CsCl-type structure increased ethylene selectivity from 74% to 92% (B).[51] Moreover, PdCu alloys with a ordered body-centered cubic (B2) structure have shown superior ethylene selectivity compared to those with a face-centered cubic (FCC) structure.[48,52,53]

3.2.2.3 PdX alloy. In addition to widely investigated PdAg and PdCu, other bimetallic PdX catalysts have been developed for acetylene selective hydrogenation. The secondary metal (X) includes Au, Zn, Co, Sn, Ga, Ti, In, La, and Mn.[57,64,208,209] Due to variations in reaction evaluation conditions and selectivity benchmarks across studies, direct comparisons of catalytic performance among these bimetallic catalysts remain difficult. To assess the effectiveness of bimetallic catalysts, researchers typically provide performance data for the corresponding monometallic Pd catalysts as references. Fig. 8 compares the catalytic performance of monometallic and bimetallic catalysts under identical reaction conditions, using a similar Pd metal loading within the same study. In these investigations, the catalysts were primarily synthesized *via* the impregnation or colloidal solution methods, resulting in bimetallic NPs that generally form an alloy phase without a well-defined structure. Introducing a secondary metal (X) consistently improves ethylene selectivity, though its effect on catalytic activity depends on the specific element. Notably, metals like Zn, Sn, In, La, and Mn enhance both selectivity and activity, outperforming monometallic Pd catalysts.

Table 6 Pd-based SA catalysts for acetylene hydrogenation

Catalyst	T, °C	Feed[a], %	X, %	S, %	Activity[b]	Method[c]	Ref.
Carbon material supported							
Pd_1/C_3N_4	100	0.5/1/25	40	95		D	96
Pd_1/ND@G	120	1/10/20	15	95	388.7	D	97
Pd_1/Graphene	50	1/2/0	64	78	364.9	E	98
Pd_1/C_3N_4	50	1/2/0	30	96	171.0	E	
Pd-SAs-900	100	0.5/5/50	75	95	13.4	B	99
Pd_1/MPNC	110	0.5/5/50	84	82	483.9	B	100
Pd_1–N_8/CNT	40	2/4/50	62.6	96.4	2163.0	E*	101
Pd_1Cu_1/ND@G	90	1/10/20	67	93	2122.1	C	102
Pd_1–N_1C_3	100	0.65/5/50	92	80	968.5	—	103
Pd/GDY	160	0.33/0.66/32.8	75	100		E*	104
Pd_1/N-graphene	125	1/10/20	99	93.5		D	105
Pd_1/N,S-C	150	0.5/5/50	100	80	2024.5	D	106
Pd_1-Ndicy/hNCNC	160	1/215	90	87	3644.2	D	107
Metal oxide supported							
Pd_1/ZnO	80	2/20/40	99	84	33864.4	D	108
Pd_1/MgO	150	1/10/0	25	74	49884.4	E	109
Pd_1/MgO	120	1/10/20	30	94		D	110
Pd_1–Fe_1/Fe_2O_3(012)	40	1/10/20	85	97	227.2	G	111
Pd_1/MgO	120	1/2/0	39	42	1208.4	E	112
Pd_1/CeO_2	140	2/20/40	35	90	299.3	D	113
Pd_1/α-Fe_2O_3	120	2/20/40	50	85	427.6	D	
Single atom alloy							
$AuPd_{0.01}/SiO_2$	120	1/20/20	50	80	6334.5	D	114
$AgPd_{0.01}/SiO_2$	160	1/20/20	60	80	3694.0	D	115
$CuPd_{0.006}/SiO_2$	160	1/20/20	100	85	5770.3	D	116
Pd_1Ni/SiO_2	80	1/10/20	90	88	10126.9	D	117
PdCu-SAA	160	0.45/0.9/45	60	96	529.1	E*	118
$Pd_{0.1}Ni_2/SiO_2$-GR-500R	130	1/10/20	60	90	2565.5	D	119
Pd_xAg/Al_2O_3	60	1/10/20	96	94	1368.3	—	120
Pd30 ppm/Fe_5C_2	80	1/3/0	38	82		E	121
Pd_1-NiGa	110	0.5/2.5/40	100	96.8	593.9	C	122
Pd_1Ag_{10}/Al_2O_3	75	0.5/2.65/45.1	65	97	395.3	D	123
Pd_1Cu_n/Al_2O_3	120	0.33/0.66/33	100	82		D	124
Others							
Pd_1@Cu-SiW	80	0.5/5/50	12	92	2.8	B	125
Pd_1@NENU-1	80	0.5/5/50	75	88	0.2	B	
Pd_1@Y	80	0.5/5/50	35	60	7.6	B	
T-Pd_1/UiO-66-NH_2	150	0.33/0.66/34.5	45	93	582.0	E*	126
BmimBF4-0.021Pd/HAP	100	2/20/40	95	88		D	127
Pd/Ni$(OH)_2$	105	0.65/5/50	80	75	14822.8	B	128
0.8 Pd/WS2	25	1/20/0	65	65		C	129

[a] The feed composition listed in the table corresponds to $C_2H_2/H_2/C_2H_4$. [b] Activity is calculated as the number of moles of acetylene converted per hour per total molar Pd active metal ($mol_{C_2H_2}$ mol_{Pd}^{-1} h^{-1}). [c] Method refers to the calculation method specified in Table 2. E* indicates that Method E was applied under ethylene-rich feed conditions.

The structure of PdX bimetallic NPs significantly influences their catalytic performance in acetylene hydrogenation. Core–shell bimetallic catalysts, such as Au@Pd,[210] Pd@Pt,[211] and Ru@Pd,[212] have been extensively developed for acetylene hydrogenation. Core–shell architectures offer a distinct approach to modulating the electronic and geometric properties of catalysts due to their unique strain effects and coordination environments, while maintaining a continuous and abundant exposure of shell–metal ensembles. The shell thickness plays a critical role in determining catalytic performance. A monolayer of the shell metal exhibits the strongest electronic interaction with the core metal, maximizing its electronic effects. Studies have shown that a thinner shell generally provides higher hydrogenation activity than a thicker one. For example, a Ru(5.1 nm)@0.7ML-Pd catalyst with a 0.7 monolayer Pd shell exhibited more than twice the hydrogenation activity compared to Ru(5.1 nm)@2.3ML-Pd with a 2.3 monolayer Pd shell, while ethylene selectivity increased from 51% to 71% (D).[212]

Trimetallic catalysts have also been investigated to enhance the performance of acetylene hydrogenation, with examples including Ni–Pd–Ag, Pd–Au–Ag, Al–Pd–Ru, and Pd–Cu–Zn.[30,47,59,213] Compared to the corresponding bimetallic systems, trimetallic catalysts often exhibit better performance. For instance, under conditions ensuring 100% acetylene conversion, the $PdAuAg_2$ catalyst achieved an ethylene selectivity of over 75% (E*), whereas monometallic Pd and bimetallic PdAu and PdAg catalysts all exhibited selectivity below 65% (E*).[59] However, the introduction of a third metal increases the structural complexity of the catalysts, making it more difficult to identify

Table 7 Monometallic non-Pd-based catalysts for acetylene hydrogenation

Catalyst	Description	T, °C	Feed[a], %	X, %	S, %	Activity[b]	Method[c]	Ref.
Au								
Au/CeO_2	Au-2 nm	270	0.1/0.7/0	75	100	7.4	G	130
Au/Fe_2O_3	Au-3.5	169	0.11/15.4/0	50	95.9	3.0	E	131
Au/SiO_2-R250	O_2 plasma	150	0.8/16/83.2	80	76		D	132
Au/C-TiO_2-R250		150	1.0/10.2/88.7	62	43	334.8	D	133
Au/C-TiO_2-R250		150	1.1/5.4/93.5	40	79	227.6	D	
Au/ZnO–F–O		200	1/20/0	66	80	63.3	E	134
Au/CNA		250	0.6/3/0	14	98	81.0	E	135
$Au/Ce_{0.9}Zr_{0.1}O_2$		250	0.6/3/0			9.4	E	136
Au/C-TiO_2-am		185	1.1/2.2/96.7	98	78		D	137
Ni								
Ni/MCM-41		250	1 : 3 : 0	100	40	524.1	E	138
Ni/AC-N-0.5		200	1 : 3 : 0	96	46		E	139
Ni/MCM-41		200	1 : 2 : 0	82	85		E	140
Cu								
$Cu(OH)_2$-derived	CuC	110	0.45/10/88.8	98	82	0.1	D	141
Cu-derived	Cu_xC–Cu	110	0.47/7/91.8	100	80	0.1	D	142
Cu_2O derived	Cu_xC	110	0.45/10/0	100	52.4		E	143

[a] The feed composition listed in the table corresponds to $C_2H_2/H_2/C_2H_4$. [b] Activity is calculated as the number of moles of acetylene converted per hour per total molar active metal ($mol_{C_2H_2}\ mol_{metal}^{-1}\ h^{-1}$). [c] Method refers to the calculation method specified in Table 2. E* indicates that Method E was applied under ethylene-rich feed conditions.

active sites and hindering mechanistic understanding. Unraveling the structure–performance relationships in trimetallic systems remains a challenge.

3.2.3 Active sites with well-defined IMC structure. IMC phases exhibit well-defined atomic compositions and ordered structures, which endows IMC with unique electronic properties and geometric configurations. The incorporation of a secondary metal modifies the electronic properties of Pd, optimizing the adsorption strength of reactant species and suppressing the over-hydrogenation of ethylene. Additionally, the ordered arrangement of the secondary metal spatially isolates adjacent Pd sites, inhibiting C–C coupling reactions. Secondary metals such as Ga, Zn, and In form IMC phases with Pd over a wide range of metal ratios and structural configurations, leading to improved ethylene selectivity compared to monometallic Pd (Fig. 9). Notably, the formation of PdGa IMCs not only enhances ethylene selectivity but also promotes acetylene hydrogenation activity.

3.2.3.1 PdGa IMC. PdGa IMCs are among the most extensively studied IMC catalysts for acetylene hydrogenation.[79,80,214] Schlögl *et al.* first proposed that the well-defined crystal structure of PdGa IMCs could effectively isolate Pd atoms, thereby modifying their catalytic properties.[14,76,77] They synthesized bulk PdGa and Pd_3Ga_7 *via* the metal melting method and evaluated their performance for acetylene hydrogenation. These bulk samples exhibited excellent long-term stability and significantly higher ethylene selectivity (70–75%, B) compared to the Pd/Al_2O_3 reference (17%, B).[75] However, the catalytic activity was relatively low due to the presence of surface oxide species, which formed during the grinding or milling process. Surface etching, which removed these oxide species, enhanced the surface activity ($g\ m_{cat}^{-2}\ h^{-1}$) to a level comparable to that of Pd/Al_2O_3. However, the ethylene selectivity decreased to ~50% (B), likely due to partial decomposition of the IMC phase, leading to Pd-enriched surfaces.[76]

To improve the dispersion of PdGa IMCs and enhance their catalytic activity, researchers have focused on synthesizing well-defined PdGa IMC NPs. Two-step synthesis and precursor-based methods have proven effective in producing GaPd and $GaPd_2$ NPs with particle sizes below 7 nm.[78,215] Investigations of nanoscale PdGa IMC catalysts have demonstrated their intrinsically higher activity compared to monometallic Pd in acetylene hydrogenation. For instance, nano-$GaPd_2$@Al_2O_3 and nano-GaPd@Al_2O_3 exhibited hydrogenation activities of 7120 and 4140 $mol_{C_2H_4}\ mol_{Pd}^{-1}\ h^{-1}$, which were 2.9 and 1.7 times higher than that of Pd/Al_2O_3, respectively.[78] Moreover, the ethylene selectivity over nano-GaPd@Al_2O_3 increased to 82% (B). The significantly enhanced catalytic performance of PdGa IMCs was attributed to the presence of isolated Pd atoms within their intermetallic structure. This conclusion was further validated through precise atomic-level engineering of the catalyst surface.[81] The exposed surface structures of Pd_2Ga IMC were tailored *via* reactive metal–support interactions, where increasing the reduction temperature induced a transition from the energetically favorable (013)/(020) facets to (011)/(002). This structural evolution resulted in two distinct configurations (Fig. 10): $Pd_2Ga(Pd_1)$, characterized by isolated Pd atoms (Pd_1), and $Pd_2Ga(Pd_3)$, characterized by consecutive Pd trimers (Pd_3). Notably, $Pd_2Ga(Pd_1)$ exhibited a higher ethylene selectivity (80%, C) compared to $Pd_2Ga(Pd_3)$ (60%, C).

3.2.3.2 PdZn IMC. PdZn bimetallic catalysts exhibit both ill-defined alloy phases and well-defined IMC phases. The formation of a well-defined structure is highly dependent on the catalyst preparation method. Various PdZn IMC catalyst,

Table 8 Multi-metallic alloy catalysts for acetylene hydrogenation

Catalyst	T, °C	Feed[a], %	X, %	S, %	Activity[b]	Method[c]	Ref.
NiX alloy							
$NiZn_2/MgAl_2O_4$	100	2/20/0	75	60	84.2	E	144
$Ni/MgAl_2O_4$	100	2/20/0	75	47	29.5	E	
Ni_6In/SiO_2	180	1/10/0	100	60	11.8	E	145
$Ni_{10}In/SiO_2$	180	1/10/0	100	60	11.8	E	
$AgNi_{0.25}/SiO_2$	120	1/20/20	50	50	97.1	D	146
$NiGa/\alpha\text{-}Al_2O_3$	160	15/58.2/0.8	37	72	46.5	E	147
$NiZn/TiO_2$	150	2/20/0	67	81	842.8	—	148
Ni/Al_2O_3	200	0.5/10/20	100	−60	12.6	D	149
$NiCo/Al_2O_3$	200	0.5/10/20	55	87	6.9	D	
$NiFe/Al_2O_3$	200	0.5/10/20	99	79	12.5	D	
$NiMn/Al_2O_3$	200	0.5/10/20	98	65	12.3	D	
$NiMo/Al_2O_3$	200	0.5/10/20	64	95	8.1	D	
Ni_5Ga/SiO_2	180	1/5/0	100	78	11.8	E	150
$Ni_7Sn/ZSM\text{-}12$	250	1/2/0	100	84		E	151
$Ni/ZSM\text{-}12$	250	1/2/0	100	70		E	
Ni/SiO_2	250	1/2/0	97	55		E	152
Ni_7Mg/SiO_2	250	1/2/0	100	31		E	
Ni_7Sn/SiO_2	250	1/2/0	100	65		E	
$Ni/8\%Sn\text{–}CeO_2$	250	1/2/0	100	83			153
NiCu alloy							
$NiCu/Al_2O_3$	115	0.31/3.1/30.4	80	86	4.5	E	154
pre-NiCu/MMO	160	0.33/0.66/34.5	100	70	9.1	—	155
$Ni\&Cu\text{-}NP/Al_2O_3$	130	1/2/0	100	71		E	156
$CuNi_{0.125}/SiO_2$	160	1/20/0	95	62	364.3	E	157
$NiCu_{0.125}/MCM\text{-}41$	250	1/3/0	100	62		E	158
$CuNi_7/ZSM\text{-}12$	250	33.3/66.7/0	100	55		E	159
$NiCu/ZrO_2$	220	1/10/20	100	93	1.1	D	160
$Ni_{2.5}Co_{2.5}Cu_5@C/Al_2O_3$	120	0.5/10/0	98	80		E	161
$CuNiCs/TiO_2$	180	0.33/6.6/33	98	92		E*	162
Au–Ni alloy							
$AuNi/\gamma\text{-}Al_2O_3$	58	4.3/8.7/87.0	64	>99.99	17.6	—	163
$AuNi_{0.5}/SiO_2$	100	1/20/0	48	39	1.7	E	164
Others							
$PtCoO_x/Z$	140	1/20/20	85	88	185.0	C	165
$PtCuO_x/Z$	140	1/20/20	85	95	185.0	C	
$PtCu/Al_2O_3$	150	1.1/11.1/22.2	65	85	17.8	C	166
$Cu_{0.8}Zn_{0.2}(OH)$	90	0.48/4/94.75	80	96		D	167
CuZnCo/HEOs	—	0.71/2.86/70.72	100	90		—	168
$AuAg/SiO_2$	250	0.8/16/83.2	82	55		D	169

[a] The feed composition listed in the table corresponds to $C_2H_2/H_2/C_2H_4$. [b] Activity is calculated as the number of moles of acetylene converted per hour per total molar active metal ($mol_{C_2H_2}\ mol_{metal}^{-1}\ h^{-1}$). [c] Method refers to the calculation method specified in Table 2. E* indicates that Method E was applied under ethylene-rich feed conditions.

including Pd_1Zn_1, $Pd_{3.9}Zn_{6.1}$, and the (Pd,Zn) γ-brass phase, have been successfully synthesized for acetylene hydrogenation.[13,86,87,216] Pd/ZnO, which predominantly contained the Pd_1Zn_1 phase (Fig. 11a), achieved a high ethylene selectivity of 89% (D) under ethylene-rich feed conditions.[86] The high selectivity suggests that the Pd_1Zn_1 phase effectively suppresses ethylene over-hydrogenation to ethane. DFT calculations revealed that the Pd–Zn–Pd ensembles in the Pd_1Zn_1 phase exhibited a weak π-bonding interaction with ethylene (Fig. 11b), consistent with the experimental findings. However, it is noteworthy that the Pd/ZnO catalyst does not effectively suppress the formation of oligomers. Under ethylene-free feed conditions, Pd/ZnO showed an ethylene selectivity of ∼70% (E), while the selectivity toward oligomer (C_{4+}) products exceeded 20% (E).[86]

The site-isolation effect in acetylene hydrogenation was further examined using the intermetallic (Pd, Zn) γ-brass phase. Pd_8Zn_{44}, which featured completely isolated Pd sites, exhibited an extremely low formation rate of ethane (Fig. 11c and d). Isotope labeling experiments enabled a direct calculation of the intrinsic ethylene selectivity (Method E) under ethylene-rich feed conditions, revealing an ethylene selectivity of ∼80%. However, it should be noted that the acetylene hydrogenation rate over Pd_8Zn_{44} was significantly lower than that of Pd_9Zn_{43}, which contained Pd_3 trimer sites on the surface. This difference is attributed to the limited ability of Pd_8Zn_{44} to activate H_2 dissociation, highlighting a trade-off between site isolation and H_2 activation in PdZn IMCs.

3.2.3.3 PdX IMC. Given its structural similarity to Pd_2Ga, Pd_2In (*Pnma*) has been proposed as a potential IMC catalyst for acetylene hydrogenation. DFT calculations revealed that Pd_2In

Table 9 Non-Pd-based IMC catalysts for acetylene hydrogenation

Catalyst	Description	T, °C	Feed[a], %	X, %	S, %	Activity[b]	Method[c]	Ref
NiX IMC								
Ni_3Ga-MIHMs	Ni_3Ga	120	0.65/5/50	70	80	0.6	B	170
Ni/MHMs	Ni	120	0.65/5/50	23	70	0.2	B	
NiGa/MgAlO	Ni_5Ga_3	190	1/10/20	80	75	30.2	C	171
NiGa/MgAlO	Ni_5Ga_3	90	1/10/0	75	78	28.3	C	
NiGa/MgAlO	NiGa	190	1/10/20	70	10	26.4	C	
NiGa/MgAlO	NiGa	90	1/10/0	25	82	9.4	C	
Ni	Ni	90	1/10/0	65	78	24.5	C	
$Ni_3ZnC_{0.7}$/oCNT	$Ni_3ZnC_{0.7}$	200	0.5/4.5/20	98	95	61.6	D	172
Ni/oCNT	Ni	200	0.5/4.5/20	70	88	29.4	D	
$Ni_3ZnC_{0.7}$/C		160	1/15/0	95	85		E	173
NiFeCuGaGe/SiO_2	CsCl0-type	150	1.7/16.7/16.7	39	85	61.3	C	174
NiGa/SiO_2	Ni_1Ga_1	150	1.7/16.7/16.7	54	90	14.2	C	
Crystalline $CeNi_2$	$CeNi_2$	100	2/10/0	3	85		G	175
Amorphous $CeNi_2H_x$	$CeNi_2H_x$	100	2/10/0	90	26		G	
NiGa/MgAlO	Ni_3Ga	110	0.5/2.5/10	100	65.1		C	176
	$Ni_3GaC_{0.5}$	110	0.5/2.5/10	100	89.1		C	
	Ni	110	0.5/2.5/10	100	46.7		C	
NiSb/MgAlO	*P*63/*mmc* NiSb	180	0.5/2.5/10	50	93	0.4	C	177
Ni_3Zn/ZnO	Ni_3Zn	100	1/20/0	98	80	9.1	E	178
Ni_3Zn/ZnO	Ni_3Zn	125	1/20/20	20	70	1.8	D	
NiZn/ZnO	NiZn	100	1/20/0	16	12	1.5	E	
NiZn/ZnO	NiZn	125	1/20/20	54	75	5.0	D	
Ni_3Ga/TiO_2	NI_3Ga	150	1.8/18.2/9.1	30	90	59.0	C	179
$(Ni_{0.8}Cu_{0.2})_3Ga/TiO_2$		130	1.8/18.2/9.1	40	95	78.6	C	
$(Ni_{0.67}Cu_{0.33})_3Ga/TiO_2$		110	1.8/18.2/9.1	60	92	117.9	C	
$NiMn_{0.88}Fe_{0.12}Ge$		210	1/20/20	30	95	0.0	C	180
$Ni_3GaC_{0.5}$/oCNT	$Ni_3GaC_{0.5}$	160	0.5/5/20	89	75		C	181
PtX IMC								
PtGe/MCM-41	Pt_1Ge_1	200	14/29/0	72	64	—	E	182
$PtSn_{1.0}$@MSW	Pt_1Sn_1	200	0.5/5.0/49.8	20	83	58.5	B	183
Pt_3Fe/SiO_2	L1-Pt_3Fe	180	1/2/0	99	83	27.4	E	184
Pt_3Fe/SiO_2	A1-Pt_3Fe-alloy	180	1/2/0	50	77	13.8	E	
Others								
BiRh	Bulk-Rh_1Bi_1	200	0.5/5/50	95	88	0.6	—	185
$RhZn/SiO_2$	Rh_1Zn_1	150	1/15/0	50	92	275.9	E	186
$RhZn/SiO_2$	Rh_1Zn_1	217	1/15/0	100	91		E	
$Al_{13}Fe_4$		200	0.5/5/50	78	82		B	187
$Al_{13}Fe_4$		200	2/10/88	16.5	75		—	188
CoSb		240	0.5/2.5/40	92	92		C	189

[a] The feed composition listed in the table corresponds to $C_2H_2/H_2/C_2H_4$. [b] Activity is calculated as the number of moles of acetylene converted per hour per total molar active metal site ($mol_{C_2H_2}$ mol_{metal}^{-1} h^{-1}). [c] Method refers to the calculation method specified in Table 2. E* indicates that Method E was applied under ethylene-rich feed conditions.

and Pd_2Ga exhibited only minor differences in their electronic structures, as reflected in their density of states (DOS).[82] Catalytic performance evaluations revealed that Pd_2In demonstrated good stability and a slightly higher ethylene selectivity of 80% (B) compared to $GaPd_2$ (75%, B).[82] To further explore PdIn IMCs for acetylene hydrogenation, compositions with varying In/Pd ratios, such as Pd_3In, PdIn, and Pd_2In_3, have been developed. Generally, an increase in the In/Pd ratio enhanced ethylene selectivity but reduced acetylene hydrogenation activity. For example, as the In/Pd ratio increased from 1/3 to 1/1, the selectivity to ethylene significantly improved from 10% to 90% (C), whereas acetylene conversion decreased from 90% to 50%.[82]

Pd_1Bi_1 has been reported to exhibit highly dispersed Pd sites, which result in an extremely weak adsorption of ethylene.[90] This unique electronic structure effectively suppressed the formation of β-PdH_x and inhibited over-hydrogenation of ethylene to ethane. Consequently, the PdBi/Calcite catalyst (Pd_1Bi_1 phase) achieved an exceptionally high ethylene selectivity (>99%, D) under ethylene-rich feed conditions. Pd_3Bi_1 was employed for acetylene hydrogenation under ethylene-free feed conditions, where it exhibited an ethylene selectivity of ~80% (E) at full acetylene conversion.[91]

Several other IMCs, including Pd_2Sn, Pd_3P, PdP_2, and $CaPdH_2$, have been investigated for acetylene hydrogenation.[92,93,217] These IMC phases effectively modify the Pd ensemble structure and tune its electronic properties, leading to enhanced catalytic performance. In addition, ternary IMC catalysts have been developed to further improve the selective hydrogenation of acetylene to ethylene.[89,94,218] Notable examples include $Pd_2Ga_{1-x}Sn_x$ ($0 \leq x \leq 1$) and $Pd_{11}Bi_2Se_2$. The introduction of Sn into Pd_2Ga was found to enhance catalytic activity. Specifically, bulk-$Ga_{0.7}Sn_{0.3}Pd_2$ exhibited an acetylene hydrogenation rate of 9.5 $mol_{C_2H_2}$ mol_{Pd}^{-1} h^{-1}, nearly doubling

Table 10 Non Pd-based SA catalysts for acetylene hydrogenation

Catalyst	Description	T, °C	Feed[a], %	X, %	S, %	Activity[b]	Method[c]	Ref.
Ni SA								
Ni_1/N–C		150	0.5/10/50	70	95		—	190
cal-Ni_1@CHA		100	1/16/0	60	95	5.4	G	191
Ni_1MoS/Al_2O_3		100	0.15/3.03/15	50	~100	1.1	E*	192
		120	0.15/3.03/15	100	90	2.2	E*	
Ni_1Cu_2/g-C_3N_4	Ni_1–Cu_2	160	0.5/5/25	80	90	4.1	C	193
Ni_1/g-C_3N_4		160	0.5/5/25	13	85	0.7	C	
Ni_n/ND@G	Fully exposed	190	1/10/20	100	85	91.0	C	194
Cu SA								
Cu_1/ND@G		180	1/10/20	40	98	13.6	C	195
Cu_1/ND@G		200	1/10/20	90	98	30.6	C	
Cu_n/ND@G	Cu cluster	200	1/10/20	20	93	6.8	C	
0.5Cu/Al_2O_3	Single atom	178	1/10/20	82	93	18.6	C	196
0.8Cu/Al_2O_3	3.4 nm Cu NPs	172	1/10/20	60	92	13.6	C	
Cu_1/ND@G		200	1/10/20	100	92	38.7	C	197
CuZn/NC2	Cu_1–Zn_1	160	0.33/0.66/33	73	98		E*	198
Pt SA								
Pt_1–In_2O_3		135	0.5/2.5/5	95	90		C	199

[a] The feed composition listed in the table corresponds to $C_2H_2/H_2/C_2H_4$. [b] Activity is calculated as the number of moles of acetylene converted per hour per total molar active metal ($mol_{C_2H_2}\ mol_{metal}^{-1}\ h^{-1}$). [c] Method refers to the calculation method specified in Table 2. E* indicates that Method E was applied under ethylene-rich feed conditions.

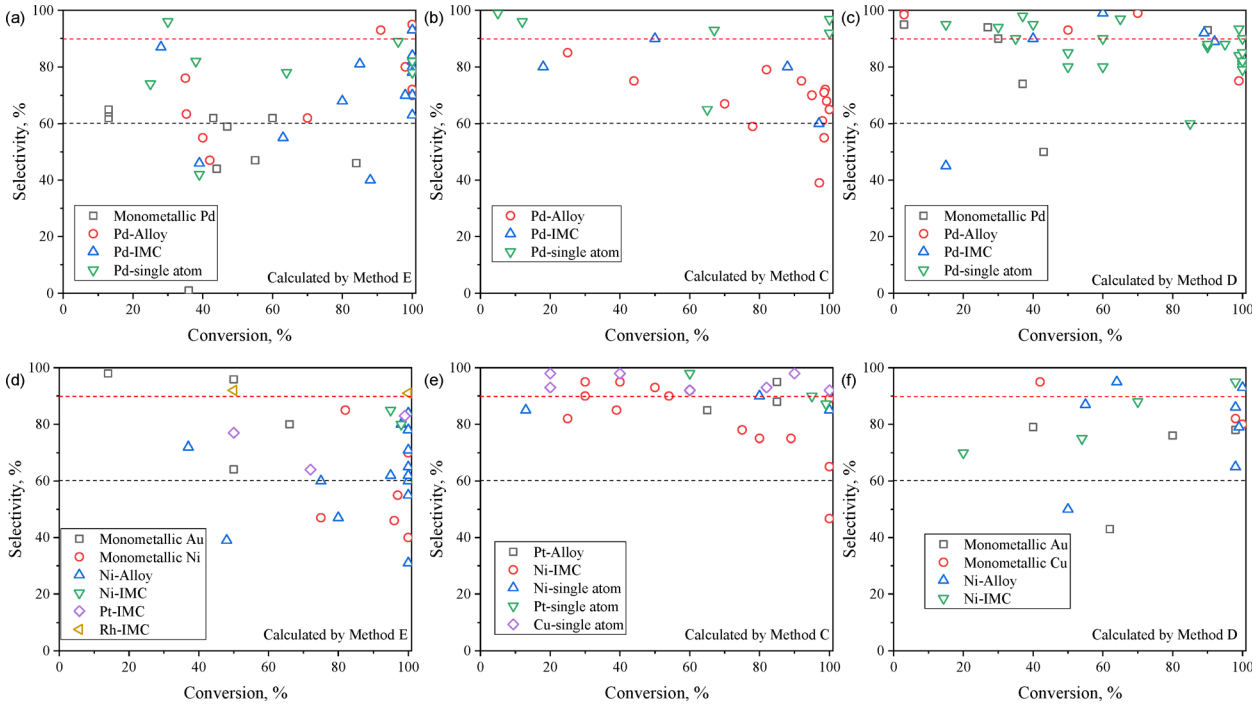

Fig. 5 Ethylene selectivity *versus* acetylene conversion over (a)–(c) Pd-based and (d)–(f) non-Pd-based catalysts. Methods C, D, and E in the figures correspond to the ethylene calculation methods specified in Table 2. The data are summarized from Tables 3–10.

that of bulk-Ga_1Pd_2 (5.5 $mol_{C_2H_2}\ mol_{Pd}^{-1}\ h^{-1}$), while maintaining the same ethylene selectivity.[94]

3.2.4. Pd SA active sites

3.2.4.1 Pd SA sites supported on carbon materials. Carbon-based materials are among the most widely used supports for anchoring SA sites (Fig. 12). Through defect sites or nitrogen doping, atomically dispersed Pd species can be stabilized *via* Pd–N or Pd–C bonds.[96,100,103,105] The unique structure of single-atom Pd sites effectively inhibits the formation of non-selective subsurface hydrogen species while facilitating the desorption of surface C_2H_4 species, thereby preventing the over-hydrogenation of ethylene to ethane. Under ethylene-rich feed

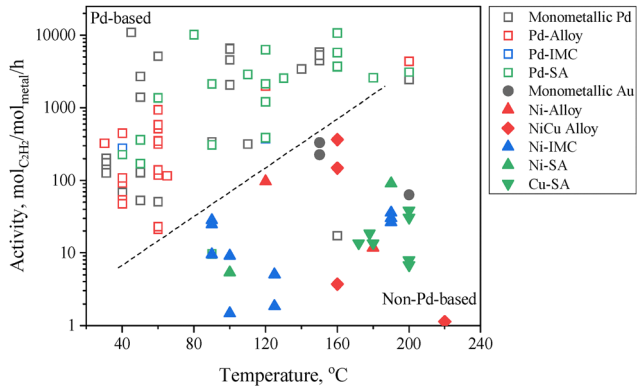

Fig. 6 Acetylene hydrogenation activity over Pd-based and non-Pd-based active sites. Data are summarized from Tables 3–10.

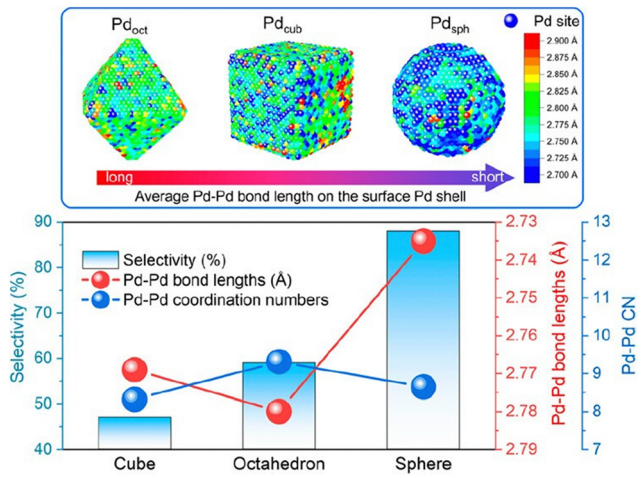

Fig. 7 Comparison of partial Pd–Pd interatomic distances and Pd–Pd coordination numbers at the surface of Pd NPs with their selectivity for acetylene hydrogenation. Reprinted with permission from ref. 202. Copyright 2023 American Chemical Society.

conditions, Pd_1/ND@G achieved a high ethylene selectivity of 90% (D) at full acetylene conversion.[97] Li *et al.*[99] developed a Pd SA catalyst *via* the atomization of Pd NPs, achieving an ethylene selectivity of 95% (B) at ~75% acetylene conversion.

The formation of Pd–N or Pd–C bonds weakened ethylene adsorption and reduced H_2 activation, which leaded to sluggish H_2 dissociation kinetics and alters the reaction pathway due to the absence of metal ensembles in Pd SA.[102] In the acetylene hydrogenation over Pd SA sites, the support atoms forming bonds with Pd were considered to participate in H_2 activation.[98,99,101,219] However, the inherently low H_2 dissociation ability of isolated Pd atoms limits hydrogenation activity, necessitating significantly higher reaction temperatures to achieve nearly 100% conversion compared to Pd NP catalysts (180 °C *vs.* 20 °C).[97] To overcome this limitation, dual-atom[102,220] and triatomic[104] catalysts have been proposed to introduce cooperative sites that facilitate H_2 dissociation and acetylene hydrogenation. Ma *et al.*[102] designed a Pd_1–Cu_1 dual-atom catalyst (Pd_1Cu_1/ND@G), which exhibited a fivefold increase in catalytic activity compared to Pd_1/ND@G (Fig. 12d–f). The proposed mechanism suggests that Cu sites serve as active centers for H_2 activation, while Pd sites catalyze acetylene hydrogenation, thereby significantly improving catalytic performance.

3.2.4.2 Pd SA sites supported on metal oxide and other materials. Metal oxides, such as ZnO, MgO, Fe_2O_3, CeO_2, and Al_2O_3, have been utilized as supports for anchoring Pd single atoms in acetylene hydrogenation.[108,110,111,113,221] These catalysts have demonstrated good performance in suppressing the over-hydrogenation of ethylene to ethane, achieving ethylene selectivity exceeding 80% (D) under ethylene-rich feed conditions (Table 6). Similar to carbon-supported Pd SA, Pd SA sites on metal oxides exhibit limited efficiency in cleaving the H–H bond, thereby restricting hydrogenation activity. The reduced hydrogenation activity may accelerate the polymerization pathways. A 20% (E) selectivity to C_4 products was observed over the Pd_1/MgO catalyst. Atomic Pd anchored on α-Fe_2O_3(012) exhibited a unique Pd–Fe pair structure, which enhanced d-electron dominance near the Fermi level, thereby accelerating H_2 dissociation.[111]

Beyond metal oxides, Pd single atoms have also been stabilized on other supports, including MOFs, hydroxyapatite, and $Ni(OH)_2$.[125,126,128] These catalysts typically enhance the ethylene selectivity to some extent and leverage the intrinsic properties of the supports to further enhance acetylene hydrogenation. For instance, the abundant hydroxyl groups in $Ni(OH)_2$ promoted acetylene hydrogenation activity.[128]

3.2.4.3 Pd single atom alloy. Pd_1Cu single-atom alloy (SAA) is among the earliest reported SAA catalysts for acetylene hydrogenation. While monometallic Cu catalysts exhibit intrinsic activity for acetylene hydrogenation, their weak H_2 dissociation ability limits overall hydrogenation efficiency. To overcome this limitation, researchers introduced isolated Pd single atoms onto Cu surfaces as active sites for efficient hydrogen dissociation. Through a combination of DFT calculations and ultrahigh vacuum (UHV) surface experiments, Sykes *et al.*[222] demonstrated that Pd_1/Cu(111) exhibits efficient H_2 dissociation and highly selective hydrogenation of acetylene (Fig. 13a). Zheng *et al.*[223] further revealed that Pd single atoms anchored on Cu(100) displayed a higher hydrogen spillover rate and enhanced hydrogenation activity compared to those on Cu(111). Supported Pd_1Cu catalysts were synthesized with an ultralow Pd content, achieving a Cu/Pd atomic ratio of up to 160.[116,224] The isolation of Pd by Cu weakened C_2H_4 adsorption (Fig. 13b), leading to a high ethylene selectivity of 85% (D) at nearly 100% acetylene conversion. Beyond Pd_1Cu, analogous Pd SAA incorporating Au,[114] Ag,[115,120,225,226] Ni,[117,119] and Fe_5C_2[121] have also been evaluated for acetylene hydrogenation. Compared to Pd_1Au (<70%, D), Pd_1Ag exhibited higher ethylene selectivity (~80%, D), particularly at acetylene conversion levels exceeding 70%.[115]

3.2.5 Active sites coated with carbon or metal oxide layer. Studies have reported that coating a thin carbon layer over metal active sites can significantly enhance ethylene

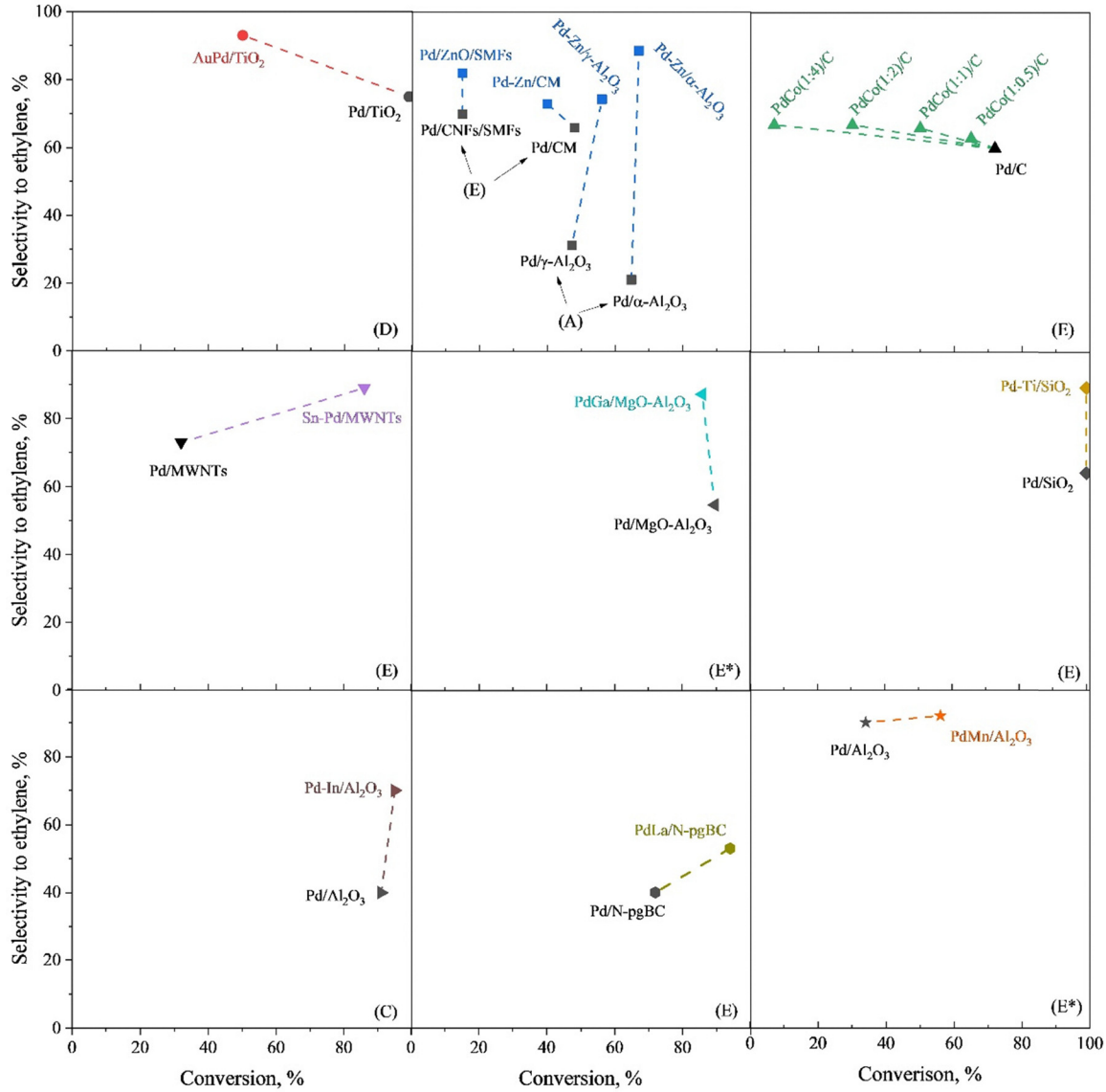

Fig. 8 Catalytic performance of monometallic and bimetallic Pd-based alloy catalysts for acetylene hydrogenation. Letters in parentheses indicate the selectivity calculation method as specified in Table 2. E* indicates that Method E was applied under ethylene-rich feed conditions.

selectivity.[227–230] This effect has been observed for various metal catalysts. For example, PdZn alloy NPs encapsulated within a few layers of graphene (PdZn@C/ZnO) exhibited an increase in ethylene selectivity from 75% to 95% (D) compared to PdZn/ZnO.[231] The enhanced selectivity resulting from the carbon layer is primarily attributed to its electronic modulation and confinement effects, which weaken ethylene adsorption. DFT calculations by Fu *et al.*[232] further demonstrated that within the confined sub-nanospace between two-dimensional graphene monolayers and the Pd(111) surface, ethane formation was thermodynamically unfavorable, effectively suppressing ethylene over-hydrogenation reactions.

Metal oxides such as Bi_2O_3 and Ga_2O_3 have been deposited onto metal cores to enhance acetylene hydrogenation performance.[73,233] These metal oxides can selectively decorate specific regions of the metal core and improve both selectivity and catalytic activity. Through precise structural design, researchers have successfully enhanced catalytic performance. For instance, atomic layer deposition (ALD) was employed to deposit controlled amounts of Ga_2O_3 adlayers on Pd NPs.[234] This selective modification preferentially covered the edges and open facets of Pd, effectively suppressing oligomer formation (Fig. 14a). Lu *et al.*[233] developed a Ga_2O_3 coating of Ag@Pd core–shell NP catalysts, which significantly enhanced the selectivity and activity (Fig. 14b). Additionally, Pd/Bi_2O_3 catalysts featuring nanometer-scale metal/oxide interfaces were designed to facilitate intra-cluster electron transfer, weakening ethylene adsorption and improving selectivity (Fig. 14c).

3.3 Non-Pd-based active sites

Non-Pd-based metals, such as Au, Ni, and Cu, had already been reported to exhibit selective hydrogenation activity for acetylene.

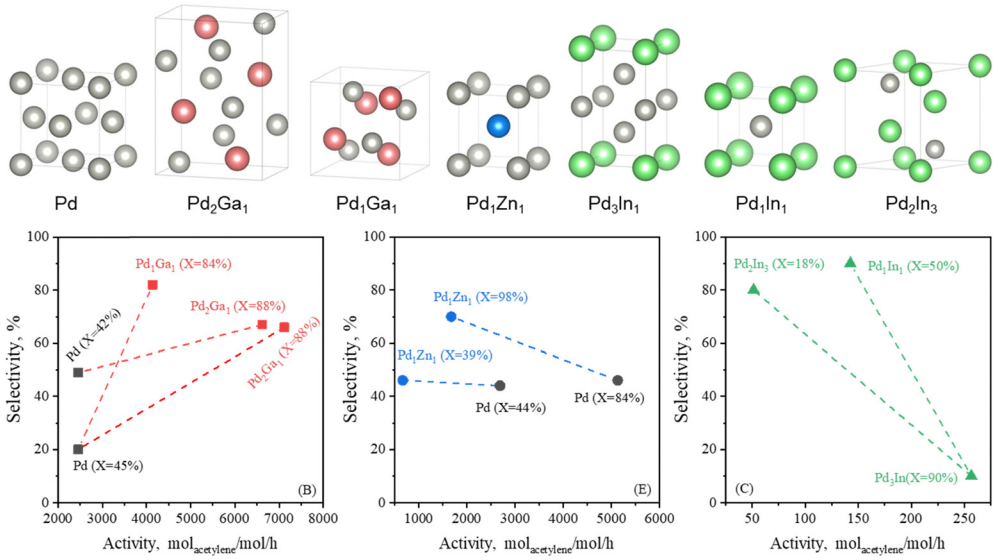

Fig. 9 Catalytic performance of Pd-based IMC catalysts for acetylene hydrogenation. Letters in parentheses indicate the selectivity calculation method as specified in Table 2.

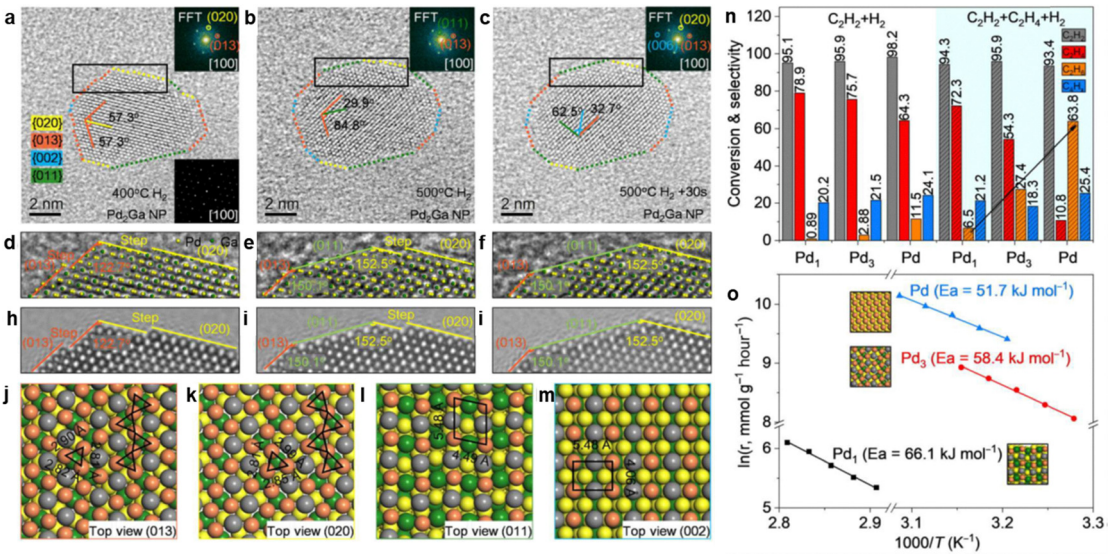

Fig. 10 (a)–(m) Surface atom arrangement and variation during Pd_2Ga refacetting, and (n) and (o) Hydrogenation properties of different surface Pd geometries. Reprinted with permission from ref. 81 Copyright 2022 The American Association for the Advancement of Science.

Although their hydrogenation activity is significantly lower than that of Pd-based catalysts, ongoing research continues to develop catalysts based on less expensive and more abundant metals. The development of non-Pd-based catalysts follows a similar trajectory to Pd-based catalysts, where the design of active sites evolve from monometallic sites to disordered alloy structures, and further to well-defined IMC structures and SA sites. This section discusses the research progress of non-Pd-based active sites across these categories. Additionally, a non-metallic type of active site, known as frustrated Lewis pairs (FLPs), has also been applied in acetylene selective hydrogenation and is further discussed in Section 3.3.5.

3.3.1 Monometallic active sites. Pd-based catalysts do not fully resolve the challenges of selectivity at elevated temperatures and oligomer formation. To address these limitations, researchers have explored alternative non-Pd-based catalysts for acetylene hydrogenation. Among them, Au is one of the earliest metals evaluated due to its promising performance in other hydrogenation processes.[130,236] Au exhibits the capability of suppressing the over-hydrogenation of ethylene to ethane under specific conditions. When considering only C_2 product, Au achieved nearly 100% ethylene selectivity (G) at an acetylene conversion of 75%.[130] Despite this, Au catalysts suffered from rapid deactivation, with conversion dropping from 100% to

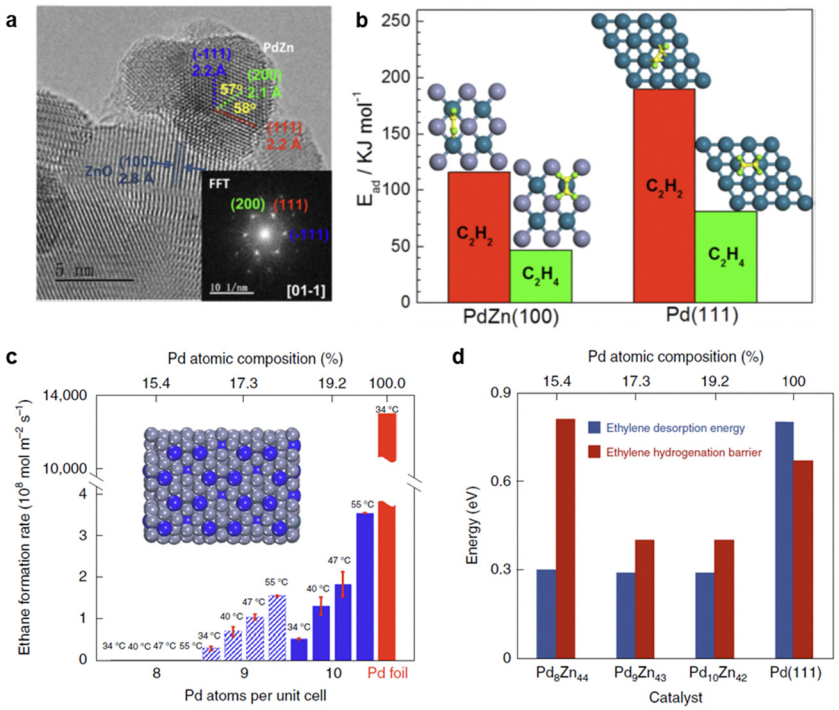

Fig. 11 (a) HRTEM image of the Pd/ZnO catalyst with the formation of Pd_1Zn_1 phase; (b) DFT calculations of acetylene and ethylene adsorption on PdZn(100) or Pd(111) surfaces. Reprinted with permission from ref. 86. Copyright 2016 American Chemical Society. (c) Ethylene hydrogenation activity at different temperatures over Pd_8Zn_{44}, Pd_9Zn_{43}, $Pd_{10}Zn_{42}$ and Pd foil; (d) DFT-calculated ethylene hydrogenation barrier and desorption energy. Reprinted with permission from ref. 13. Copyright 2022 Springer Nature.

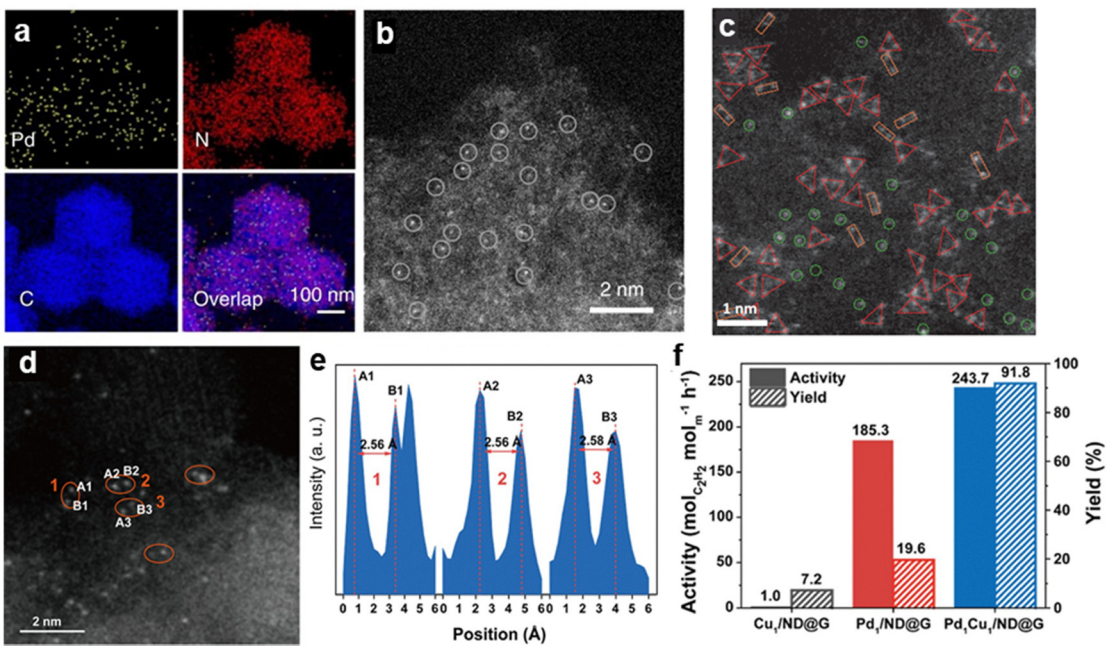

Fig. 12 (a) EDS mapping and (b) HAADF-STEM image of Pd_1/CN-900. Reprinted with permission from ref. 99. Copyright 2018 Springer Nature. (c) HAADF-STEM image of Pd_3 trimer active site. Reprinted with permission from ref. 104. Copyright 2022 Springer Nature. (d) HAADF-STEM image and (e) intensity profile of Pd_1Cu_1/ND@G; (f) activity and C_2H_4 yields of the different catalysts. Reprinted with permission from ref. 102. Copyright 2022 American Chemical Society.

below 60% within a 5-hour test.[130] This instability is attributed to the oligomer deposition that negatively impacts the inherently low hydrogen coverage over Au active sites.[131] Increasing the H_2/C_2H_2 ratio can mitigate oligomer formation

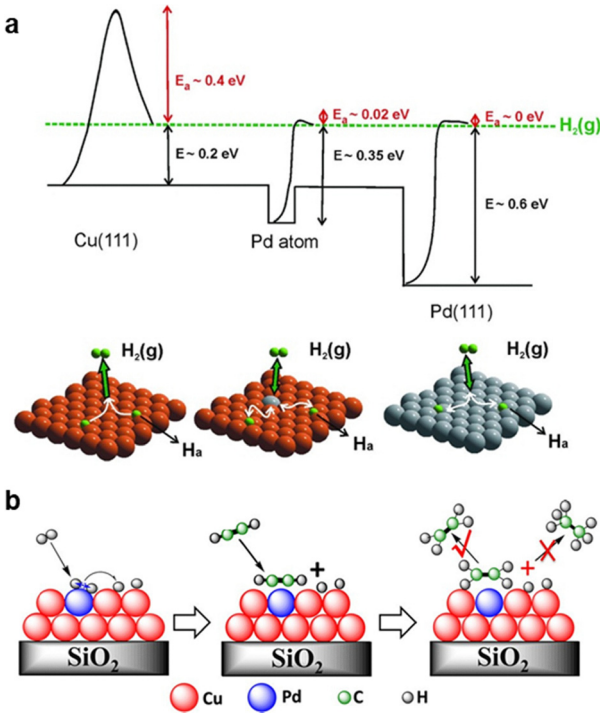

Fig. 13 (a) Potential energy diagram of H_2 dissociation over the Pd_1/Cu(111) surface, where the orange and gray atoms are Cu and Pd, respectively. Reprinted with permission from ref. 222. Copyright 2012 The American Association for the Advancement of Science. (b) Proposed reaction pathway for semihydrogenation of acetylene over silica-supported Cu-alloyed Pd SA. Reprinted with permission from ref. 116. Copyright 2017 American Chemical Society.

to some extent, but excessive hydrogen concentrations also promote ethylene over-hydrogenation. For instance, as the H_2/C_2H_2 ratio increased from 5 to 10, ethane selectivity rose from 21% to 57% (D).[133] Enhancing the interaction between Au and its support has been shown to improve catalytic performance.[134–136,237] Notable strategies include the use of flower-like ZnO to generate a higher concentration of Au^{3+} species[134] and C/N co-decorated alumina to modulate the electronic properties of Au.[135]

Both Pd and Au are precious metals, and from the perspective of reducing catalyst costs, non-precious metals such as Ni[138,238,239] and Cu[143,240] have been explored for acetylene hydrogenation. Among them, Ni is considered one of the most promising active metals due to its high efficiency in H_2 dissociation. However, acetylene can easily decompose on the sites of three-nickel-atom arrangements to form ethylidine species.[241] A major challenge associated with monometallic Ni catalysts is the formation of substantial amounts of C_4 and GO during hydrogenation.[138–140] The selectivity toward oligomers exceeded 40%, leading to rapid catalyst deactivation, with acetylene conversion dropping from 100% to below 50% within a 5-hour test.[138] In comparison, monometallic Cu catalysts suffer from intrinsically low activity due to their poor ability to dissociate H_2. Compared to Au, the activity of Cu can be lower by up to two orders of magnitude.[141,143] Additionally, other transition metals such as Co[242] and Fe[243] have also been investigated for acetylene hydrogenation, but these catalysts typically show low activity and selectivity for acetylene selective hydrogenation.

3.3.2 Multi-metallic sites with disordered alloy structure

3.3.2.1 NiCu alloy. Monometallic Ni and Cu each exhibit distinct advantages in terms of catalytic activity and selectivity, respectively. To take advantage of both metals, researchers have proposed Ni–Cu alloy catalysts as a strategy to enhance acetylene hydrogenation performance.[154,155,160] Compared to monometallic Ni, NiCu alloy catalysts showed improved ethylene selectivity. Long-term stability tests revealed that pre-NiCu/MMO (derived from NiCuMgAl layered double hydroxide) maintained an ethylene selectivity above 50%, whereas imp-Ni/MMO (prepared by impregnation method) experienced a decline in selectivity to ~10%.[155] To further optimize catalytic performance, the Cu/Ni atomic ratio was varied[156–159] and the optimal Cu/Ni ratio was identified to be in the range of 0.05–1. For instance, while the ethylene selectivity over $NiCu_1$ and $NiCu_{0.05}$ was ~55% (E), it increased to 62% (E) over $NiCu_{0.125}$.[158] However, suppressing C–C coupling reactions on NiCu catalysts remains a significant challenge.

3.3.2.2 NiX alloy. In addition to NiCu alloys, other Ni-based bimetallic catalysts have been studied for acetylene hydrogenation. Using DFT calculations, Nørskov *et al.*[244] predicted that Ni–Zn alloys should exhibit selectivity comparable to Pd–Ag systems. Experimental evaluations confirmed that a 25%Ni–75%Zn catalyst displayed remarkably low selectivity to ethane, even lower than that of a 25%Pd–75%Ag catalyst, under ethylene-rich feed conditions. Subsequent research efforts have focused on developing highly selective Ni–Zn alloy catalysts and evaluating their intrinsic ethylene selectivity under ethylene-free feed conditions.[144,148] Compared to the ethylene selectivity of 47% (E) over $Ni/MgAl_2O_4$, the selectivity was enhanced to 60% (E) over $NiZn_2/MgAl_2O_4$.[144] Further increasing the Zn/Ni atomic ratio increased ethylene selectivity, reaching 80% (E) over $NiZn_5$.[148] However, rapid deactivation was observed during long-term stability tests. Beyond Ni–Zn, several other secondary metals have been explored in Ni-based bimetallic catalysts for acetylene hydrogenation, including In, Ag, Co, Fe, Mo, Mn, Ga, and Sn.[145–147,150–152,245] Notably, NiGa catalysts exhibited enhanced ethylene selectivity of 70–80% (E) at nearly 100% acetylene conversion.[147,150] Among the Ni-based bimetallic catalysts with Fe, Co, Mn, and Mo as the secondary metals, NiMo demonstrated the most effective suppression of ethylene over-hydrogenation to ethane, achieving an ethylene selectivity of 95% (D).[149]

3.3.2.3 Others multi-metallic alloy. Pt-based bimetallic catalysts have been explored for acetylene hydrogenation (Table 9). Chen *et al.*[246] investigated acetylene hydrogenation over a Ni/Pt(111) model surface in a batch reactor, demonstrating that PtNi bimetallic catalysts exhibited both higher hydrogenation activity and improved selectivity than monometallic Ni and Pt catalysts. Further research has been conducted on supported

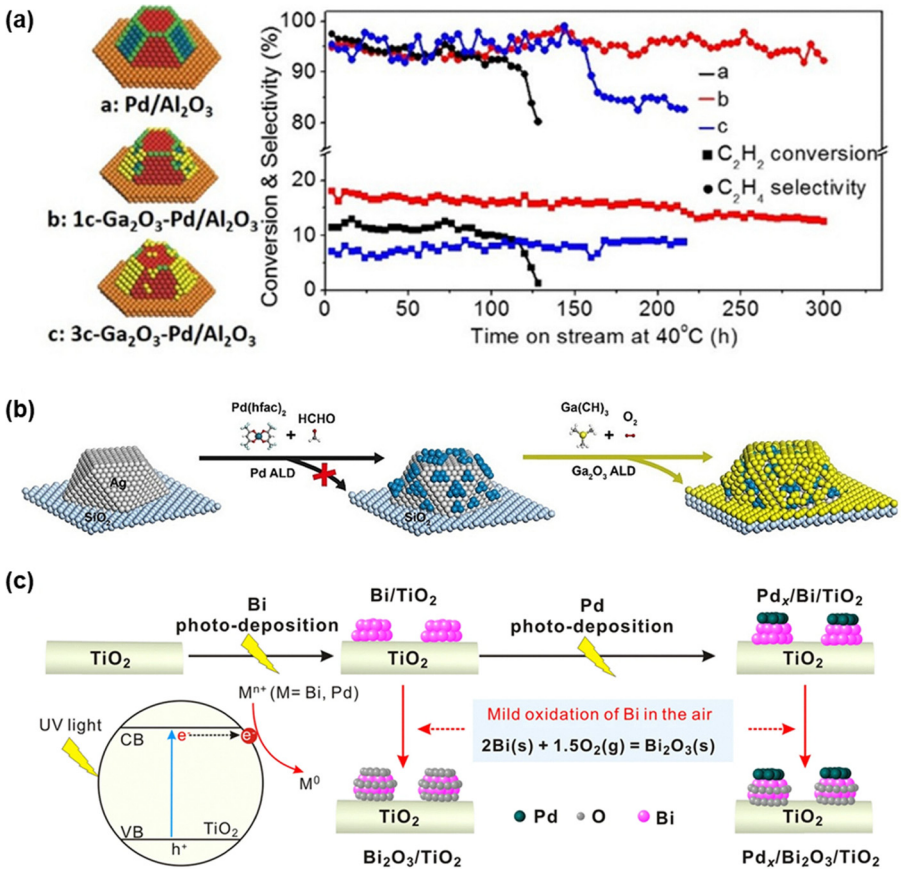

Fig. 14 (a) Acetylene hydrogenation over Ga_2O_3-coated Pd particles. Reprinted with permission from ref. 234. Copyright 2016 American Chemical Society. (b) Ga_2O_3-coated Pd@Ag/SiO_2 catalysts prepared by the ALD method. Reprinted with permission from ref. 233. Copyright 2021 Wiley-VCH GmbH. (c) Grafting nanometer metal/oxide interface of $Pd_x/Bi_2O_3/TiO_2$ catalyst. Reprinted with permission from ref. 235. Copyright 2021 Springer Nature.

Pt-based bimetallic catalysts, including PtAg, PtNi, PtCo, PtFe, and PtCu, for acetylene hydrogenation.[165,166,247–249] Notably, PtCo and PtCu catalysts achieved ethylene selectivity >85% (C).[165,166] In contrast, Au-based bimetallic catalysts, such as AuAg and AuNi, showed limited improvement in ethylene selectivity.[163,164,169] Under ethylene-free feed conditions, the ethylene selectivity over AuNi remained below 80% (E).[164] Other metal alloy catalysts, including CuZn[167] and ternary NiCoCu[161] alloys, demonstrated the ability to suppress ethylene over-hydrogenation to ethane. However, they still face challenges in effectively suppressing the oligomerization reaction.

3.3.3 Active sites with well-defined IMC structure

3.3.3.1 NiX IMC. Ni-based IMC catalysts are the most extensively studied non-Pd-based IMC catalysts for acetylene hydrogenation. Fig. 15 summarizes the catalytic performance in terms of activity and selectivity compared with benchmark catalysts.

Initially, intermetallic NiZn was identified as a cost-effective alternative to PdAg catalysts through DFT descriptor-based analysis across late 3d transition metal alloys.[244] However, early studies primarily synthesized NiZn as a disordered alloy phase rather than a well-defined IMC phase, limiting the ability to establish clear structure–performance relationship. Rioux *et al.*[250] successfully synthesized a series of bulk Ni–Zn IMC phases, including Ni_4Zn, Ni_1Zn_1, and Ni_5Zn_{21}, and evaluated their catalytic performance using isotopic labeling in a batch reactor. As the Zn/Ni ratio increased, the intrinsic ethylene selectivity (E) increased from <10% (Ni) to ~20% (Ni_4Zn & Ni_1Zn_1) and further to ~50% (Ni_5Zn_{21}). Despite these advancements, a major challenge remains in effectively suppressing the formation of oligomer products.[178]

NiGa IMCs have also been investigated for acetylene hydrogenation, exhibiting a similar trend between the Ga/Ni ratio and ethylene selectivity as observed in the NiZn IMC system.[170,171] As the Ga/Ni ratio increased from 0 to 1, ethylene selectivity increased from 78% to 82% (C).[171] Atomically isolating Ni sites has been proposed as a strategy to mitigate oligomer formation. Furthermore, coupling this approach with the electronic modification effect of a secondary metal can further enhance catalytic performance. For instance, Sb, which has a higher electronegativity than Ni, was incorporated into the Ni lattice, forming Ni_1Sb_1. This IMC catalyst exhibited high ethylene selectivity (93%, C) at nearly 100% acetylene conversion.[177]

Incorporating interstitial carbon atoms into the lattice of NiX IMCs has been demonstrated as an effective strategy to

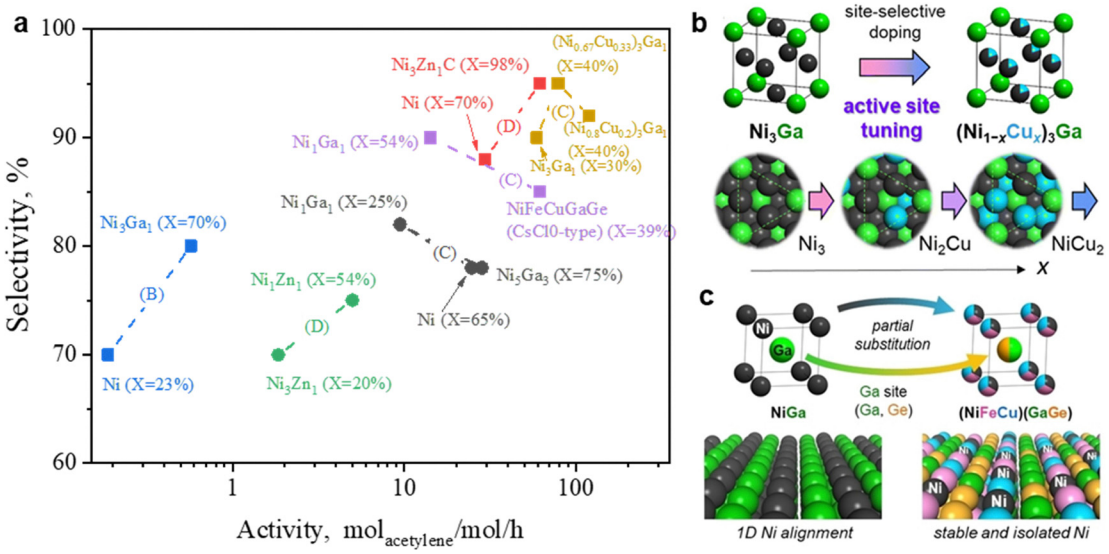

Fig. 15 (a) Catalytic performance of Ni based IMC catalysts for acetylene hydrogenation. (b) Site-selective doping of Cu to the Ni sites of Ni_3Ga IMC. Reprinted with permission from ref. 179. Copyright 2024 Royal Society of Chemistry. (c) Multi-metallization of intermetallic NiGa to (NiFeCu)(GaGe) HEI. Reprinted with permission from ref. 174. Copyright 2022 Wiley-VCH GmbH. Letters in parentheses indicate the selectivity calculation method as specified in Table 2.

simultaneously enhance both catalytic activity and selectivity. Representative intermetallic carbides include $Ni_3ZnC_{0.7}$ and $Ni_3GaC_{0.5}$.[172,173,176] Compared with Ni/CNT, the $Ni_3ZnC_{0.7}$/CNT catalyst exhibited a twofold increase in activity, while the ethylene selectivity improved from 88% to 95% (D).[172] Under ethylene-free feed conditions, the ethylene selectivity was enhanced from ~70% (E) over Ni_3Zn/CNT to 85% (E) over $Ni_3ZnC_{0.7}$/C.[173]

Recently, multi-metallic IMC and high-entropy intermetallic (HEI) catalysts have been proposed for acetylene hydrogenation (Fig. 15b and c). Multi-metallic IMCs offer additional opportunities for tuning the electronic properties of the Ni active sites while preserving the geometric structure essential for reactant adsorption and activation. For instance, partial substitution of Ni in the Ni_3Ga IMC phase with Cu ($(Ni_{0.67}Cu_{0.33})_3Ga/TiO_2$) nearly doubled the hydrogenation activity.[179] Moreover, the HEI NiFeCuGaGe/SiO_2 catalyst exhibited more than a fourfold increase in activity compared to Ni_1Ga_1/SiO_2.[174]

3.3.3.2 Other IMCs. PtX IMC catalysts, including Pt_1Ge_1, Pt_1Sn_1, and Pt_3Fe ($L1_2$), have been evaluated for acetylene hydrogenation.[182–184] The transformation of disordered Pt_3Fe (A1) particles into an ordered Pt_3Fe ($L1_2$) phase resulted in the formation of isolated three-fold hollow Pt sites, with electronic properties finely tuned by neighboring Fe single atoms (Fig. 16). This structural modification led to a twofold increase in acetylene hydrogenation activity, while ethylene selectivity increased from 77% to 83% (E).[184]

Rh-based IMCs, such as Rh_1Bi_1 and Rh_1Zn_1, have demonstrated enhanced performance for acetylene hydrogenation as well.[185,186] Lan *et al.*[186] proposed a Zn atom emitting–trapping–ordering (Zn-ETO) strategy, which enabled the synthesis of highly pure-phase IMC catalysts. Compared with monometallic

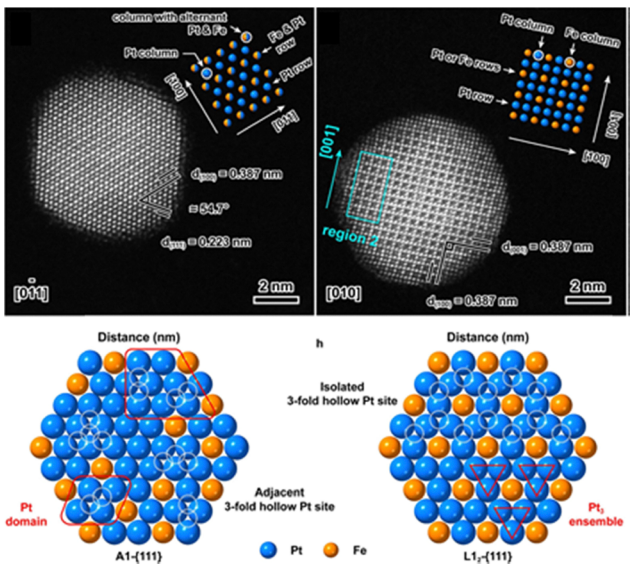

Fig. 16 Geometric arrangements of Pt and Fe atoms in the Pt_3Fe A1 and $L1_2$ NPs. Reprinted with permission from ref. 184. Copyright 2023 Elsevier.

Rh/SiO_2, the Rh_1Zn_1/SiO_2 catalyst synthesized *via* the Zn-ETO method significantly enhanced ethylene selectivity from 50% to 92% (E).

Another approach in IMC catalyst development involves replacing noble metals with cost-effective alternatives. MoP and $Al_{13}Fe_4$ have been explored for acetylene hydrogenation, exhibiting moderate hydrogenation activity and selectivity.[187,188,251] Specifically, $Al_{13}Fe_4$ achieved an ethylene selectivity of 82% (B) at a conversion of 78%.[187] However, challenges remain in terms of limited activity and rapid deactivation.

3.3.4 Non-Pd-based SA sites. Non-Pd-based SACs for acetylene hydrogenation primarily involve single atom of Pt, Rh, Ni, and Cu anchored on carbon materials or metal oxide

supports.[190–192,252,253] Similar to Pd-based SACs, these non-Pd-based catalysts also face a trade-off between activity and selectivity, governed by the linear free energy and Brønsted–Evans–Polanyi (BEP) relationships.[254]

Karim *et al.*[255] investigated the electronic and catalytic properties of TiO_2 supported Pt SA and subnanometer clusters (Fig. 17a). Their results demonstrated that as the size of Pt species decreased from 2.1 nm to single atoms, the TOF significantly dropped from 2.5×10^{-2} s^{-1} to 6.0×10^{-5} s^{-1} (at 70 °C), while ethylene selectivity within the C_2 products increased from 50% to 100% (G). A comparable trend was observed for Cu-based SA catalyst (Fig. 17b). As the size of Cu in Cu/Al_2O_3 decreased from 9.3 nm to single atoms, the TOF dropped from 147 h^{-1} to 4 h^{-1}, while ethylene selectivity improved from 84% to 91% (C).[196] In addition to enhancing selectivity, SACs also demonstrated a certain degree of suppression of undesired coupling side reactions, leading to significantly improved catalyst stability.[194,195,197] Compared with Cu NP catalysts, Cu SACs exhibited a much lower coking rate after ~5 h on stream, achieving a steady state following an initial deactivation.[196]

To further enhance catalytic performance in acetylene hydrogenation, multi-heteronuclear SA catalysts have been proposed, such as $Ni_1Cu_2/g\text{-}C_3N_4$[193] and dual-atom CuZn/NC_2.[198] Compared with $Ni_1/g\text{-}C_3N_4$, $Ni_1Cu_2/g\text{-}C_3N_4$ exhibited higher catalytic activity, ethylene selectivity, and catalyst stability. Characterization and computational studies revealed that the Ni active site, confined within two stable hydroxylated Cu grippers (Fig. 17c and d), underwent dynamic structural rearrangements. These rearrangements involved the breaking of interfacial Ni-support bonds upon reactant adsorption and their reformation upon product desorption, thereby optimizing the overall catalytic efficiency.[193]

3.3.5 Frustrated Lewis acid–base pair site. FLPs represent a class of non-metallic hydrogenation catalysts. FLPs have been shown to effectively activate small molecules such as H_2 and alkynes, exhibiting low activation barriers. Many FLP-based catalysts have been developed for acetylene hydrogenation (Table 11). Li *et al.*[256] recently reviewed the role of non-metallic catalysts for acetylene hydrogenation, emphasizing the catalytic mechanisms over FLPs, including the adsorption and activation of acetylene and H_2, as well as the formation of ethylene. In the current review, we focus primarily on the catalytic performance of these types of catalysts.

FLP catalysts for acetylene hydrogenation include both metal oxide and carbon materials. Carbon materials such as graphene, graphene oxides, and multi-walled carbon nanotubes generally exhibited higher hydrogenation activity, with rates exceeding 1.0 $g_{C_2H_2}\, g_{cat}^{-1}\, h^{-1}$.[258,265–267] However, these materials typically showed low selectivity for ethylene, due to over-hydrogenation of ethylene to ethane and the formation of a significant amount of oligomers.

Metal oxides, including CeO_2,[257,260,262,268] In_3O_5,[259] CrO_x,[261] and FeO_x,[263,269] have also been investigated for acetylene hydrogenation, where the intrinsic selectivity to ethylene can be enhanced to >70% (E). It has been demonstrated that ceria catalysts with stoichiometric surface OH groups (Ceria-O) were crucial for enhancing ethylene selectivity. Compared to ceria with surface oxygen vacancies (Ceria-V_O) or hydride species (Ceria-H), the Ceria-O catalyst increased ethylene selectivity from <20% to 75%.[264] However, it should be noted that metal oxides face significant challenges in terms of hydrogenation

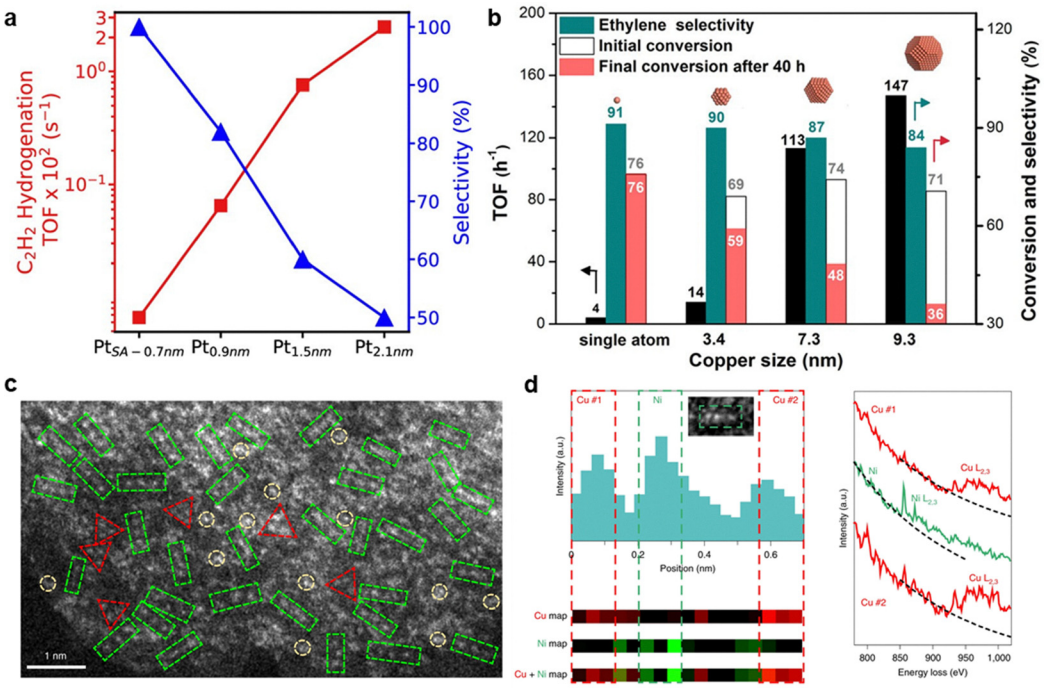

Fig. 17 Size effect of (a) Pt active site and (b) Cu active site on the activity and selectivity for acetylene hydrogenation. Reprinted with permission from refs. 255 and 196. Copyright 2019 American Chemical Society and 2020 American Chemical Society. (c) and (d) Structural characterization of $Ni_1Cu_2/g\text{-}C_3N_4$ catalyst. Reprinted with permission from ref. 193. Copyright 2021 Springer Nature.

Table 11 FLPs catalysts for acetylene hydrogenation

Catalyst	T, °C	Feed[a], %	X, %	S, %	Activity[b]	Method[c]	Ref.
CeO_2	250	1/30/0	80	85	11.86*	E	257
Graphenes	110	1.05/3.2/95.7	81	—	56.63		258
In_3O_5	300	1/30/0	70	84	3.63*	E	259
Ni–CeO_2	75	0.5/2.0/0	46	63	2.05	D	260
CrO_x/γ-Al_2O_3	120	0.48/36.5/9.3	55	—	2.53		261
r-CeO_2-500	200	2.5/75/0	13	74	2.09	E	262
h-Al_2O_3/$FeO_{1.25}$	130	0.7/13.5/52.7	83	85	—	E*	263
Cerial-V_O	200	2.5/75/0	3	12	0.12	E	264
Cerial-H	200	2.5/75/0	2	20	0.08	E	
Cerial-O	200	2.5/75/0	7	75	0.28	E	

[a] The feed composition shown corresponds to the ratio of $C_2H_2/H_2/C_2H_4$. [b] Activity is expressed as the amount of acetylene converted per hour per gram of catalyst mass ($mmol_{C_2H_2}\ g_{cat}^{-1}\ h^{-1}$); values marked with an asterisk (*) are calculated per unit volume of catalyst ($mmol_{C_2H_2}\ mL_{cat}^{-1}\ h^{-1}$). [c] Method refers to the selectivity calculation method defined in Table 2. E* denotes Method E applied under ethylene-rich feed conditions.

activity. Even at high reaction temperatures of 200 °C, the catalytic activity was lower than 0.1 $g_{C_2H_2}\ g_{cat}^{-1}\ h^{-1}$.

4. Theoretical studies of acetylene hydrogenation

Experimental studies have demonstrated that the composition and structure of active sites significantly influence the performance of acetylene hydrogenation. In earlier studies, researchers could only infer possible reaction mechanisms based on the adsorption behavior and kinetic fitting models from experimental results. With the rapid advancement of computational quantum chemistry, researchers now have a powerful toolkit to investigate the structure–performance relationships of active sites at the atomic level. In the past two decades over 100 studies have focused on the reaction mechanisms of acetylene selective hydrogenation from a theoretical perspective. These computational studies have not only rationalized experimental observations but also offered theoretical insights to guide the design of improved active sites.

To summarize these theoretical investigations, we categorize these studies according to the structural characteristics of the studied active sites. The computational models are classified into Pd-based and non-Pd-based categories and further subdivided into monometallic, disordered alloy, IMC, and SA site types, following the framework established in Sections 3.2 and 3.3 for experimental studies. The key research themes and major findings are summarized in Tables 12 and 13. DFT studies on the reaction mechanism of acetylene selective hydrogenation typically focus on three key aspects:

(1) Adsorption energetics and geometries. This is the common type of DFT calculation, where researchers model the adsorption behavior of reactants on different active sites, analyzing their binding energy and geometric configurations.

(2) Energy profiles of reaction pathways. These studies go beyond adsorption and map out the transition state pathways for elementary reaction steps, providing a deeper understanding of reaction barriers and intermediates.

(3) Activity and selectivity analysis based on DFT-calculated energy profiles. Several models have been proposed to evaluate catalytic activity and selectivity, helping to rationalize experimental observations and guide the design of more efficient catalysts.

This section will discuss the progress of DFT studies on acetylene selective hydrogenation from the above three perspectives.

4.1 Adsorption energetics and catalyst structural evolution

DFT calculations are widely used to model adsorption energetics and geometries of reactants and intermediates. Surface science experiments have postulated possible adsorbed species and adsorption geometries in acetylene hydrogenation (Fig. 18a), including π-adsorbed acetylene, di-σ-adsorbed acetylene, vinyl species, ethylidyne, ethylidene, top-adsorbed acetylene, and vinylidene.[362] DFT calculations can determine the adsorption energies (E_{ad}) of these surface intermediates on different model surfaces. An effective catalyst should exhibit relatively strong acetylene adsorption ($E_{ad\text{-}C_2H_2}$ as negative as possible) to enhance acetylene hydrogenation and weak ethylene adsorption ($E_{ad\text{-}C_2H_4}$ as positive as possible) to improve selectivity. Nørskov *et al.*[244] proposed scaling relations between adsorption energies of reactants and intermediates and identifying a descriptor for catalytic activity and selectivity, which should enable efficient screening of high-performance acetylene hydrogenation catalysts (Fig. 18b and c). Charge analysis and density of states (DOS) calculations further quantify charge transfer and electronic properties of adsorption models, providing additional insights into the electronic interactions between active sites and adsorbed species.[363,364]

DFT calculations are also used to analyze catalyst structure evolution during acetylene hydrogenation. Experiments have reported dynamic changes in the structure and composition of active sites, such as PdC_x phase formation and surface-segregated Pd in PdAg catalysts, which have been investigated and confirmed by DFT calculations.[273,290] Sautet *et al.*[276] combined DFT calculations with atomistic *ab initio* thermodynamics to study the influence of reaction conditions on PdC_x phase formation (Fig. 18d). They introduced the Gibbs free energy of formation($\Delta\gamma^f$) as a criterion to evaluate the likelihood and stability of carbide phase formation.

4.2 Energy profile of reaction pathways

Acetylene hydrogenation generally proceeds *via* the Horiuti-Polanyi mechanism,[320,365] with the reaction network (Fig. 19) classified into three main pathways: C_2 hydrogenation, C–C

Table 12 DFT calculations for Pd-based active sites

Active site	Investigation theme	Key observations	Ref.
Monometallic Pd	Pd_n (n = 2–12) cluster size effect	• Pd_2 cluster showed more selectivity while Pd_{12} showed higher activity.	270 and 271
	Exposed Pd crystal surface	• Clean Pd(111) surface exhibits higher selectivity and activity compared to Pd(100). • Pd(100) is more prone to forming PdC_x phase, and in its carbide form, Pd(100) demonstrates higher activity than Pd(111).	272–274
	Subsurface or interstitial atoms of C, B, H, *et al.*	• Subsurface H increase the overall activity while decrease in the ethylene selectivity. • Subsurface C increase the ethylene selectivity. • B-modified Pd surfaces show similar properties with C-modified Pd.	275–280
	Molecule coverage effect	• Coverage-dependent microkinetic model gives a much more reasonable TOF (1.41 s^{-1}).	281 and 282
PdX (X = coinage metals of Ag, Cu, Au)	Promotion effect of Ag	• Ag promotes ethylene and hydrogen desorption, reducing their further reaction. • Pd–Ag(100) hinders carbon deposit migration, leading to low selectivity due to hydrogenation of carbonaceous species.	283–285
	Ratio of Ag to Pd and Pd_xAg_y cluster structure	• Pd_1Ag_3 is proposed as a potential phase with optimized catalytic performance	286–289
	Surface restructure	• Surface Pd contents in PdAg and PdAu tend to increase under acetylene hydrogenation conditons	290 and 291
	Core–shell structure	• Cu@Pd core–shell structure showed better activity and selectivity than Au@Pd and Ag@Pd	292 and 293
	Screen of PdX alloy	• Coinage metals in Pd promote the ethylene selectivity and hinder the formation 1,3-butadiene. • Pd_1Cu_3, Pd_1Ag_1 and Pd_1Au_1 catalysts show better activity and ethylene selectivity and inhibit the formation of oligomer.	294–301
Pd-based IMC	PdGa IMC	• PdGa IMC surface terminations significantly impact catalytic pathways, activity and selectivity. • Ga-enriched $GaPd_2$(010) surfaces showed enhanced ethylene selectivity.	302–307
	Pd_2Sn, and AlPd IMC	• The B20-type AlPd compound exhibits potential as an active and selective hydrogenation catalyst. • High-coverage model calculations show comparable hydrogenation barriers on Pd(111) and Pd_3Sn(111).	308,309
Pd SA	Pd_1/gC_3N_4, Pd_1/TiO_2, Pd_1/Fe_3O_4	• H diffusion is significantly modified by the type of single metal atoms	310–312
Pd SAA	Screen the Pd-based SAA	• Pd_1M(100) (M = Cu, Ag, Au) with surface Pd coordination number of 8 exhibits the best catalytic performance	313 and 314
	Pd_1Ag	• H_2 and C_2H_2 can simultaneously bind with a single Pd doping atom in Ag clusters	225, 315 and 316
	Pd_1Cu	• High selectivity on Pd_1Cu(111) arises from facile ethylene desorption and moderate H_2 dissociation activity.	317–320

bond breaking, and C–C coupling. In the C_2 hydrogenation pathway, acetylene undergoes sequential hydrogenation to ethylene, which can be further hydrogenated to ethane under excess hydrogen conditions. In the C–C breaking pathway, intermediates such as CH, CCH, CCH_2, and CCH_3 are formed through C–C and/or C–H bond cleavage, which can lead to PdC_x formation and coke deposition.[283,317,339] In the C–C coupling pathway, reactive species like CCH, CCH_2, CHCH, and $CHCH_2$ can couple to form 1,3-butadiene, a known precursor to green oil.[297,299] When calculating the energy profiles of each pathway, the transition state (TS) of each step is identified, and the activation energy (ΔE_a) is determined as the difference between the transition state energy (E_{TS}) and the corresponding initial state energy (E_{IS}).

Many studies evaluate catalytic performance based solely on the C_2 hydrogenation pathway, where catalytic efficiency is determined by the energy barrier of the rate-determining step. For ethylene selectivity, ethylene from the gas phase can re-adsorb onto the surface and undergo further hydrogenation to ethane. A selective active site should have a higher activation barrier for ethylene hydrogenation ($\Delta E_{a\text{-}C_2H_4}$) than for ethylene desorption ($\Delta E_{des\text{-}C_2H_4}$). On Pd(111), $\Delta E_{a\text{-}C_2H_4}$ and $\Delta E_{des\text{-}C_2H_4}$ were comparable, leading to ethylene over-hydrogenation to ethane. In contrast, PdAg catalysts exhibited a much higher activation barrier for ethylene hydrogenation, thereby enhancing ethylene selectivity (Fig. 20a). Similarly, NiZn has been predicted to suppress ethane formation due to a much higher $\Delta E_{a\text{-}C_2H_4}$ than $\Delta E_{des\text{-}C_2H_4}$ (Fig. 20b).

DFT calculations limited to the C_2 hydrogenation pathway reveal the ability of a catalyst to inhibit ethylene over-hydrogenation, but they do not address the competing C–C coupling pathway. Experimental studies have shown that some catalysts produce significant amounts of oligomers, sometimes even exceeding ethane formation. Thus, incorporating C–C coupling pathway analysis is essential for a comprehensive evaluation of catalytic performance. 1,3-Butadiene formation is often used as a representative descriptor of the C–C coupling

Table 13 DFT calculations for non-Pd-based active sites

Active site	Investigation theme	Key observations	Ref.
Monometallic	Cu	• B- or N-doped Cu(111) has excellent C_2H_4 activity and selectivity and greatly inhibits green oil. • $Cu_{GCN4.8}$ with defect site is screened out to inhibit green oil and presents excellent C_2H_4 activity and selectivity	321–324
	Ni	• Ni(111) surface with defect sites showed better catalytic activity and selectivity of ethylene	325 and 326
	Pt	• Pt/α-WC(0001)–W enables selective C_2H_2 hydrogenation to C_2H_4 (−0.44 eV) while preventing over-hydrogenation and catalyst deactivation by suppressing CCH_3 formation.	327,328
	Others (Au, transition metal carbide, Rh)	• α-MoC(101) exhibits Pt-like electronic properties with enhanced C_2H_4 activity, selectivity, and stability against green oil formation.	329–333
Multi-metallic	Cu-based	• PdCu(211) and AgCu(211) surfaces favor C_2H_4 desorption, indicating Pd and Ag enhance selectivity for C_2H_4 formation.	334 and 335
	Ni-based	• Au, Ag, and Cu doping on Ni modulates acetylene adsorption, enhancing catalytic activity.	149 and 336
	Pt-based	• $PtCu_3$ IMC is screened out as the optimal catalyst among Pt–M (M = Au, Ag, Cu) for acetylene hydrogenation	337
IMC	NiX IMC (X = Ga, In, Sn, Ti)	• A targeted subspace of IMC enables access to new Brønsted–Evans–Polanyi relationships. • NiIn and Ni_2In_3 suppressed ethane formation but promoted oligomerization.	338–341
	$Al_{13}Co_4$ and Al_5Co_2	• Active sites are pentagonal $CoAl_5$ clusters but not isolated Co atoms. • The rate-limiting activation energies on $CoAl_5$ are comparable to those of conventional Pd or PdAg.	342–345
	Metal phosphide	• FeP(101)–I exhibits Pd-like performance with enhanced performance compared to Pd and other M_xP_γ catalysts (M = Mo, W, Fe, Co, Ni, and Pd).	346
SA	Supported Ni single atom	• Single-Ni-doped catalysts with four-N-modified C34 universally exhibit high ethylene selectivity • $Ni_1(OH)_2/TiO_2(101)$ favors acetylene adsorption and promotes the heterolytic dissociation of H_2	347–350
	Pd_1/TiO_2 and Pt_1/Cu	• Pd_1/TiO_2 shows the highest ethylene selectivity but lowest activity among Pt_n/TiO_2, • Pt_1–Cu(111) exhibits the highest selectivity and stability among Pt_1–X(111) (X = Cu, Ag, Au),	351–353
FLPs	CeO_2 and TiO_2	• Ce/O FLPs facilitate heterolytic H_2 dissociation and the resulting O–H and Ce–H species drive acetylene hydrogenation. • Doped metals such as Ga, Cu, Ni, Pd, Pt, or Co promote surface oxygen vacancy formation and generate diverse FLP types with surface O atoms.	354–359
	Perovskite oxyhydride (POHs) and carbon nitride	• POHs are capable of selective hydrogenation due to their rich hydrogen surface-redox chemistry	360 and 361

pathway in DFT calculations. Previous studies suggest that oligomerization on Ni surfaces occurs *via* C–C bond formation between adsorbed acetylene and vinyl, with the reaction pathway beginning with partial acetylene hydrogenation to vinyl, followed by C_4H_5 formation and subsequent hydrogenation to butadiene (Fig. 20c). Zhang *et al.*[297,323,324,366] proposed three primary C–C coupling routes, including CHCH–CHCH coupling, CHCH–$CHCH_2$ coupling, and $CHCH_2$–$CHCH_2$ coupling (Fig. 20d). DFT results further reveal that Group 1B metals in Pd-based catalysts, such as Cu_3Pd_1, can effectively suppress the C–C coupling pathway and consequently green oil formation.

Experimental studies revealed that the PdC_x phase forms during acetylene hydrogenation, with carbon species derived from acetylene decomposition. DFT calculations have been employed to investigate the C–C breaking pathway, showing that reducing the size of Pd ensembles can inhibit C–C bond cleavage. Specifically, carbon deposition on the 0.01 ML Pd/Cu(111) surface exhibited a significantly higher activation energy (2.00 eV) compared to the 1.00 ML Pd/Cu(111) surface (1.30 eV), suggesting that smaller Pd ensembles suppress carbon accumulation by making C–C cleavage less favorable.[317]

4.3 Activity and selectivity analysis from DFT calculations

The energy profile results provide activation energies for each step, which can be used to calculate elementary reaction rates based on transition state theory (TST). Several models have been proposed to further evaluate the overall activity of reaction pathways, including the energetic span model, the two-step model, and the microkinetic model.

The energetic span model, originally introduced by Amatore and Jutand[367] and further developed by Kozuch and Shaik,[368] quantifies the efficiency of catalytic cycles through TOF, which is closely related to the highest transition state and the most stable intermediate in the energy profile. By applying this model, researchers can analyze acetylene hydrogenation activity over different catalyst structures.[270,286,336,340] For instance,

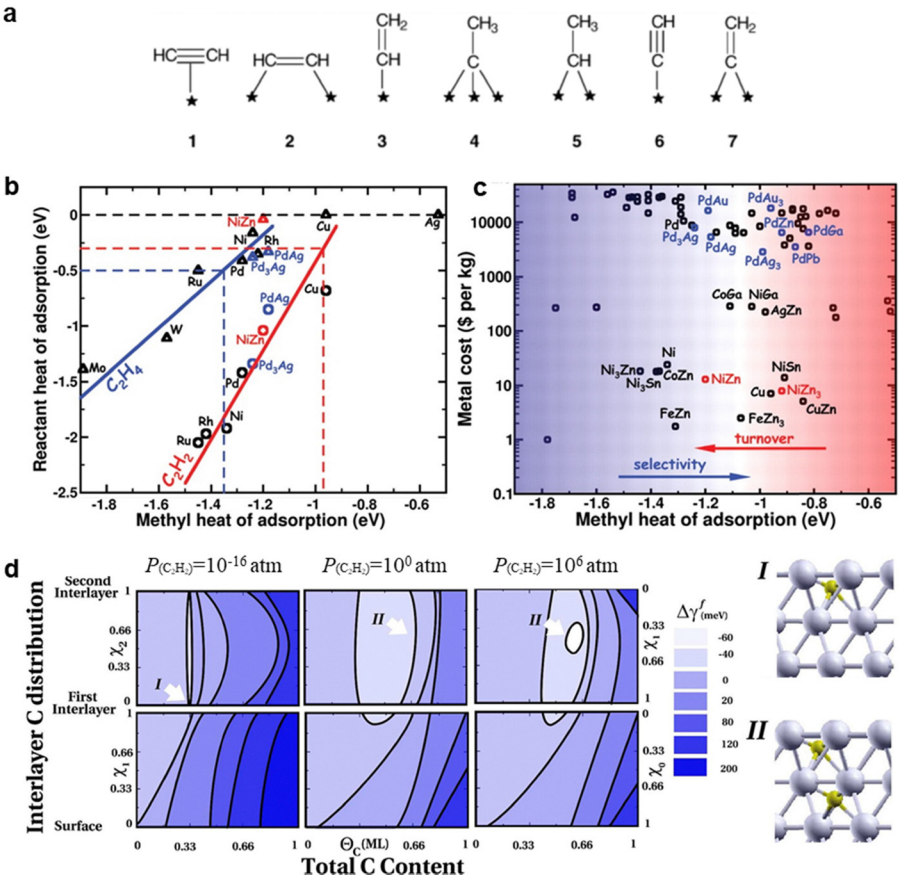

Fig. 18 (a) Proposed surface intermediates in hydrogenation of acetylene. Reprinted with permission from ref. 362. Copyright 2001 Elsevier. (b) Heats of adsorption for C_2H_2 and C_2H_4 and (c) Price (in 2006) of 70 binary IMC plotted against the heat of adsorption for methyl. Reprinted with permission from ref. 244. Copyright 2008 The American Association for the Advancement of Science. (d) Computed two-dimensional Gibbs free energy maps for the accumulation and dissolution of C atoms on the two outermost Pd(111) interlayers. Reprinted with permission from ref. 276. Copyright 2013 American Chemical Society.

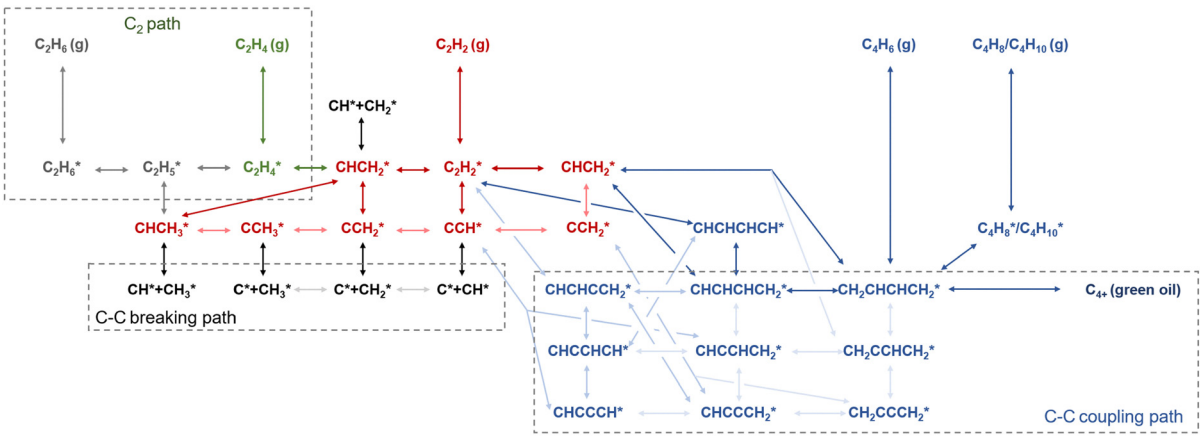

Fig. 19 Reaction network of acetylene hydrogenation for DFT calculation.

Pd_2Ag_2C exhibited the highest TOF among Pd_4, Pd_3Ag_1, Pd_1Ag_3, Pd_2Ag_2, and Pd_2Ag_2C catalysts,[286] while Au/Ni(111) demonstrated higher activity than Ni(111), Cu/Ni(111), Ag/Ni(111), and Au(111).[336]

The two-step model, proposed by Hu *et al.*,[254,272,289] treats acetylene hydrogenation as a kinetic process consisting of two steps: adsorption and desorption. The adsorption rate (r_{ad}) and desorption rate (r_{de}) are determined by the effective energy

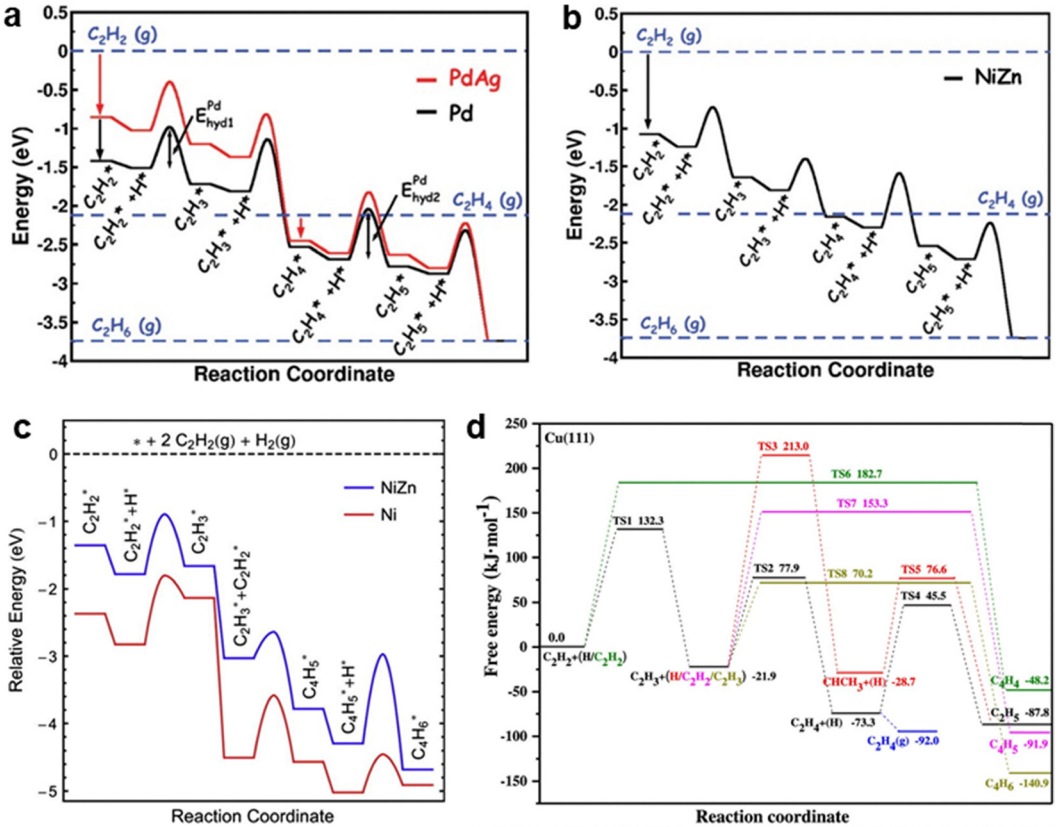

Fig. 20 (a) and (b) Energy diagrams of C_2 path for acetylene hydrogenation on Pd(111), PdAg(111) and NiZn(110). Reprinted with permission from ref. 244. Copyright 2008 The American Association for the Advancement of Science. (c) Energy diagram for the oligomerization of acetylene on Ni(111) and NiZn(101). Reprinted with permission from ref. 250. Copyright 2014 Elsevier. (d) Energy diagram for the possible oligomerization paths over Cu(111). Reprinted with permission from ref. 323. Copyright 2022 American Chemical Society.

barriers for reactant adsorption and product desorption, respectively. Under steady-state conditions, the overall reaction rate (r) is obtained from $r = r_{ad} = r_{de}$.[272] Using this model, reaction rates can be predicted, as demonstrated by the case of Pd_6Ag_7, which exhibited the highest reaction rate among $Pd_{13-m}Ag_m$ clusters.[289]

The microkinetic model for acetylene selective hydrogenation was developed based on the Langmuir–Hinshelwood (L–H) mechanism, where the adsorption and desorption of C_2H_2 and H_2 were assumed to be in equilibrium, and TST was applied to determine rate constants for each elementary step based on the energy profile.[281,288,299,351] Additionally, the model assumes that the sum of the total coverage of all intermediates and free adsorption sites equals to unity. The steady-state approximation is employed by setting the time derivatives of all intermediate coverages to zero. The microkinetic model provides insights into each step of various reaction pathways as a function of reaction temperature and reactant ratio. For instance, studies based on the microkinetic model have identified CHCH and $CHCH_2$ as the main fragments responsible for C–C coupling on PdM(111) (M = Cu, Ag, Au), and revealed that high temperatures and high H_2-to-C_2H_2 ratios inhibited of green oil formation.[299] Furthermore, coverage-dependent microkinetic models have been proposed to incorporate the effects of surface coverage on E_{ad} for all intermediates. For example, a model was used to quantify the coverage (θ) effect on E_{ad}, demonstrating that the coverage-dependent microkinetic model obtained a significantly more reasonable TOF (1.41 s^{-1} at 300 K) compared to the coverage-independent model (3.16×10^{-24} s^{-1}).[281]

Ethylene selectivity was also analyzed based on the energy profiles.[7,250,335] A simplified metric for ethylene selectivity was defined as the difference between the activation energy for C_2H_4 hydrogenation and the desorption energy of C_2H_4:

$$\Delta E_{select} = \Delta E_{a\text{-}C_2H_4} - \Delta E_{des\text{-}C_2H_4} \quad (9)$$

A more positive ΔE_{select} value indicates a higher selectivity toward C_2H_4 formation. This approach has been widely used to evaluate the selectivity of different model surfaces and the effects of crystal structure and metal composition.[7]

5. Effect of catalyst supports on acetylene hydrogenation

Acetylene hydrogenation catalysts are typically metal catalysts supported on solid materials, making the selection of support material crucial to overall catalytic performance. On one hand,

the inherent properties of the support can directly affect acetylene hydrogenation. For instance, the acid–base characteristics of the support can influence C–C coupling reaction pathways. On the other hand, the support can modulate the properties of metal active sites, further influencing the overall catalytic performance. For example, high-surface-area supports enhance metal dispersion, while reducible supports (*e.g.*, TiO_x) exhibit the strong metal–support interactions (SMSI) effect. The most commonly used supports for acetylene hydrogenation catalysts are metal oxides and carbon-based materials. In addition, porous materials, such as zeolites and metal–organic frameworks (MOFs), have also been explored. The performance of active sites on different supports for acetylene hydrogenation is summarized in Tables 14 and 15. This section summarizes the effect of supports on acetylene hydrogenation.

5.1 Metal oxides

5.1.1 Al_2O_3-based supports. Al_2O_3-based oxide materials are among the most widely studied supports for acetylene hydrogenation. Researchers have investigated how the physical and chemical properties of Al_2O_3-based oxides influence the catalytic performance of active metals, focusing on factors such as the Al_2O_3 crystal phase and acidity. To further optimize the catalytic properties, secondary metal oxides have also been introduced to modify the characteristics of Al_2O_3.

Al_2O_3 exists in several crystalline phases, including β, γ, η, χ, κ, ρ, δ, θ, and α, each of which exhibits distinct structural, physical, and chemical properties.[369,370,410–413] The choice of phase has a significant impact on catalytic performance for acetylene hydrogenation. Using Pd/Al_2O_3 as an example, the α-Al_2O_3 phase had a low surface area (0.1–2 $m^2\ g^{-1}$), which limited Pd dispersion and consequently reduced catalytic activity. In contrast, the γ-Al_2O_3 phase typically exhibited a much higher surface area, promoting metal dispersion, however, it also introduced a greater number of acidic sites, which accelerated the formation of oligomer products.[369] It is reported that oligomer formation was about four to five times faster on Pd/γ-Al_2O_3 compared with the α-Al_2O_3-supported catalyst.[414] The phase transformation of Al_2O_3 is highly dependent on the calcination temperature. As the heating temperature increased from 900 °C to 1100 °C, the phase transition proceeded as follows: γ → (γ+ δ + θ) at 900 °C → (δ + θ) at 1000–1050 °C → α at 1100 °C. During this transformation, the surface area of Al_2O_3 decreased significantly from 244 $m^2\ g^{-1}$ to 16.4 $m^2\ g^{-1}$.[370] Catalytic evaluations have shown that Pd/Al_2O_3 calcined at 1050 °C (containing δ and θ phases) exhibited the highest ethylene selectivity. However, some studies have reported that α-Al_2O_3 generally resulted in the lowest hydrocarbon deposition and the highest ethylene selectivity, while at the cost of catalytic activity.[410] Although some variations exist in reported results, a common conclusion is that reducing the acidity of the Al_2O_3 support can effectively suppress the formation of oligomer products, thereby improving ethylene selectivity.

Basic oxides, such as MgO, have been introduced to reduce the acidity of Al_2O_3 while preserving its high surface area, thereby balancing both acetylene hydrogenation activity and ethylene selectivity. MgO can be directly deposited onto the Al_2O_3 surface *via* impregnation with a magnesium precursor.[380,415] Alternatively, it can be incorporated into the support during synthesis to form Mg–Al composite oxides, such as Mg–Al-layered double hydroxide (MgAl-LDH),[378,382,416] hydrotalcite (HT),[379] palygorskite,[381] and spinel.[383] The incorporation of MgO significantly improves ethylene selectivity. For instance, Pd supported on HT (Pd/HT) exhibited an ethylene selectivity of 75% (E), considerably higher than that of Pd/MgO (48%, E) and Pd/Al_2O_3 (38%, E).[379] Additionally, MgO-Al_2O_3 composite oxides derived from MgAl-LDH exhibited a larger surface area and lower surface acidity, which not only enhanced ethylene selectivity but also improved catalytic activity compared with Pd/Al_2O_3.[378,416]

The properties of Al_2O_3 can also be tuned by incorporating second metal species such as Zn, Fe, and Ce.[375–377,417–419] Studies have shown that doping α-Al_2O_3 with Zn and Fe *via* the sol–gel method effectively reduced the acidity of the support, which mitigated deactivation caused by oligomer formation and enhanced ethylene selectivity.[375,417] Similarly, impregnating Al_2O_3 with a Ce precursor decreased its acidity, but an optimal Ce loading was necessary to achieve the best catalytic performance.[376] In addition to acidity regulation, electronic interactions between CeO_x and the active metal were observed, which also contributed to the catalytic activity enhancement.[376,377]

Al_2O_3-based oxide supports with unique structures have been designed to improve catalytic performance, including α-Al_2O_3@SiC core–shell structures, microfibrous AlOOH/Al-fiber, microrod Al_2O_3, and array-modified molded alumina.[371–373,420,421] These tailored structures exhibited optimized acidic properties, enhanced the interaction between the support and active metal to improve metal dispersion, and modified the electronic properties of the active metal *via* electronic effects. These synergistic effects contribute to enhanced catalytic activity and selectivity.

5.1.2 Ti-containing oxides. TiO_2 is a reducible metal oxide that exhibits the SMSI effect, where Ti species migrate onto the surface of active metal under specific reduction conditions. These migrated Ti species reduce the number of multi-coordinated Pd sites through geometric effects while also altering the electronic properties of active sites, thereby enhancing ethylene selectivity and suppressing oligomer formation.[387,422–424] It should be noted, however, that the surface coverage of Ti species also decreases the hydrogenation activity. Experimental results revealed that Pd/TiO_2/MCM-1 catalysts without high-temperature reduction treatment underwent rapid deactivation, with acetylene conversion decreasing from 100% to below 60% within 10 h.[390] In contrast, samples reduced at 500 °C exhibited significantly improved stability, maintaining a conversion of ~50%. Additionally, plasma treatment was reported to further enhance ethylene selectivity by generating more Ti^{3+} species.[425]

To further optimize catalytic performance, secondary metal oxides such as La, Ni, and Mg have been incorporated into Ti-containing oxides.[386,388,389] These additional oxides further modified the geometric and electronic properties of the active

Table 14 Catalysts with metal oxides as supports for acetylene hydrogenation

Catalyst	Description	T, °C	Feed[a], %	X, %	S, %	Activity[b]	Method[c]	Ref.
Al_2O_3-based oxides								
Pd/γ-Al_2O_3		40	1.5/1.7/96.8	52	78		—	369
Pd/α-Al_2O_3		40	1.5/1.7/96.8	70	82		—	
Pd/α&γ-Al_2O_3	65% α-Al_2O_3	40	1.5/1.7/96.8	80	88		—	
Pd/γ,θ,δ-Al_2O_3		60	1/1.5/60	16	18		C	370
Pd/θ,δ-Al_2O_3		60	1/1.5/60	78	65		C	
Pd/α-Al_2O_3		55	0.45/0.71/92.4	99	36		E	371
Pd/α-Al_2O_3@SiC		65	0.45/0.71/92.4	95	48		E	
Pd–Ag/α-Al_2O_3		55	0.45/0.71/92.4	100	41		E	
Pd–Ag/α-Al_2O_3@SiC		65	0.45/0.71/92.4	99	57		E	
0.05Pd-Cat-600/400		70	0.33/0.66/33.3	55	62	180.5	C	372
0.05Pd-Cat-100/400		70	0.33/0.66/33.3	100	36	313.6	C	
Pd/meso-Al_2O_3		130	0.33/0.66/33.3	100	85		D	373
Pd/com-Al_2O_3		130	0.33/0.66/33.3	98	25	4008.1	D	
Pd/α-Al_2O_3-C		50	0.3/1.5/6	45	61	188.5	C	374
Pd/Al_2O_3-1400		50	0.3/1.5/6	64	63	320.4	C	
Pd/α-Al_2O_3			1.5/1.7/96.8	82	65		E	375
Pd/Fe-modified α-Al_2O_3			1.5/1.7/96.8	84	72		E	
Au/Al_2O_3		250	0.6/3/0	4	87	17.5	E	376
Au/0.3%CeO_2–Al_2O_3		250	0.6/3/0	7	100	30.7	E	
Pd/Zn/0.1Ce/Al_2O_3		100	2/2.2/80(1MPa)	84	93	19969.7	D	377
Pd/Al_2O_3		40	0.3/0.6/33.1	12	88	44.6	D	234
Pd/Al_2O_3		100	0.3/0.6/33.1	90	<0	334.6	D	
1c-Ga_2O_3–Pd/Al_2O_3	Ga_2O_3-ALD	40	0.3/0.6/33.1	15	95	55.8	D	
1c-Ga_2O_3–Pd/Al_2O_3	Ga_2O_3-ALD	100	0.3/0.6/33.1	100	0	371.8	D	
Pd/Al_2O_3		80	0.91/1.82/97.3	68	83		E*	378
Pd/MgO–Al_2O_3		80	0.91/1.82/97.3	95	95		E*	
Pd/HT		55	0.35/0.6/0	97	75	195.3	E	379
Pd/MgO		80	0.35/0.6/0	96	48	198.1	E	
Pd/Al_2O_3		100	0.35/0.6/0	85	38	177.6	E	
Au/Al_2O_3		250	0.6/3/0	5	92	7.3	E	380
Au/3%MgO_x–Al_2O_3	Reduced at 550	250	0.6/3/0	12	92	20.9	E	
Pd/A-Pal	Air roasting	70	1/2/0	98	52	3491.9	E	381
Pd/N-Pal	NH_3-roasting	70	1/2/0	50	58	890.8	E	
3D-Al-Pd/MMO		55	0.33/0.66/34.5	95	88	126.5	F	382
Pd/Al_2O_3		55	0.33/0.66/34.5	30	90	40.2	F	
Pd/Al_2O_3		100	0.33/0.66/34.5	98	10		F	
Pd/$MgAl_2O_4$-400		80	1/5/20	48	92	5473.0	D	383
Pd/$MgAl_2O_4$-600		80	1/5/20	17	98	1938.4	D	
Cu/$MgAlO_x$		225	0.33/1.02/32.86	64	95		E*	384
Cu/$Fe_{0.12}MgO_x$		215	0.33/1.02/32.86	79	98		E*	
Pd/MgO		50	4/96/0	79	49	18015.4	—	385
Ti-containing oxides								
Pd–SiO_2/300		60	1/10/0	87	5		—	386
Pd–1La–0.2Ti/300		60	1/10/0	87	40		—	
Pd–0.2Ti/300		60	1/10/0	87	5		—	
Pd–1Nb–0.2Ti/300		60	1/10/0	94	48		—	
Pd–Ti/SiO_2		60	0.98/1.96/97.05	95	34		—	387
Pd/SiO_2		60	0.98/1.96/97.05	93	15		—	
PdAg/TiO_2		85	0.32/0.6/32.9	90	75	238.7	E*	388
PdAg/NiTi-LDH		70	0.32/0.6/32.9	90	82	242.1	E*	
PdAg/TiO_2		65	0.33/0.66/32.8	50	68	76.4	E*	389
PdAg/$Mg_{0.3}Ti_{0.7}O_y$		65	0.33/0.66/32.8	67	71	102.4	E*	
PdAg/$Mg_{0.5}Ti_{0.5}O_y$		65	0.33/0.66/32.8	92	86	140.6	E*	
PdAg/$Mg_{0.7}Ti_{0.3}O_y$		65	0.33/0.66/32.8	81	79	123.8	E*	
PdAg/MgO		65	0.33/0.66/32.8	64	62	97.8	E*	
Pd/1c-TiO_2/MCM-41	Reduced at 500 °C	40	0.1/0.2/2.5	50	75		E*	390
Si containing oxides								
I-Pd/M–SiO_2		50	1/7/0	87	38		E	391
Pd/C–SiO_2		80	1/7/0	95	66		E	
PdAg/Na + -β-zeolite		50	2.5/10/2.5	35	52	807.0	E*	392
PdAg/K + -β-zeolite		50	2.5/10/2.5	18	68	415.0	E*	
PdAg/Rb + -β-zeolite		50	2.5/10/2.5	47	50	1083.6	E*	
Pd(v)/FG	Fiberglass	85	0.49/0.74/59.4	99	60	356.8	B	393
Pd-HNT-az-Ac	Halloysite nanotube	30	1.05/1.94/5.01	27	76		E*	394
Others								
Au/CeO_2(R)–air		250	0.6/3/0	17	100	18.2	E	395

Table 14 (*continued*)

Catalyst	Description	*T*, °C	Feed[a], %	*X*, %	*S*, %	Activity[b]	Method[c]	Ref.
$Au/CeO_2(R)–H_2$		250	0.6/3/0	6	93	6.4	E	
$Ni–Cu/CeO_2$-NP		90–180	0.6/2.4/5.4	85	84		E	396
$Ni–Cu/CeO_2$-NC		90–180	0.6/2.4/5.4	85	50		E	
$Pd_{1.0}/Bi_2O_3/TiO_2$		40	1/20/20	61	93	151.2	D	235
$Pd–SrTiO_3$		100	1/10/20	96	90	1094.6	C	397

[a] The feed composition listed in the table corresponds to $C_2H_2/H_2/C_2H_4$. [b] Activity is calculated as the number of moles of acetylene converted per hour per total molar active metal ($mol_{C_2H_2}$ mol_{metal}^{-1} h^{-1}). [c] Method refers to the calculation method specified in Table 2. *E** indicates that Method E was applied under ethylene-rich feed conditions.

Table 15 Catalysts with different supports for acetylene hydrogenation

Catalyst	*T*, °C	Feed[a], %	*X*, %	*S*, %	Activity[b]	Method[c]	Ref.
Carbon material as support							
$Ni_{10}Co_{90}$@C		0.5/10/20	95	81		D	398
Pd/C	85	0.49/20.77/34.27	80	30	376.3	E*	399
Pd/CNTs-out	80	0.87/0.87/42.26	97.7	83.1	30.3	E*	400
Pd/CNTs-in	80	0.87/0.87/42.26	95.4	73.3	29.6	E*	
Pd/CNT	80	1/3/20	80	15	684.1	C	401
Pd/N2.1-CNT	80	1/3/20	100	40	855.2	C	
Pd@NMC-850	100	0.35/0.70/30.5	65	83		C	402
Pd/Al_2O_3	60	0.35/0.70/30.5	90	30		C	
chrGO/Pd-NP	90	1/2/80	89.68	41.72	12.2	E	403
Pd/CMK-3	180	11.25/45/0	95	84		E	404
Porous material							
PdZn-1.2@ZIF-8C	120	0.65/5/50	88	79	186.3	B	405
PdZn-2.7/ZIF-8C	60	0.65/5/50	88	84	26.1	B	
Pd@SOD	80	0.6/6/0	20	95		E	406
Pd/SOD	80	0.6/6/0	60	23		E	
Other supports							
Pd/TiO_2	80	1/2/0	98	65	172.4	E	407
Pd/SiC	80	1/2/0	90	85	160.3	E	
1.06-Pd/Si_3N_4	160	0.66/6.6/32.9	100	95	91.3	E*	408
Pd/C	160	0.66/6.6/32.9	100	77	89.6	E*	
Pd/β-Mo_2C-600	120	1/10/0	70	80		E	409

[a] The feed composition listed in the table corresponds to $C_2H_2/H_2/C_2H_4$. [b] Activity is calculated as the number of moles of acetylene converted per hour per total molar active metal ($mol_{C_2H_2}$ mol_{metal}^{-1} h^{-1}). [c] M refers to the calculation method specified in Table 2. *E** indicates that Method E was applied under ethylene-rich feed conditions.

metal while also tuned the surface acid–base characteristics, contributing to improved catalytic activity and selectivity.

5.1.3 Si-containing oxides. SiO_2 is generally regarded as an inert support for acetylene hydrogenation due to its inability to exhibit SMSI effects under high-temperature reduction treatment. To evaluate the influence of Si species on the catalytic performance of active metals, chemical vapor deposition (CVD) was employed to deposit Si onto the active metal surface.[426–428] Experimental results demonstrated that Si modification had a similar effect to TiO_x, reducing the number of multi-coordinated Pd sites and thereby suppressing oligomer formation. Moreover, surface Si exhibited synergistic effects with other catalytic components, such as La oxide and NiZn alloy, further enhancing catalytic performance.[426,428]

Beyond SiO_2, other Si-containing materials have also been explored for the design of highly efficient acetylene hydrogenation catalysts, including zeolites, fiberglass, halloysite and porous hollow silica nanoparticles.[392–394,429–431] These materials offered unique properties that promoted small particle sizes and uniform dispersion of Pd NPs.[430,431] Additionally, these supports have also been reported to regulate the adsorption of reaction intermediates to improve the catalytic activity and selectivity.[393,430]

5.1.4 Other oxides. Ohter metal oxides, including CeO_2, Ga_2O_3, Bi_2O_3, ZnO, and $SrTiO_3$, have been investigated for acetylene hydrogenation.[235,395–397,432] These oxides can either serve directly as supports for active metals or function as promoters to modify metal NPs. The morphology of the metal oxide support also plays a crucial role in catalytic performance. For example, Au supported on ZnO with a needle-like morphology (exposing non-polar planes) exhibited higher activity compared to Au supported on platelet-shaped ZnO (exposing polar planes).[432]

5.2 Carbon-based materials

Carbonaceous materials represent another widely used class of supports for heterogeneous catalysis. Owing to their varied sp^2

carbon atom arrangements and structures, these materials exhibit unique electronic properties that can effectively modify active metal sites. Studies have shown that Pd supported on carbonaceous materials demonstrated higher ethylene selectivity and reduced oligomer formation compared to Pd/Al_2O_3 catalysts.[399,433] Various carbonaceous materials have been explored for acetylene hydrogenation, including carbon nanotubes (CNTs), carbon nanofibers (CNFs), and graphene oxide.[400,403,434,435] Notably, compared with CNTs, CNFs with a stacked structure provided a more finely dispersed Pd phase, leading to enhanced hydrogenation activity.[435]

Nitrogen doping in carbonaceous materials has been shown to further improve catalytic performance.[401,402,436–438] Specifically, graphitic nitrogen modulates the electronic properties of active sites, facilitating the desorption of ethylene and thereby increasing ethylene selectivity. For example, Pd supported on nitrogen-doped CNTs ($Pd/N_{1.4}$–CNT) exhibited 1.5 times higher hydrogenation activity compared to Pd/CNTs, with ethylene selectivity improving from 40% to 55% (C) at 90% conversion.[401]

5.3 Porous materials

In acetylene hydrogenation reactions, porous materials such as zeolites,[406,439] MOFs,[405,440–443] and covalent triazine frameworks[444] have also been explored as catalyst supports. The confinement effect of these materials facilitates the formation of smaller active metal NPs, while the electronic interactions and spatial constraints between the porous support and the active metal further enhance catalytic performance. Additionally, novel reaction mechanisms have been proposed. For instance, encapsulating Pd within sodalite (SOD) zeolite prevented the direct interaction of acetylene and ethylene with Pd active sites, while H_2 could diffuse into the SOD pores and be activated by the encapsulated Pd nanoclusters. A hydrogen spillover process subsequently generated OH species on the SOD surface, which then reacted with acetylene, leading to selective hydrogenation. As a result, Pd@SOD exhibited significantly higher ethylene selectivity compared to Pd/SOD.[406]

6. Effect of catalytic modifiers and reaction media on acetylene hydrogenation

In addition to catalytic active sites and catalyst supports, modifiers also play a crucial role in influencing reaction performance. Among them, CO has been employed as a modifier to suppress the over-hydrogenation of ethylene to ethane. In industrial ethylene purification, small amounts of CO are intentionally introduced into the feed gas to enhance hydrogenation selectivity and mitigate the risk of temperature runaway. Alkali metals are effective catalyst modifiers that enhance catalytic performance of acetylene hydrogenation. The mechanism and effects of CO and alkali modification have been reviewed in previous work.[1,2] DFT calculations revealed that CO exhibited a comparable adsorption strength to acetylene but bound more strongly than ethylene on the Pd(111) surface,[445,446] reducing the number of available active sites for hydrogenation. Moreover, the remaining free sites on the CO-covered Pd(111) surface led to significantly weaker ethylene adsorption, further suppressing ethylene over-hydrogenation.[445] However, it should be noted that CO also accelerated green oil formation on Pd catalysts, particularly in tail-end process. A similar phenomenon has been observed on Ni-based catalysts.[144,447,448] For instance, it was reported that the addition of 550 ppm CO reduced ethane selectivity from 20% to 10%, while increasing oligomer selectivity from 35% to 51%.[448]

Beyond CO and alkali, other modifiers, such as sulfur, organic ligands, and ionic liquids, have been employed as catalyst additives, which will be further discussed in Section 6.1. Additionally, the liquid phase has been reported as a process modifier, as it influences the reactant concentration around active sites due to the solubility differences of reactant gases in the liquid solvent. This aspect will be further discussed in Section 6.2.

6.1 Catalytic modifiers

6.1.1 Sulfur. Sulfur species have been introduced into catalysts for acetylene hydrogenation, leading to enhanced catalytic performance due to the formation of metal sulfides. Among various metal sulfides, Pd sulfide exhibited the highest ethylene selectivity compared to Ni and Cu sulfides.[449–451] It has been reported that increasing the reduction temperature resulted in sulfur loss from the catalyst, leading to a phase transition from sulfur-rich PdS to intermediate $Pd_{16}S_7$, and finally to sulfur-lean Pd_4S.[451] Experimental results revealed that Pd_4S exhibited the best catalytic performance, achieving an ethylene selectivity of 82.8% at 250 °C. Zhang *et al.*[366,452–455] investigated the effect of sulfur on Cu- and Pd-based catalysts for acetylene hydrogenation using DFT calculations. Their theoretical results indicated that sulfur-decorated model surfaces, such as S/Pd_1Ag_1 and S/Pd_1Au_1, exhibited a d-band center shifted further away from the Fermi level, which improved ethylene selectivity and catalytic activity.[366] Additionally, the reduced spatial availability of active sites due to the presence of sulfur effectively suppressed the formation of oligomer byproducts.

6.1.2 Ionic liquid. Ionic liquids (ILs) are non-volatile due to their extremely low vapor pressure, making them promising additives and catalyst coatings for enhancing selectivity in hydrogenation reactions. Coating supported metal catalysts with ILs introduces an additional diffusion barrier between reactant molecules and metal active sites.[456–460] Studies have shown that ILs exhibit high solubility for acetylene while maintaining low solubility for ethylene. For instance, the solubility of C_2H_2 in [Prmim][Cl] reached 1.05 mmol g^{-1}, which was 5.5 times higher than that of C_2H_4 (0.19 mmol g^{-1}). This selective solubility reduces the extent of over-hydrogenation of ethylene to ethane.[461] Compared to Pd/SiO_2, the introduction of an IL layer increased ethylene selectivity from 70% to 85% (E).[462]

Beyond the solubility effects, ILs also modify the electronic properties of active metals. It has been reported that certain ILs

formed unique carbene structures around Pd active sites, facilitating the desorption of ethylene.[463] This electronic effect enhances ethylene selectivity. However, catalyst deactivation due to oligomer formation remains a challenge for IL-coated catalysts.[462,464] The use of Pd@S-1 core–shell materials coated with ILs has been reported, showing improved stability for acetylene hydrogenation.[461]

6.1.3 Organic ligands and polymers. Organic ligands have been employed to tune the electronic properties of metal active sites, thereby enhancing the ethylene selectivity for acetylene hydrogenation. Early studies evaluated phenyl phosphine and phenyl sulfide as modifiers for Pd-based catalysts.[465–468] These ligands effectively altered the electronic structure of Pd, improving ethylene selectivity by suppressing the over-hydrogenation of ethylene. Another class of ligands includes nitrogen-containing compounds, such as amines,[469,470] amino acids,[471] and 1,10-phenanthroline-5,6-dione (PDO).[472] On one hand, the strong interaction between Pd and histidine influenced the structural characteristics of the active metal, leading to increased metal dispersion. On the other hand, the electronic effect of nitrogen atoms weakened reactants adsorption on Pd, thereby improving ethylene selectivity. More recently, hydrophobic ligands have been explored to modify catalyst surfaces (Fig. 21a). The presence of hydrophobic chains on Cu surfaces introduced steric hindrance, effectively suppressing undesired C–C coupling side reactions, thereby improving ethylene selectivity.[473]

The concept of dynamic metal–polymer interaction was proposed by Choi *et al* for acetylene hydrogenation.[474–478] In their study, polyphenylene sulfide (PPS) chains were utilized to encapsulate Pd particles through strong metal–polymer interactions, effectively suppressing the over-hydrogenation of ethylene to ethane. The proposed mechanism (Fig. 21b) suggested that the Pd–PPS interface selectively facilitated H_2 activation only in the presence of acetylene, which strongly bound to Pd and disrupted the Pd–PPS interaction. Once acetylene underwent hydrogenation to form ethylene, which exhibited weaker binding on Pd, the PPS chains rapidly re-adsorbed onto the Pd surface. This dynamic re-adsorption repelled ethylene, preventing its further hydrogenation to ethane and thereby enhancing ethylene selectivity.[474,479]

6.2 Acetylene hydrogenation in liquid phase

The introduction of a liquid phase medium in acetylene hydrogenation was first reported by Edvinsson *et al.* in 1995.[480] In their study, heptane was used to form a liquid film on the catalyst layer within a monolith reactor, which improved catalyst stability by efficiently removing green oil deposits. Later, Shitova *et al.*[481] employed *N*-methylpyrrolidone (NMP) as a liquid solvent in a shaker-type flow reactor, achieving high ethylene selectivity. Acetylene exhibits high solubility in polar solvents such as acetone, NMP, dimethylformamide (DMF), and certain ionic liquids, whereas ethylene has much lower solubility in these solvents.[482–484] For instance, the selective solubility factor (α) of acetylene to ethylene in NMP exceeded 11 at temperatures below 100 °C.[482] As a result, the actual reactant concentration in the vicinity of the active sites is significantly modified by the liquid solvent, effectively suppressing the over-hydrogenation of ethylene to ethane (Fig. 22a). Compared to the gas-phase process over Pd/SiO_2 catalysts, the introduction of the liquid phase media increased ethylene selectivity from $<60\%$ to $>80\%$ (E).[482]

The liquid phase hydrogenation is typically conducted in a stirred-tank reactor (CSTR) (Fig. 22b), where the dissolved composition in the solvent remains nearly constant and closely matches the outlet composition once a steady state is reached. At high acetylene conversions, acetylene rapidly and uniformly dissolves within the liquid phase upon entering the reactor, maintaining a relatively low acetylene concentration. This characteristic reduces the formation of oligomerization products. A theoretical model was developed for the liquid phase hydrogenation process, integrating reaction kinetics, mass transfer, and reactor modeling under different reaction conditions.[485] The simulation results suggested that the liquid phase process

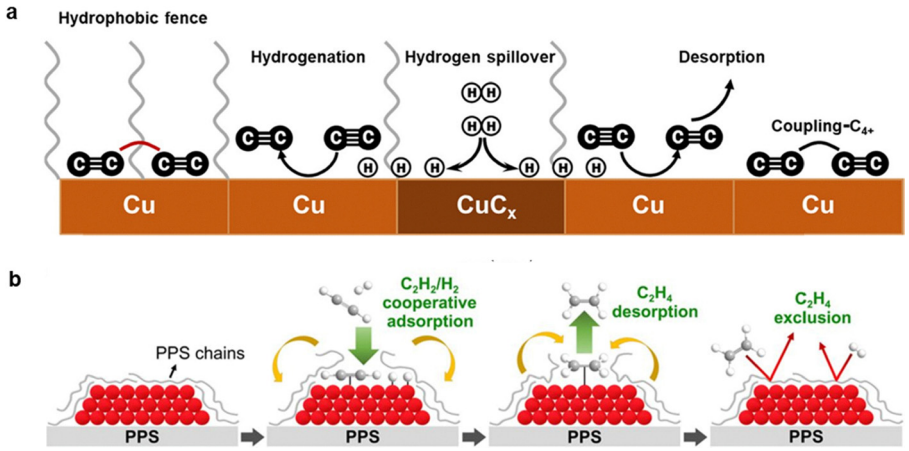

Fig. 21 (a) Schematic illustration of the semihydrogenation of alkyne on $Cu_2O–C_{16}$. Reprinted with permission from ref. 473. Copyright 2024 American Chemical Society. (b) Reversibility of Pd–PPS interaction and proposed acetylene hydrogenation scheme over Pd/PPS. Reprinted with permission from ref. 474. Copyright 2020 The American Association for the Advancement of Science.

operated at a lower acetylene concentration and a higher H_2/C_2H_2 ratio, particularly at high acetylene conversions, effectively inhibiting the formation of oligomer byproducts.

The choice of the liquid solvent has a significant impact on the performance in liquid phase hydrogenation. A solvent with a higher α value is expected to enhance ethylene selectivity. A typical comparison was made between NMP and decane. Decane exhibited a lower α value of 0.8, meaning that acetylene and ethylene had comparable solubilities in this solvent. As a result, when decane was used as the liquid phase over Pd/SiO_2, the ethylene selectivity remained below 70%, lower than that observed with NMP ($>80\%$, E).[482] ILs exhibited extremely high α values, making them promising candidates for acetylene selective hydrogenation. For instance, 1,3-dimethylimidazolium methylphosphite ([DMIM][$MeHPO_3$]) had an α value of 45, suggesting its potential as an effective liquid solvent. However, [DMIM][$MeHPO_3$] also possessed a high viscosity (363 mPa·s), which was much larger than that of NMP (1.65 mPa s). The high viscosity leaded to severe mass transfer resistance, significantly reducing the overall reaction activity when ILs are directly used as the liquid phase.[462]

Building on the liquid phase hydrogenation process, researchers have further investigated the catalytic performance of different bimetallic catalysts, including PdGa,[486–488] PdFe,[489] PdZn,[490,491] and PdAg.[485,492] It has been reported that the intrinsic selectivity of the bimetallic active sites can be partially combined with the benefits of liquid phase hydrogenation. For example, PdAg/C catalysts exhibited higher ethylene selectivity than PdZn/C and PdGa/C in the liquid phase process.[486,493] However, optimizing the combination of specific catalysts with liquid phase hydrogenation processes requires further study.

7. Conclusions and perspectives

Acetylene selective hydrogenation has undergone extensive development over the past two decades. This review attempts to establish a standardized framework for evaluating catalytic performance and summarizes trends and advances in active site design. Multiple classes of active sites, including monometallic, disordered alloy, IMC, and SA sites, have been strategically engineered to achieve high activity and selectivity. In addition, catalyst supports and modifiers have emerged as effective strategies for enhancing catalytic performance. Despite these advancements, further research is needed to improve both the intrinsic activity and ethylene selectivity of catalysts. Key challenges and future opportunities are discussed below to guide the continued development of efficient catalytic systems for acetylene hydrogenation.

7.1 Reaction mechanism and structure–performance relationship

Understanding the reaction mechanism and structure–performance relationship is crucial for designing high-performance catalysts. However, this remains challenging for acetylene hydrogenation due to difficulty in identifying the true active sites under reaction conditions and the structural evolution of these sites during the reaction. For instance, monometallic Pd active sites may form PdC_x and PdH_x phases under reaction conditions, while certain Pd-based active site structures, such as Pd_1Ga_1 IMC and Pd SA, have been reported to suppress the formation of PdC_x and PdH_x. The Pd species in PdAg catalysts tend to segregate to the surface under reaction conditions, while some IMCs, such as Ni_3Zn, gradually transform into a Ni_3ZnC phase. These structural evolutions can have varying effects on catalytic performance. For example, the formation of the Ni_3ZnC phase has been shown to enhance ethylene selectivity, whereas PdAg segregation may promote side reactions, leading to catalyst deactivation. Therefore, unraveling the real-time structural evolution of active sites under reaction conditions and its correlation with catalytic performance is essential for the rational design of improved catalysts. Furthermore, acetylene hydrogenation involves multiple reaction pathways, each consisting of various elementary steps and intermediate species (Fig. 19). The specific elementary reactions at different active sites require further investigation. A deeper understanding of these aspects will facilitate theoretical modeling and computational studies to elucidate the reaction mechanism, ultimately providing valuable guidance for the design and optimization of catalytic active sites.

In situ characterization technologies play a crucial role in gaining the above-mentioned insights. These techniques have been widely employed to determine the structure of active sites under reaction conditions.[494–496] For instance, *in situ* XANES and EXAFS have been used to investigate carbide formation and decomposition in Pd NPs under different gas atmospheres. It was observed that a mixture of acetylene and hydrogen induced the formation of a hydride phase, whereas exposure to pure acetylene leaded to the decomposition of the hydride phase and rapid formation of carbide species.[497,498] *In situ* TEM revealed that under reaction conditions, Pd(100) facets transformed into stepped facets, resulted in a decline in ethylene selectivity.[499] Surface-sensitive techniques such as *in situ* XPS and *in situ* prompt gamma activation analysis (PGAA) have provided valuable insights into the surface chemical properties of active sites under reaction conditions. These studies demonstrated that PdGa exhibited high stability, effectively inhibiting both alloy segregation and subsurface chemical interactions involving C and/or H atoms, which were phenomena commonly observed in monometallic Pd.[500] Additionally, various *in situ* spectroscopic techniques, including polarization-dependent reflection absorption infrared spectroscopy (RAIRS),[495] diffuse reflectance infrared Fourier transform spectroscopy (DRIFTS),[501] inelastic neutron scattering spectroscopy (INS),[502] and Raman spectroscopy,[503] have been employed to identify reaction intermediates and probe their adsorption geometries on active sites.

DFT calculations serve as a powerful tool for investigating the reaction mechanism of acetylene selective hydrogenation and have been widely applied to elucidate the structure–activity relationships of different active sites (Section 4). However, DFT calculations are inherently limited by their static nature, as they require assumptions about surface structures and reaction

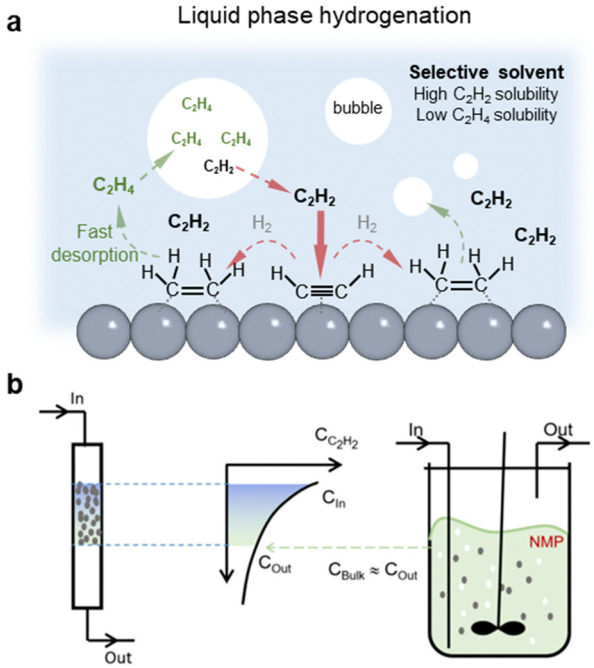

Fig. 22 (a) Schematic illustration of the liquid phase hydrogenation. (b) Reactor models for gas phase (PBR) and liquid phase (CSTR) hydrogenation. Reprinted with permission from ref. 485. Copyright 2024 Elsevier.

mechanisms. In this regard, *in situ* characterization techniques provide crucial information about active site structures and reaction intermediates under realistic conditions, which greatly benefits for constructing more accurate DFT models and reaction pathways. Moreover, DFT calculations should comprehensively consider all possible reaction pathways, especially the C–C coupling reaction pathway. Many DFT studies have primarily focused on the C_2 hydrogenation pathway, which have contributed to understanding the mechanism of ethylene overhydrogenation. However, in many cases, the formation of C–C coupling products is non-negligible and can even constitute the major side reactions. Understanding the oligomerization mechanism is therefore crucial for designing catalysts with high selectivity and stability. It is important to note that the elementary reaction network of C–C coupling is significantly more complex than that of the C_2 hydrogenation pathway. Establishing a simplified yet accurate elementary reaction scheme remains a key challenge in DFT calculations of acetylene hydrogenation. In addition, combining DFT calculations with microkinetic modeling provides a more effective and accurate approach (Section 4.3). By incorporating coverage effects and real reaction conditions, microkinetic models enable the evaluation of intrinsic catalytic performance for different active sites under practical conditions, thereby enhancing the predictive power of DFT calculations.

7.2 Catalyst design for acetylene selective hydrogenation

The ideal catalyst for acetylene selective hydrogenation should efficiently adsorb and activate H_2 and C_2H_2, facilitate the conversion of acetylene to ethylene, and exhibit weak adsorption of ethylene to prevent its over-hydrogenation to ethane.[244] To achieve this, the site isolation concept has been proposed and widely applied in active site design. In this review, the active sites are categorized into monometallic, disordered alloy, IMC, and SA sites (Section 3). The introduction of a secondary metal has proven to be an effective strategy for developing active sites with enhanced ethylene selectivity. Additionally, engineering bimetallic active sites into ordered phases has been demonstrated to modulate the adsorption strength of key intermediates, thereby improving ethylene selectivity. Another critical approach is to maximize the spatial separation of metal centers, forming SA sites, which effectively minimize the side reactions.

A trade-off between activity and selectivity exists due to the linear free energy relationships and BEP scaling on metal surfaces. Achieving higher ethylene selectivity often comes at the cost of reduced hydrogenation activity, as weakening ethylene adsorption also decreases the ability to activate H_2. To overcome the trade-off between activity and selectivity, further efforts are required to design novel active sites. Dual-atom sites and fully exposed atomic sites have been proposed as strategies to retain the site isolation concept while simultaneously providing additional sites for H_2 activation and intermediate stabilization. Additionally, multi-metallic active sites, such as trimetallic IMCs, offer an alternative approach to balancing activity and selectivity. Recently, machine learning (ML) has emerged as a promising tool for catalyst-design and for uncovering the atomic-scale reaction mechanisms of acetylene hydrogenation.[504] The integration of DFT calculations and ML has provided deeper insights into the PdAg catalytic system, guiding the identification of the optimal Pd_1Ag_3 alloy crystal active sites.[287,505] Furthermore, ML has been employed to screen and predict potential single-atom alloys,[506] metal oxides,[507] and Ni-based IMCs[508] for acetylene hydrogenation. ML holds great promise for accelerating the development of highly efficient acetylene hydrogenation catalysts. Further research is necessary to elucidate the reaction mechanisms and establish key catalytic descriptors, particularly for the complex reaction pathways involved in acetylene hydrogenation.

For catalyst active site design, the choice between Pd-based and non-precious metals is also an important consideration. In Section 3, we have summarized the performance of Pd-based and non-Pd-based active sites for acetylene hydrogenation. Non-Pd-based active sites are primarily based on non-precious metals such as Ni and Cu. Pd-based catalysts generally exhibit activities that are more than two orders of magnitude higher than those of non-precious metal catalysts. Additionally, Pd-based catalysts typically offer superior ethylene selectivity and stability compared to Ni- and Cu-based catalysts. However, from the perspective of cost and sustainability, non-precious metal catalysts have significant advantages over Pd-based systems. Although Pd-based catalysts have been widely applied in industrial acetylene hydrogenation, developing advanced non-precious metal catalysts remains a key research direction. For Pd-based active sites, enhancing intrinsic activity and reducing Pd loading, such as through SA or cluster sites, are important strategies, while catalyst stability and

regenerability should be considered. For non-precious metal systems, active site design regarding metal composition and atomic arrangement is essential to improve activity and selectivity, especially by suppressing C–C coupling reactions to achieve long-term stability.

Catalyst performance is also closely related to the support and modifiers (Sections 5 and 6). Supports play a crucial role in stabilizing active sites and providing synergistic effects, while modifiers can enhance catalyst selectivity and stability by tuning the electronic structure of active sites and regulating the local reaction environment. Beyond designing high-performance active sites, optimizing suitable supports and modifiers is essential for further improving catalytic performance and advancing industrial catalyst development. In addition, the development of high-performance catalysts also relies on effective synthesis strategies. For example, traditional impregnation methods often lead to heterogeneous metal distributions in the synthesis of targeted active sites, resulting in a mixture of monometallic species, disordered alloys, and IMC at the nanoscale. Such structural complexity hinders the establishment of a clear structure–activity relationship. Therefore, developing strategies for precise catalyst synthesis to achieve desired active sites with high-phase purity and scalability is crucial for both fundamental mechanistic understanding and catalyst design for industrial applications.

7.3 Effect of feeding composition in acetylene selective hydrogenation

The selective hydrogenation of acetylene is primarily applied in two industrial processes: (1) the removal of trace acetylene impurities in ethylene production *via* naphtha cracking and (2) the hydrogenation of acetylene derived from non-oil alternative resources such as natural gas and coal. It is important to note that the composition of feed gases in these two processes differs significantly (as detailed in Section 2.1 and Table 1). The feed composition has a profound impact on the catalytic performance. For instance, a high concentration of acetylene tends to promote C_4 hydrocarbon formation, while an increased hydrogen concentration can suppress oligomerization to some extent but potentially promotes the side reaction of ethylene over-hydrogenation. Therefore, when developing industrial catalysts, it is crucial to distinguish between the targeted processes and select representative feed compositions accordingly.

In the petrochemical industry, acetylene hydrogenation requires the removal of trace acetylene to a residual concentration below 10 ppm, or even lower, while minimizing ethylene loss. Therefore, an ideal catalyst must achieve an exceptionally high conversion ($>99.5\%$) while preventing ethylene loss as much as possible. When evaluating catalysts under ethylene-rich feed conditions, particular attention should be paid to the benchmarks for selectivity and conversion calculations (Section 2.3). Direct measurement of ethylene concentration changes to calculate ethylene selectivity is not recommended unless isotope labeling experiments are conducted. Given the stringent requirement for acetylene removal, researchers are more concerned with catalyst performance at high acetylene conversions. Due to the challenges in direct calculation of selectivity, it is suggested to evaluate the individual concentration changes of acetylene and ethylene instead (Section 2.3 and Fig. 3). Another critical parameter for catalyst evaluation is the operating window (OW), as a wider OW ensures better catalyst stability at the required temperature for acetylene removal. Currently, industrial catalysts for this process are Pd-based catalysts, with lifespans exceeding one year. To reduce catalyst costs, the development of non-precious metal catalysts or more efficient Pd-based catalysts is of great significance. When developing alternative catalysts, researchers should consider catalyst stability to ensure long-term industrial viability.

For the potential application of acetylene hydrogenation in ethylene production from natural gas or coal, the feed gas is ethylene-free, and the acetylene concentration is significantly higher (Table 1). Most reported catalysts are designed for feeds with acetylene concentration of $\leq 2\%$, whereas higher acetylene concentrations impose more stringent requirements on catalyst performance. Under such conditions, C–C coupling reactions become more pronounced, with selectivity to coupling products exceeding 10%.[38,54,147,159,182] Notably, over monometallic Pd and bimetallic PdCu catalysts, the selectivity to GO can even surpass 40%.[54] Therefore, suppressing C–C coupling reactions remains a major challenge in catalyst development for high-acetylene-concentration hydrogenation. An alternative strategy involves reactor and process design to regulate the actual acetylene concentration adjacent to the catalytic active sites. For example, replacing the PBR with the CSTR can help mitigate high local acetylene concentrations (Fig. 22b). Acetylene hydrogenation in liquid phase reactors has been reported to effectively suppress oligomer formation. Additionally, acetylene hydrogenation is a highly exothermic reaction, and higher acetylene concentrations further intensify heat transfer challenges. Efficient heat removal is essential to maintain catalyst stability and prevent runaway reactions. In this regard, liquid phase hydrogenation offers distinct advantages due to its superior heat transfer properties. Therefore, the development of catalysts tailored for high-acetylene-concentration liquid phase hydrogenation represents a promising research direction.

The gas products derived from partial oxidation (POX) and pyrolysis (PPY) processes contain large amounts of CO and H_2. Direct acetylene hydrogenation under such CO- and H_2-rich conditions can simplify the overall process. CO can effectively inhibit the over-hydrogenation of ethylene to ethane, however, excessive CO concentrations significantly reduce catalyst activity and promote C–C coupling reactions. Additionally, gas products from POX and PPY often contain sulfur species, which are highly toxic to catalysts. Although sulfur species can be removed *via* adsorption or other desulfurization pretreatments, their complete removal significantly increases operational costs. In addition, CO is also often present in the feed that can lead to the poison of metal active sites from competitive adsorption. Therefore, developing high-performance catalysts with tolerance to sulfur and CO is essential for such systems. One effective approach is tuning the intrinsic electronic properties of active sites to enhance sulfur tolerance. For instance,

trace sulfur can actually improve the selectivity of Pd catalysts (as discussed in Section 6.1.1), but maintaining active sites in a sulfur-lean phase, such as Pd_4S, is critical, as excess sulfur can severely poison catalytic activity. Other Pd-based active sites, including Pd_5P_2 and Pd_2Si, have also demonstrated good sulfur tolerance in hydrogenation reactions.[509,510] Furthermore, confinement strategies, such as encapsulating active sites within N-doped graphene shells or zeolites, can effectively prevent sulfur poisoning.[511,512] Future catalyst development for these systems must carefully balance sulfur tolerance with high hydrogenation activity and selectivity. To improve CO tolerance, tailoring the electronic structure of active sites to weaken CO adsorption is critical. Studies have shown that SA sites and tightly coupled metallic Ru–Ni clusters exhibit weakened CO binding, thereby enhancing CO tolerance in hydrogenation.[513,514] From the perspective of balancing the adsorption energies of CO and reactants, combining DFT calculations with ML to screen active sites offers a promising approach.

7.4 Catalyst stability and regeneration for acetylene selective hydrogenation

Catalyst stability plays a crucial role in industrial applications. It is widely accepted that catalyst deactivation during acetylene hydrogenation mainly arises from the formation of GO and coke. A deactivation process has been proposed for monometallic Pd catalysts.[515,516] In the initial stage, light green oil accumulates on the Pd surface, resulting in a slight decline in catalytic activity. As deactivation progresses, 1,3-butadiene undergoes polymerization, forming heavy green oil that blocks catalyst pores and restricts hydrogen diffusion, leading to a substantial loss in activity.

The formation of coke and GO primarily arises from side reactions, including C–C bond cleavage and C–C coupling. Section 3 summarizes how active site design strategies can mitigate these pathways. Since C–C coupling generally requires adjacent active metal sites, one effective approach is to dilute the active metal using secondary metals to adjust active site geometry, thereby suppressing oligomer formation. In multimetallic systems, two typical geometric structures exist: disordered alloys and IMC. Disordered alloy structures tend to feature adjacent active metal sites and, under reaction conditions, active metal segregation can occur at the nanoparticle surface (*e.g.*, in PdAg alloys), limiting their ability to inhibit C–C coupling. In comparison, the ordered arrangement of secondary metals in IMC structures spatially isolates adjacent active sites, providing a unique geometry that effectively suppresses C–C coupling. Another approach is the use of SA structures, which completely eliminate neighbouring active sites. Although both IMC and SA structures geometrically favour the suppression of C–C coupling, active site design must also account for H_2 activation. It is important to recognize that the C_2 path and C–C coupling path are competitive parallel reactions. Insufficient H_2 activation can lead to increased selectivity toward C–C coupling products, as activated C_2H_2 species tend to couple in the absence of adequate hydrogenation sites. Although site isolation is designed to eliminate neighbouring active metal sites and suppress C–C coupling reactions, experimental results showed that a certain extent of oligomerization can still occur, even on IMC or SA sites. The exact reaction mechanism for C–C coupling pathways remains unclear, and interactions between active metal sites and support materials, such as acidic-basic properties, may also contribute to oligomer formation.

Beyond the geometry of active sites, catalyst supports and reaction conditions also play critical roles in determining catalyst stability. Metal oxides are the most widely used supports for acetylene hydrogenation, with Al_2O_3 being commonly employed in industrial PdAg catalysts. It is well established that support acidity promotes C–C coupling reactions; thus, reducing support acidity can enhance catalyst stability. However, this must be balanced against other important support properties, such as surface area, which is crucial for effective metal dispersion. Regarding reaction conditions, the ratio of H_2/C_2H_2 significantly affects catalyst stability. In industrial practice, acetylene hydrogenation is typically performed *via* two main processes: the tail-end and the front-end processes. The front-end process offers better catalyst stability due to a much higher H_2/C_2H_2 ratio compared to the tail-end process.[1,2] For industrial acetylene hydrogenation, these typical reaction compositions are generally fixed by upstream processes and are difficult to adjust. However, for potential applications of acetylene hydrogenation in ethylene production from natural gas or coal, optimizing reaction conditions remains essential for achieving high ethylene selectivity and catalyst stability. While a high H_2/C_2H_2 ratio improves catalyst stability, it also promotes over-hydrogenation of ethylene to ethane. Striking a balance between these factors is a key challenge in future process design. Additionally, the introduction of solvents can help modulate the local concentrations of reactive species near the catalyst surface.

Regeneration is another crucial aspect for the industrial application of catalysts. Under practical reaction conditions, it is nearly impossible to completely avoid the formation of GO and coke. As these deposits accumulate, catalytic activity gradually declines. A common approach to compensate for this decline is to incrementally increase the reaction temperature until catalyst activity drops below acceptable production levels. At that point, catalytic activity is typically restored through high-temperature calcination (up to 350 °C) in an oxygen-rich atmosphere. However, this regeneration process can induce metal sintering, causing irreversible loss of catalytic activity.[517–520] Since sintering originates from the high-temperature hydrothermal environment of regeneration, optimizing the regeneration process and developing milder regeneration conditions remain challenging yet essential for extending catalyst lifetime. Some studies have addressed this by adjusting parameters such as regeneration temperature and O_2/steam feed rates to reduce sintering.[521,522] Others have explored alternative regeneration strategies, such as using supercritical carbon dioxide instead of conventional oxidative treatments.[523,524] It is worth noting that most current regeneration studies focus on the industrially established $PdAg/Al_2O_3$ catalysts. Although the active site design strategies discussed in Section 3 can partially mitigate the formation of GO and coke, the regeneration ability of these advanced catalysts remains relatively

underexplored. Further efforts are needed to evaluate and improve catalyst regeneration performance for broader industrial applications.

7.5 Extension to selective hydrogenation of other alkynes and dienes

Selective hydrogenation is a critical process for removing trace alkynes and dienes from alkene streams to meet polymer-grade requirements (<10 ppm).[525–527] In addition to acetylene hydrogenation for polymer-grade ethylene production, selective hydrogenation is also applied to propyne (for polymer-grade propylene), 1,3-butadiene and butynes (for polymer-grade C4 olefins), and phenylacetylene (for polymer-grade styrene). Similar to acetylene, these alkynes undergo hydrogenation pathways including semi-hydrogenation to target alkenes, over-hydrogenation to alkanes, and side reactions such as C–C coupling to form oligomers.[526,527]

For terminal alkynes such as propyne, 1-butyne, 1-pentyne, and phenylacetylene, the adsorption configurations on active sites are in general analogous to those of acetylene, including end-on (vinyl or vinylidene) and flat-lying (π- or di-σ-bonded) configurations.[1,525] Therefore, the design principles of active sites for acetylene selective hydrogenation should also be applicable to these systems. Catalyst development for terminal alkynes has followed a similar trend, where active sites evolve from monometallic sites to disordered alloy structures, and further to well-defined IMC structures and SA sites. Pd-based systems (*e.g.*, PdAg, PdCu, PdZn) are the most widely investigated,[528–531] among which PdAg catalysts are already industrially employed for propyne removal from propylene-rich streams. IMC catalysts such as Pd_2Ga, which enable electronic and geometric tuning of C≡C and C=C groups adsorption, have shown promising performance in phenylacetylene hydrogenation.[532] To replace precious metal Pd, non-precious metal IMCs such as Ni_1Sb_1 and Ni_3Sn_2 have been developed for propyne hydrogenation, achieving improved propylene selectivity.[533,534] Additionally, the site isolation strategy for constructing SA sites have been effective in suppressing over-hydrogenation and C–C coupling pathways for alkynes hydrogenation.[535–539] While terminal alkynes have mechanistic similarities with acetylene, the effect of substituent groups on the C≡C bond introduces additional complexity. For instance, phenylacetylene, with its bulky phenyl group, exhibits different adsorption behavior from acetylene. DFT calculations revealled that phenylacetylene preferentially adsorbed on top of isolated Pd atoms, whereas acetylene favored bridge sites at the Pd–Ag interface on Pd_1/Ag(111) surfaces.[539]

For 1,3-butadiene selective hydrogenation, the reaction pathway is inherently linked to that of acetylene hydrogenation (Fig. 19), as 1,3-butadiene serves as a key intermediate in the C–C coupling of acetylene, which contributes to the formation of GO. Several catalysts that demonstrated promising performance in acetylene hydrogenation have also been investigated for 1,3-butadiene selective hydrogenation. These include disordered alloy (*e.g.*, PdAg and PdCu)[540–542] and IMC (*e.g.*, Ni_3ZnC and Ni_3In)[543,544] catalysts, which exhibited enhanced 1-butene selectivity. More recently, SA sites engineering has emerged as an effective strategy to further improve 1-butene selectivity.[545–548] The mechanism by which SA sites enhance 1-butene selectivity is largely attributed to the distinct adsorption configurations of 1,3-butadiene. On conventional Pd(111) surfaces, the most stable adsorption configuration for 1,3-butadiene was the 1,2,3,4-tetra-σ mode, in which the molecule interacts with four adjacent Pd atoms.[541] When Pd was maximally isolated into SA sites, the adsorption mode shifted toward mono-π interaction,[546,547] which favored the formation of 1-butene while significantly suppressing its further hydrogenation to butane due to steric hindrance, ultimately leading to improved 1-butene selectivity.[546]

7.6 Emerging alternatives to thermocatalytic acetylene selective hydrogenation

Electrocatalytic and photocatalytic acetylene hydrogenation (EAH and PAH) have recently emerged as promising alternatives to traditional thermocatalytic process. EAH can be conducted in aqueous media using water as the proton source and powered by renewable electricity under ambient conditions.[549,550] PAH utilizes visible light as the energy input and typically employs water or other non-H_2 proton sources.[551–553] PAH has demonstrated exceptionally high ethylene selectivity (≥99%), but still faces significant challenges in terms of overall process efficiency and the production of polymer-grade ethylene.[551–553] Compared with PAH, EAH has been more extensively studied and holds greater potential for replacing traditional thermocatalytic routes in industrial applications.

In addition to conventional performance indicators such as acetylene conversion, ethylene selectivity, and catalyst stability, EAH introduces several electrochemical metrics, including overpotential, current density, and faradaic efficiency (FE), which are critical for evaluating electrocatalytic performance.[550] Besides the typical side reactions of over-hydrogenation and C–C coupling observed in thermocatalysis, EAH faces a unique challenge from the competitive hydrogen evolution reaction (HER), which significantly diminishes the FE toward ethylene ($FE_{C_2H_4}$). For practical and industrial relevance, achieving high $FE_{C_2H_4}$ at elevated current densities is essential. Zhang *et al.* have shown that ethylene production *via* EAH became economically viable when $FE_{C_2H_4}$ exceeded 85% at current densities ≥200 mA cm^{-2}.[554]

EAH was first reported in 1964 using a palladized cathode in an alkaline aqueous solution, demonstrating the feasibility of this approach.[555] However, the inherently low solubility of acetylene in aqueous media limited the performance of early EAH systems operated in batch cell reactors, resulting in low $FE_{C_2H_4}$ (<70%) and restricting operation to low current densities (<3.5 mA cm^{-2}), even when using precious metal-based electrocatalysts such as Pd, Pt, and Ag.[549,555,556] The development of flow cells and membrane electrode assemblies has successfully overcome mass transport limitations caused by poor acetylene solubility, significantly enhancing the feasibility of EAH using water as the proton source. Over the past decade, substantial efforts have been devoted to designing advanced electrocatalysts for EAH in flow-cell configurations.[5,557] Among

them, Cu-based catalysts have received the most attention due to their earth abundance and theoretically predicted suitability for EAH catalysis.[558] Various Cu-based architectures, including Cu dendrites,[559] microparticles,[5] single atoms,[560,561] and nanodots,[562] have been developed to improve EAH performance. For instance, Cu dendrites supported on gas diffusion electrodes achieved a high $FE_{C_2H_4}$ of 97% at −0.7 V *vs.* RHE and an ethylene partial current density of ∼130 mA cm^{-2} under a pure C_2H_2 feed.[559] Cu nanodots have also exhibited excellent performance, delivering a $FE_{C_2H_4}$ of ∼95.9% at −0.15 V *vs.* RHE and current density exceeding 450 mA cm^{-2}.[562] Bimetallic Cu catalysts, such as Cu NP/Fe-NC,[563] Cu–Cd,[564] Cu–Pd,[565] and Cu–Zn,[566] have been explored to tailor adsorption properties. Notably, Zn doping enhanced acetylene adsorption while increasing the *H–*H binding energy barrier, effectively lowering the overpotential and suppressing both hydrogen evolution and over-hydrogenation side reactions.[566] Beyond Cu-based systems, Ni-, Co-, and Ag-based electrocatalysts have also been developed.[567–570] For example, Ag nanocubes exposing (100) facets achieved a high partial current density of 337 mA cm^{-2} at −1.5 V *vs.* RHE, significantly outperforming (111)-facet analogues.[567] Recently, 2-thiolimidazole, a metal-free catalyst, was reported to achieve ethylene partial current density and $FE_{C_2H_4}$ values comparable to those of metal-based systems such as Cu and Pd.[571]

Although significant progress has been made in the development of advanced electrocatalysts for EAH, challenges remain before this technology can be translated into industrial-scale applications. Current research in EAH mainly focuses on two feed conditions: ethylene-rich feeds (aimed at removing trace acetylene impurities) and ethylene-free feeds (targeting ethylene production from acetylene). For ethylene-rich feed conditions, several catalysts have demonstrated the ability to reduce residual acetylene concentrations to below 5 ppm while achieving high $FE_{C_2H_4}$.[559,572] In particular, a membrane flow cell equipped with Cu dendrite catalysts achieved <5 ppm residual acetylene with a specific ethylene selectivity of 97% at a high space velocity of 9.6×10^4 mL g_{cat}^{-1} h^{-1}, comparable to those used in thermocatalysis.[559] However, the current density was relatively low (1.6 mA cm^{-2}), far from the level required for industrial-scale operation. In contrast, industrial current densities have been used under ethylene-free feed conditions.[572,573] For example, a fluorine-modified Cu catalyst achieved a partial current density of up to 760 mA cm^{-2} with an $FE_{C_2H_4}$ exceeding 90% using a 70% C_2H_2/Ar feed.[572] Nevertheless, the acetylene conversion under these conditions remained low (∼32.6%), highlighting the inherent difficulty in simultaneously achieving high ethylene current density and high acetylene conversion. This trade-off is further reflected by the inverse correlation between acetylene concentration and both $FE_{C_2H_4}$ and ethylene partial current density. As the acetylene feeding concentration decreases from 50% to 1%, $FE_{C_2H_4}$ declines from 90% to 20%, while the current density drops from ∼300 to ∼100 mA cm^{-2}.[572] Therefore, significant efforts are still required to develop EAH processes that can simultaneously deliver high activity, ethylene selectivity, and durability under industrially relevant current densities and acetylene conversion. Moreover, the scalable synthesis of high-performance electrocatalysts and the scale-up of electrochemical reactors are critical steps toward the commercial implementation of the EAH technology.[550]

Conflicts of interest

There are no conflicts to declare.

Data availability

No primary research results, software or code have been included and no new data were generated or analysed as part of this review.

Acknowledgements

X. C. L. and T. F. W. acknowledge the support from the National Natural Science Foundation of China (no. 22378224, 22108148, and 22178195). J. G. C. acknowledges support from the United States Department of Energy, Division of Chemical Sciences, Geosciences, & Biosciences, Office of Basic Energy Sciences (contract number DE-SC0012704).

References

1 A. Borodziński and G. C. Bond, *Catal. Rev.*, 2006, **48**, 91–144.
2 A. Borodziński and G. C. Bond, *Catal. Rev.*, 2008, **50**, 379–469.
3 J. Guo, Y. Lei, H. Liu, Y. Li, D. Li and D. He, *Catal. Sci. Technol.*, 2023, **13**, 4045–4063.
4 Y. Gao, L. Neal, D. Ding, W. Wu, C. Baroi, A. M. Gaffney and F. Li, *ACS Catal.*, 2019, **9**, 8592–8621.
5 S. H. Wang, K. Uwakwe, L. Yu, J. Y. Ye, Y. Z. Zhu, J. T. Hu, R. X. Chen, Z. Zhang, Z. Y. Zhou, J. F. Li, Z. X. Xie and D. H. Deng, *Nat. Commun.*, 2021, **12**, 7072.
6 E. Morais, F. Cameli, G. D. Stefanidis and A. Bogaerts, *EES Catal.*, 2025, **3**, 475–487.
7 M. Krajčí and J. Hafner, *ChemCatChem*, 2016, **8**, 34–48.
8 X. Deng, J. Wang, N. Guan and L. Li, *Cell Rep. Phys. Sci.*, 2022, **3**, 101017.
9 G. Tiwari, S. Sarkar and B. R. Jagirdar, *ChemCatChem*, 2024, **16**, e202400586.
10 L. Zhang, J. Lin, Z. Liu and J. Zhang, *Sci. China: Chem.*, 2023, **66**, 1963–1974.
11 Y. Liu, T. Wang, Q. Li and D. Wang, *Chin. J. Chem. Eng.*, 2011, **19**, 424–433.
12 B. Yan, Y. Cheng, Y. Jin and C. Y. Guo, *Fuel Process. Technol.*, 2012, **100**, 1–10.
13 A. Dasgupta, H. R. He, R. S. Gong, S. L. Shang, E. K. Zimmerer, R. J. Meyer, Z. K. Liu, M. J. Janik and R. M. Rioux, *Nat. Chem.*, 2022, **14**, 523.

14 J. Osswald, R. Giedigkeit, R. E. Jentoft, M. Armbrüster, F. Girgsdies, K. Kovnir, T. Ressler, Y. Grin and R. Schlögl, *J. Catal.*, 2008, **258**, 210–218.
15 M. Ruta, N. Semagina and L. Kiwi-Minsker, *J. Phys. Chem. C*, 2008, **112**, 13635–13641.
16 Y. N. Li and B. W. L. Jang, *Appl. Catal., A*, 2011, **392**, 173–179.
17 J. T. Feng, X. Y. Ma, Y. F. He, D. G. Evans and D. Q. Li, *Appl. Catal., A*, 2012, **413**, 10–20.
18 Y. F. He, J. T. Feng, Y. Y. Du and D. Q. Li, *ACS Catal.*, 2012, **2**, 1703–1710.
19 A. E. Yarulin, R. M. Crespo-Quesada, E. V. Egorova and L. L. K. Minsker, *Kinet. Catal.*, 2012, **53**, 253–261.
20 S. K. Kim, C. Kim, J. H. Lee, J. Kim, H. Lee and S. H. Moon, *J. Catal.*, 2013, **306**, 146–154.
21 M. Crespo-Quesada, S. Yoon, M. S. Jin, Y. N. Xia, A. Weidenkaff and L. Kiwi-Minsker, *ChemCatChem*, 2014, **6**, 767–771.
22 L. P. L. Gonçalves, J. G. Wang, S. Vinati, E. Barborini, X. K. Wei, M. Heggen, M. Franco, J. P. S. Sousa, D. Y. Petrovykh, O. Soares, K. Kovnir, J. Akola and Y. V. Kolen'ko, *Int. J. Hydrogen Energy*, 2020, **45**, 1283–1296.
23 I. T. Ellis, E. H. Wolf, G. Jones, B. Lo, M. M. J. Li, A. P. E. York and S. C. E. Tsang, *Chem. Commun.*, 2017, **53**, 601–604.
24 Q. Q. Guan, J. Zhang, L. He, R. R. Miao, Y. Z. Shi and P. Ning, *ACS Sustainable Chem. Eng.*, 2020, **8**, 11638–11648.
25 L. D. Shao, B. S. Zhang, W. Zhang, D. Teschner, F. Girgsdies, R. Schlögl and D. S. Su, *Chem. – Eur. J.*, 2012, **18**, 14962–14966.
26 T. X. Yang, M. Zhao, X. Wang, R. Ma, Y. A. Liu, Y. F. He and D. Q. Li, *Catal. Lett.*, 2022, **152**, 227–238.
27 H. Chen, Z. N. Yu, B. Yang, Y. F. Zhang, C. X. Che, X. Y. Liu, F. Zhang, W. Han, H. Wen, A. Q. Wang and T. Zhang, *Chin. J. Catal.*, 2024, **60**, 190–200.
28 A. Pachulski, R. Schödel and P. Claus, *Appl. Catal., A*, 2011, **400**, 14–24.
29 J. H. Lee, S. K. Kim, I. Y. Ahn, W. J. Kim and S. H. Moon, *Catal. Commun.*, 2011, **12**, 1251–1254.
30 J. H. Lee, S. K. Kim, I. Y. Ahn, W. J. Kim and S. H. Moon, *Korean J. Chem. Eng.*, 2012, **29**, 169–172.
31 Y. X. Han, D. Peng, Z. Y. Xu, H. Q. Wan, S. R. Zheng and D. Q. Zhu, *Chem. Commun.*, 2013, **49**, 8350–8352.
32 Y. Y. Zhang, W. J. Diao, J. R. Monnier and C. T. Williams, *Catal. Sci. Technol.*, 2015, **5**, 4123–4132.
33 M. Kuhn, M. Lucas and P. Claus, *Ind. Eng. Chem. Res.*, 2015, **54**, 6683–6691.
34 Y. F. He, Y. N. Liu, P. F. Yang, Y. Y. Du, J. T. Peng, X. Z. Cao, J. Yang and D. Q. Li, *J. Catal.*, 2015, **330**, 61–70.
35 R. Ma, Y. F. He, J. T. Feng, Z. Y. Hu, G. Van Tendeloo and D. Q. Li, *J. Catal.*, 2019, **369**, 440–449.
36 D. V. Glyzdova, T. N. Afonasenko, E. V. Khramov, N. N. Leont'eva, M. V. Trenikhin, A. M. Kremneva and D. A. Shlyapin, *Mol. Catal.*, 2021, **511**, 111717.
37 J. A. Delgado, O. Benkirane, S. Lachaux, C. Claver, J. Ferré, D. Curulla-Ferré and C. Godard, *ChemNanoMat*, 2022, **8**, e202200058.
38 K. S. Kley, J. De Bellis and F. Schueth, *Catal. Sci. Technol.*, 2023, **13**, 119–131.
39 W. Huang, W. Pyrz, R. F. Lobo and J. G. G. Chen, *Appl. Catal., A*, 2007, **333**, 254–263.
40 S. K. Kim, J. H. Lee, I. Y. Ahn, W. J. Kim and S. H. Moon, *Appl. Catal., A*, 2011, **401**, 12–19.
41 A. J. McCue, C. J. McRitchie, A. M. Shepherd and J. A. Anderson, *J. Catal.*, 2014, **319**, 127–135.
42 A. J. McCue, A. M. Shepherd and J. A. Anderson, *Catal. Sci. Technol.*, 2015, **5**, 2880–2890.
43 A. J. McCue and J. A. Anderson, *J. Catal.*, 2015, **329**, 538–546.
44 Y. N. Liu, Y. F. He, D. R. Zhou, J. T. Feng and D. Q. Li, *Catal. Sci. Technol.*, 2016, **6**, 3027–3037.
45 M. R. Ball, K. R. Rivera-Dones, E. B. Gilcher, S. F. Ausman, C. W. Hullfish, E. A. Lebrón and J. A. Dumesic, *ACS Catal.*, 2020, **10**, 8567–8581.
46 S. Y. Liu, Y. M. Niu, Y. Z. Wang, J. N. Chen, X. P. Quan, X. Zhang and B. S. Zhang, *Chem. Commun.*, 2020, **56**, 6372–6375.
47 S. Wang, J. Zhu, J. Q. Si, G. F. Zhao, Y. Liu and Y. Lu, *J. Catal.*, 2020, **382**, 295–304.
48 T. X. Yang, Y. L. Feng, R. Ma, Q. Li, H. Yan, Y. N. Liu, Y. F. He, J. T. Miller and D. Q. Li, *ACS Appl. Mater. Interfaces*, 2021, **13**, 706–716.
49 F. Xue, Q. Li, M. X. Lv, S. X. Weng, T. Y. Li, Y. Ren, Y. N. Liu, D. Q. Li, Y. F. He, Q. H. Li, X. Chen, Q. H. Zhang, L. Gu, J. X. Deng, J. Chen, L. H. He, X. J. Kuang, J. Miao, Y. L. Cao, K. Lin and X. R. Xing, *Nano Lett.*, 2024, **24**, 6269–6277.
50 X. Pei, D. Zhang, R. Tang, S. Wang, C. Zhang, W. Yuan and W. Sun, *Nanoscale*, 2024, **16**, 12411–12419.
51 M. Friedrich, S. A. Villaseca, L. Szentmiklósi, D. Teschner and M. Armbrüster, *Materials*, 2013, **6**, 2958–2977.
52 S. Liu, Y. Li, X. J. Yu, S. B. Han, Y. Zhou, Y. Q. Yang, H. Zhang, Z. Jiang, C. W. Zhu, W. X. Li, C. Wöll, Y. M. Wang and W. J. Shen, *Nat. Commun.*, 2022, **13**, 4559.
53 Q. Gao, Z. H. Yan, W. J. Zhang, H. S. Pillai, B. Q. Yao, W. J. Zang, Y. Q. Liu, X. Han, B. Min, H. Zhou, L. Ma, B. Anaclet, S. Zhang, H. L. Xin, Q. He and H. Y. Zhu, *J. Am. Chem. Soc.*, 2023, **145**, 19961–19968.
54 J. Pei, Y. Xu, Q. Yang and R. Hou, *Catal. Sci. Technol.*, 2024, **14**, 3638–3651.
55 F. Xue, Q. Li, W. H. Ji, M. X. Lv, H. K. Xu, J. R. Zeng, T. Y. Li, Y. Ren, L. H. Zhou, X. Chen, J. X. Deng, K. Lin and X. R. Xing, *Chem. Sci.*, 2024, **15**, 11837–11846.
56 C. Ma, Y. Y. Du, J. T. Feng, X. Z. Cao, J. Yang and D. Q. Li, *J. Catal.*, 2014, **317**, 263–271.
57 S. Zhang, C. Y. Chen, B. W. L. Jang and A. M. Zhu, *Catal. Today*, 2015, **256**, 161–169.
58 A. J. McCue, R. T. Baker and J. A. Anderson, *Faraday Discuss.*, 2016, **188**, 499–523.
59 J. T. Feng, Y. N. Liu, M. Yin, Y. F. He, J. Y. Zhao, J. H. Sun and D. Q. Li, *J. Catal.*, 2016, **344**, 854–864.
60 T. Sun, B. Ge, S. Huang, X. Wang, Y. Tian, X. Cai, W. Ding and Y. Zhu, *Angew. Chem., Int. Ed.*, 2025, **64**, e202420274.

61 I. S. Mashkovskii, O. P. Tkachenko, G. N. Baeva and A. Y. Stakheev, *Kinet. Catal.*, 2009, **50**, 768–774.
62 D. V. Glyzdova, T. N. Afonasenko, E. V. Khramov, N. N. Leont'eva, M. V. Trenikhin, I. P. Prosvirin, A. V. Bukhtiyarov and D. A. Shlyapin, *Top. Catal.*, 2020, **63**, 139–151.
63 E. Esmaeili, A. M. Rashidi, Y. Mortazavi, A. A. Khodadadi and M. Rashidzadeh, *J. Energy Chem.*, 2013, **22**, 717–725.
64 W. G. Menezes, L. Altmann, V. Zielasek, K. Thiel and M. Bäumer, *J. Catal.*, 2013, **300**, 125–135.
65 R. Ma, T. X. Yang, J. H. Sun, Y. F. He, J. T. Feng, J. T. Miller and D. Q. Li, *Chem. Eng. Sci.*, 2019, **210**, 115216.
66 D. V. Yurpalova, T. N. Afonasenko, I. P. Prosvirin, A. V. Bukhtiyarov, M. A. Panafidin, Z. S. Vinokurov, M. V. Trenikhin, E. Y. Gerasimov, T. I. Gulyaeva, L. M. Kovtunova and D. A. Shlyapin, *Catalysts*, 2023, **13**, 735.
67 E. Esmaeili, Y. Mortazavi, A. A. Khodadadi, A. M. Rashidi and M. Rashidzadeh, *Appl. Surf. Sci.*, 2012, **263**, 513–522.
68 L. Y. Zhao, Z. Wei, M. Y. Zhu and B. Dai, *J. Ind. Eng. Chem.*, 2012, **18**, 45–48.
69 Y. F. He, L. L. Liang, Y. N. Liu, J. T. Feng, C. Ma and D. Q. Li, *J. Catal.*, 2014, **309**, 166–173.
70 Q. Jin, Y. F. He, M. Y. Miao, C. Y. Guan, Y. Y. Du, J. T. Feng and D. Q. Li, *Appl. Catal., A*, 2015, **500**, 3–11.
71 Y. Q. Cao, Z. J. Sui, Y. Zhu, X. G. Zhou and D. Chen, *ACS Catal.*, 2017, **7**, 7835–7846.
72 D. Melnikov, V. Stytsenko, E. Saveleva, M. Kotelev, V. Lyubimenko, E. Ivanov, A. Glotov and V. Vinokurov, *Catalysts*, 2020, **10**, 624.
73 H. Q. Kang, J. Z. Wu, B. H. Lou, Y. Wang, Y. L. Zhao, J. J. Liu, S. H. Zou and J. Fan, *Molecules*, 2023, **28**, 2335.
74 Y. Chen, P. Ning, R. R. Miao, Y. Z. Shi, L. He and Q. Q. Guan, *New J. Chem.*, 2020, **44**, 20812–20822.
75 J. Osswald, K. Kovnir, M. Armbrüster, R. Giedigleit, R. E. Jentoft, U. Wild, Y. Grin and R. Schlögl, *J. Catal.*, 2008, **258**, 219–227.
76 M. Armbrüster, K. Kovnir, M. Behrens, D. Teschner, Y. Grin and R. Schlögl, *J. Am. Chem. Soc.*, 2010, **132**, 14745–14747.
77 A. Ota, M. Armbrüster, M. Behrens, D. Rosenthal, M. Friedrich, I. Kasatkin, F. Girgsdies, W. Zhang, R. Wagner and R. Schlögl, *J. Phys. Chem. C*, 2011, **115**, 1368–1374.
78 M. Armbrüster, G. Wowsnick, M. Friedrich, M. Heggen and R. Cardoso-Gil, *J. Am. Chem. Soc.*, 2011, **133**, 9112–9118.
79 M. Siebert, R. R. Zimmermann, M. Armbrüster and R. Dittmeyer, *ChemCatChem*, 2017, **9**, 3733–3742.
80 R. R. Zimmermann, M. Siebert, S. Ibrahimkutty, R. Dittmeyer and M. Armbrüster, *Z. Anorg. Allg. Chem.*, 2020, **646**, 1218–1226.
81 Y. M. Niu, Y. Z. Wang, J. N. Chen, S. Y. Li, X. Huang, M. G. Willinger, W. Zhang, Y. F. Liu and B. S. Zhang, *Sci. Adv.*, 2022, **8**, eabq5751.
82 Y. Luo, S. A. Villaseca, M. Friedrich, D. Teschner, A. Knop-Gericke and M. Armbrüster, *J. Catal.*, 2016, **338**, 265–272.
83 Q. C. Feng, S. Zhao, Y. Wang, J. C. Dong, W. X. Chen, D. S. He, D. S. Wang, J. Yang, Y. M. Zhu, H. L. Zhu, L. Gu, Z. Li, Y. X. Liu, R. Yu, J. Li and Y. D. Li, *J. Am. Chem. Soc.*, 2017, **139**, 7294–7301.
84 X. H. Ge, Y. Q. Cao, K. L. Yan, Y. R. Li, L. H. Zhou, S. Dai, J. Zhang, X. Q. Gong, G. Qian, X. G. Zhou, W. K. Yuan and X. Z. Duan, *Angew. Chem., Int. Ed.*, 2022, **61**, e202215225.
85 Q. L. Wu, C. Y. Shen, K. H. Sun, M. H. Liu and C. J. Liu, *Chem. Eng. J.*, 2024, **486**, 150333.
86 H. R. Zhou, X. F. Yang, L. Li, X. Y. Liu, Y. Q. Huang, X. L. Pan, A. Q. Wang, J. Li and T. Zhang, *ACS Catal.*, 2016, **6**, 1054–1061.
87 X. X. Cao, R. J. Tong, S. Y. Tang, B. L. Jang, A. Mirjalili, J. Y. Li, X. N. Guo, J. Y. Zhang, J. X. Hu and X. Meng, *Molecules*, 2022, **27**, 5736.
88 H. Chen, L. L. Li, Z. J. Zhao, B. Yang, Y. F. Zhang, X. Y. Liu, Q. Q. Gu, Z. N. Yu, X. F. Yang, J. L. Gong, A. Q. Wang and T. Zhang, *Nat. Commun.*, 2024, **15**, 9850.
89 I. G. Aviziotis, A. Götze, F. Göhler, H. Kohlmann and M. Armbrüster, *Z. Anorg. Allg. Chem.*, 2018, **644**, 1777–1781.
90 B. H. Lou, H. Q. Kang, W. T. Yuan, L. Ma, W. X. Huang, Y. Wang, Z. Jiang, Y. H. Du, S. H. Zou and J. Fan, *ACS Catal.*, 2021, **11**, 6073–6080.
91 W. Q. Zhang, X. B. Zhang, J. Y. Wang, A. Ghosh, J. Zhu, N. J. LiBretto, G. H. Zhang, A. K. Datye, W. Liu and J. T. Miller, *ACS Catal.*, 2022, **12**, 10531–10545.
92 R. Li, Y. Yue, Z. Chen, X. Chen, S. Wang, Z. Jiang, B. Wang, Q. Xu, D. Han and J. Zhao, *Appl. Catal., B*, 2020, **279**, 119348.
93 Y. N. Liu, A. J. McCue, C. L. Miao, J. T. Feng, D. Q. Li and J. A. Anderson, *J. Catal.*, 2018, **364**, 406–414.
94 O. Matselko, R. R. Zimmermann, A. Ormeci, U. Burkhardt, R. Gladyshevskii, Y. Grin and M. Armbrüster, *J. Phys. Chem. C*, 2018, **122**, 21891–21896.
95 Q. Guo, R. T. Chen, J. P. Guo, C. Qin, Z. T. Xiong, H. X. Yan, W. B. Gao, Q. J. Pei, A. A. Wu and P. Chen, *J. Am. Chem. Soc.*, 2021, **143**, 20891–20897.
96 X. H. Huang, Y. J. Xia, Y. J. Cao, X. S. Zheng, H. B. Pan, J. F. Zhu, C. Ma, H. W. Wang, J. J. Li, R. You, S. Q. Wei, W. X. Huang and J. L. Lu, *Nano Res.*, 2017, **10**, 1302–1312.
97 F. Huang, Y. C. Deng, Y. L. Chen, X. B. Cai, M. Peng, Z. M. Jia, P. J. Ren, D. Q. Xiao, X. D. Wen, N. Wang, H. Y. Liu and D. Ma, *J. Am. Chem. Soc.*, 2018, **140**, 13142–13146.
98 X. H. Huang, H. Yan, L. Huang, X. H. Zhang, Y. Lin, J. J. Li, Y. J. Xia, Y. F. Ma, Z. H. Sun, S. G. Wei and J. L. Lu, *J. Phys. Chem. C*, 2019, **123**, 7922–7930.
99 S. J. Wei, A. Li, J. C. Liu, Z. Li, W. X. Chen, Y. Gong, Q. H. Zhang, W. C. Cheong, Y. Wang, L. R. Zheng, H. Xiao, C. Chen, D. S. Wang, Q. Peng, L. Gu, X. D. Han, J. Li and Y. D. Li, *Nat. Nanotechnol.*, 2018, **13**, 856.
100 Q. C. Feng, S. Zhao, Q. Xu, W. X. Chen, S. B. Tian, Y. Wang, W. S. Yan, J. Luo, D. S. Wang and Y. D. Li, *Adv. Mater.*, 2019, **31**, 1901024.
101 M. C. Hu, Z. Y. Wu, Z. H. Yao, J. S. Young, L. L. Luo, Y. G. Du, C. M. Wang, Z. Iqbal and X. Q. Wang, *J. Catal.*, 2021, **395**, 46–53.
102 F. Huang, M. Peng, Y. L. Chen, X. B. Cai, X. T. Qin, N. Wang, D. Q. Xiao, L. Jin, G. Q. Wang, X. D. Wen,

H. Y. Liu and D. Ma, *J. Am. Chem. Soc.*, 2022, **144**, 18485–18493.
103 S. J. Wei, X. W. Liu, C. Wang, X. C. Liu, Q. H. Zhang and Z. Li, *ACS Nano*, 2023, **17**, 14831–14839.
104 R. R. Li, Y. X. Yue, X. L. Chen, R. Q. Chang, J. X. Zhang, B. Zhao, J. Y. Zhang, D. Cai, Y. H. Zhu, D. M. Han, J. Zhao and X. N. A. Li, *Nano Res.*, 2023, **16**, 6167–6177.
105 S. Q. Zhou, L. Shang, Y. X. Zhao, R. Shi, G. I. N. Waterhouse, Y. C. Huang, L. R. Zheng and T. R. Zhang, *Adv. Mater.*, 2019, **31**, 1900509.
106 Q. H. Li, S. J. Liu, J. C. Liu, Z. Li and Y. D. Li, *J. Am. Chem. Soc.*, 2024, **147**, 5615–5623.
107 Y. Zeng, M. Q. Xia, F. J. Gao, C. K. Zhou, X. Y. Cheng, L. W. Liu, L. Jiao, Q. Wu, X. Z. Wang, L. J. Yang, Y. N. Fan and Z. Hu, *Nano Res.*, 2024, **17**, 8243–8249.
108 H. R. Zhou, X. F. Yang, A. Q. Wang, S. Miao, X. Y. Liu, X. L. Pan, Y. Su, L. Li, Y. Tan and T. Zhang, *Chin. J. Catal.*, 2016, **37**, 692–699.
109 C. Qin, Q. Guo, J. P. Guo and P. Chen, *Chem. – Asian J.*, 2021, **16**, 1225–1228.
110 Y. L. Guo, H. F. Qi, Y. Su, Q. K. Jiang, Y. T. Cui, L. Li and B. T. Qiao, *ChemNanoMat*, 2021, **7**, 526–529.
111 R. J. Gao, J. S. Xu, J. Wang, J. Lim, C. Peng, L. Pan, X. W. Zhang, H. M. Yang and J. J. Zou, *J. Am. Chem. Soc.*, 2022, **144**, 573–581.
112 X. Tao, B. Nan, Y. A. Li, M. Du, L. L. Guo, C. Tian, L. Z. Jiang, L. Shen, N. N. Sun and L. N. Li, *ACS Appl. Energy Mater.*, 2022, **5**, 10385–10390.
113 Y. L. Guo, Y. Y. Li, X. R. Du, L. Li, Q. K. Jiang and B. T. Qiao, *Nano Res.*, 2022, **15**, 10037–10043.
114 G. X. Pei, X. Y. Liu, A. Q. Wang, L. Li, Y. Q. Huang, T. Zhang, J. W. Lee, B. W. L. Jang and C. Y. Mou, *New J. Chem.*, 2014, **38**, 2043–2051.
115 G. X. Pei, X. Y. Liu, A. Q. Wang, A. F. Lee, M. A. Isaacs, L. Li, X. L. Pan, X. F. Yang, X. D. Wang, Z. J. Tai, K. Wilson and T. Zhang, *ACS Catal.*, 2015, **5**, 3717–3725.
116 G. X. Pei, X. Y. Liu, X. F. Yang, L. L. Zhang, A. Q. Wang, L. Li, H. Wang, X. D. Wang and T. Zhang, *ACS Catal.*, 2017, **7**, 1491–1500.
117 M. Q. Zhong, J. F. Zhao, Y. X. Fang, D. F. Wu, L. N. Zhang, C. C. Du, S. X. Liu, S. F. Yang, S. L. Wan, Y. B. Jiang, J. Y. Huang and H. F. Xiong, *Appl. Catal., A*, 2023, **662**, 119288.
118 X. J. Xu, Q. Wang, L. L. Xie, Y. N. Liu, D. Q. Li, J. T. Feng and X. Duan, *AIChE J.*, 2023, **69**, e18042.
119 S. X. Liu, D. F. Wu, F. Yang, K. Chen, Z. B. Luo, J. W. Li, Z. Zhang, J. F. Zhao, L. N. Zhang, Y. C. Zhang, H. L. Zhang, S. L. Wan, Y. K. Peng, K. H. L. Zhang and H. F. Xiong, *Chem. Eng. J.*, 2024, **481**, 113043.
120 S. S. Chai, D. L. Gao, J. Xia, Y. P. Yang and X. Wang, *ChemCatChem*, 2023, **15**, e202300217.
121 M. S. Sun, F. M. Wang, G. J. Lv and X. B. Zhang, *Ind. Eng. Chem. Res.*, 2022, **61**, 13341–13353.
122 X. H. Ge, Y. D. Jing, N. N. Fei, K. L. Yan, Y. J. Liang, Y. Q. Cao, J. Zhang, G. Qian, L. N. Li, H. Jiang, X. G. Zhou, W. K. Yuan and X. Z. Duan, *Angew. Chem., Int. Ed.*, 2024, **63**, e202410979.
123 I. S. Mashkovsky, A. V. Bukhtiyarov, P. V. Markov, G. O. Bragina, G. N. Baeva, N. S. Smirnova, M. A. Panafidin, I. A. Chetyrin, E. Y. Gerasimov, Y. V. Zubavichus and A. Y. Stakheev, *Appl. Surf. Sci.*, 2025, **681**, 161516.
124 L. Y. Xu, Y. X. Qin, Q. J. Zhang, J. Zhou, J. Zhao, F. Feng, T. L. Sun, X. L. Xu, Y. H. Zhu, C. S. Lu, Q. F. Zhang, Q. T. Wang and X. N. Li, *Chem. Eng. J.*, 2024, **495**, 150582.
125 Y. W. Liu, B. X. Wang, Q. Fu, W. Liu, Y. Wang, L. Gu, D. S. Wang and Y. D. Li, *Angew. Chem., Int. Ed.*, 2021, **60**, 22522–22528.
126 W. Ru, Y. N. Liu, B. Fu, F. Z. Fu, J. T. Feng and D. Q. Li, *Small*, 2022, **18**, 2103852.
127 S. P. Ding, Y. L. Guo, M. J. Hülsey, B. Zhang, H. Asakura, L. M. Liu, Y. Han, M. Gao, J. Y. Hasegawa, B. T. Qiao, T. Zhang and N. Yan, *Chem*, 2019, **5**, 3207–3219.
128 M. Z. Hu, J. Zhang, W. Zhu, Z. Chen, X. Gao, X. J. Du, J. W. Wan, K. B. Zhou, C. Chen and Y. D. Li, *Nano Res.*, 2018, **11**, 905–912.
129 W. W. Zhang, K. Uwakwe, J. T. Hu, Y. Wei, J. T. Zhu, W. Zhou, C. Ma, L. Yu, R. Huang and D. H. Deng, *Nat. Commun.*, 2024, **15**, 9457.
130 Y. Azizi, C. Petit and V. Pitchon, *J. Catal.*, 2008, **256**, 338–344.
131 A. Sárkány, Z. Schay, K. Frey, É. Széles and I. Sajó, *Appl. Catal., A*, 2010, **380**, 133–141.
132 X. Y. Liu, C. Y. Mou, S. Lee, Y. N. Li, J. Secrest and B. W. L. Jang, *J. Catal.*, 2012, **285**, 152–159.
133 X. L. Yan, J. Wheeler, B. Jang, W. Y. Lin and B. R. Zhao, *Appl. Catal., A*, 2014, **487**, 36–44.
134 H. R. Zhou, B. X. Li, Y. X. Zhang, X. Y. Yan, W. X. Lv, X. B. Wang, B. B. Yuan, Y. Liu, Z. X. Yang and X. D. Lou, *ACS Appl. Mater. Interfaces*, 2021, **13**, 40429–40440.
135 Y. Zhang, X. Sun, Y. L. Zhao, H. J. Su, T. Murayama and C. X. Qi, *Top. Catal.*, 2021, **64**, 197–205.
136 X. Y. Hua, Y. H. Zheng, Z. X. Yang, L. B. Sun, H. J. Su, T. Murayama and C. X. Qi, *Top. Catal.*, 2021, **64**, 206–214.
137 X. L. Yan, J. H. Bao, C. Yuan, J. Wheeler, W. Y. Lin, R. F. Li and B. W. L. Jang, *J. Catal.*, 2016, **344**, 194–201.
138 S. Z. Zhou, L. H. Kang, Z. Xu and M. Y. Zhu, *RSC Adv.*, 2020, **10**, 1937–1945.
139 Z. Xu, S. Z. Zhou and M. Y. Zhu, *Catal. Commun.*, 2021, **149**, 106241.
140 J. Y. Zhao, L. He, J. D. Yu, Y. Z. Shi, R. R. Miao, Q. Q. Guan and P. Ning, *New J. Chem.*, 2021, **45**, 1054–1062.
141 C. Y. Lu, A. N. Zeng, Y. Wang and A. J. Wang, *ACS Omega*, 2021, **6**, 3363–3371.
142 C. Y. Lu, A. N. Zeng, Y. Wang and A. J. Wang, *Eur. J. Inorg. Chem.*, 2021, 997–1004.
143 C. Y. Lu, Y. Wang, R. G. Zhang, B. J. Wang and A. J. Wang, *ACS Appl. Mater. Interfaces*, 2020, **12**, 46027–46036.
144 D. L. Trimm, N. W. Cant and I. O. Y. Liu, *Catal. Today*, 2011, **178**, 181–186.
145 Y. J. Chen and J. X. Chen, *Appl. Surf. Sci.*, 2016, **387**, 16–27.
146 G. X. Pei, X. Y. Liu, A. Wang, Y. Su, L. Li and T. Zhang, *Appl. Catal., A*, 2017, **545**, 90–96.

147 Q. Y. Li, Y. X. Wang, G. Skoptsov and J. L. Hu, *Ind. Eng. Chem. Res.*, 2019, **58**, 20620–20629.
148 Z. Wang, G. Wang, C. Louis and L. Delannoy, *Res. Chem. Intermed.*, 2021, **47**, 91–116.
149 H. D. Yao, L. Y. Pan, L. W. Cui, J. F. Wang, X. Y. Wu, H. Y. Wang, Z. C. Na, D. Li and W. H. Li, *Appl. Surf. Sci.*, 2024, **648**, 159079.
150 L. Wang, F. X. Li, Y. J. Chen and J. X. Chen, *J. Energy Chem.*, 2019, **29**, 40–49.
151 D. Wang, R. Ye, C. Zhang, C. Jin, Z.-H. Lu, M. Shakouri, B. Han, T. Wang, Y. Zhang, R. Zhang, Y. Hu, J. Zhou and G. Feng, *Energy Fuels*, 2023, **37**, 13305–13318.
152 C. Zhang, L. X. Wu, R. P. Ye, G. Feng and R. B. Zhang, *Catal. Lett.*, 2024, **154**, 3619–3627.
153 X. M. Sun, R. D. Wu, M. A. Nawaz, S. Meng, T. Guan, C. Zhang, C. Y. Sun, Z. H. Lu, R. B. Zhang, G. Feng and R. P. Ye, *Inorg. Chem.*, 2024, **63**, 24313–24330.
154 Y. F. Song, S. X. Weng, F. Xue, A. J. McCue, L. R. Zheng, Y. F. He, J. T. Feng, Y. A. Liu and D. Q. Li, *ACS Catal.*, 2023, **13**, 1952–1963.
155 Y. N. Liu, J. Y. Zhao, J. T. Feng, Y. F. He, Y. Y. Du and D. Q. Li, *J. Catal.*, 2018, **359**, 251–260.
156 N. M. Hu, C. H. Yang, L. He, Q. Q. Guan and R. R. Miao, *New J. Chem.*, 2019, **43**, 18120–18125.
157 H. Liu, M. Q. Chai, G. X. Pei, X. Y. Liu, L. Li, L. L. Kang, A. Q. Wang and T. Zhang, *Chin. J. Catal.*, 2020, **41**, 1099–1108.
158 S. Z. Zhou, L. H. Kang, X. N. Zhou, Z. Xu and M. Y. Zhu, *Nanomaterials*, 2020, **10**, 509.
159 S. Hu, C. Zhang, M. Y. Wu, R. P. Ye, D. P. Shi, M. J. Li, P. Zhao, R. B. Zhang and G. Feng, *Catalysts*, 2022, **12**, 1072.
160 Z. W. Li, J. P. Zhang, J. M. Tian, K. Feng, Z. Jiang and B. H. Yan, *Chem. Eng. J.*, 2022, **450**, 138244.
161 S. H. Zhou, C. Y. Lu, Y. Bi, C. L. Zhou, Q. Li, L. X. Tan and L. C. Dong, *Chem. Eng. J.*, 2023, **476**, 146594.
162 C. X. Jin, P. Gao, S. W. Zhou, Y. X. Yue, S. S. Wang, R. Q. Chang, C. Y. Li, T. L. Sun, S. P. Zhang, Y. H. Cai, Y. H. Zhu, J. Zhao and X. N. Li, *Chem. Eng. J.*, 2025, **507**, 160617.
163 S. A. Nikolaev, V. V. Smirnov, A. Y. Vasil'kov and V. L. Podshibikhin, *Kinet. Catal.*, 2010, **51**, 375–379.
164 M. Q. Chai, X. Y. Liu, L. Li, G. X. Pei, Y. J. Ren, Y. Su, H. K. Cheng, A. Q. Wang and T. Zhang, *Chin. J. Catal.*, 2017, **38**, 1338–1346.
165 O. B. Ayodele, T. D. Shittu, O. S. Togunwa, D. Yu and Z. Y. Tian, *Chem. Eng. J.*, 2024, **479**, 147496.
166 O. B. Ayodele, R. S. Cai, J. G. Wang, Y. Ziouani, Z. F. Liang, M. C. Spadaro, K. Kovnir, J. Arbiol, J. Akola, R. E. Palmer and Y. V. Kolen'ko, *ACS Catal.*, 2020, **10**, 451–457.
167 C. Y. Lu, A. N. Zeng, Y. Wang and A. J. Wang, *Ind. Eng. Chem. Res.*, 2022, **61**, 18696–18702.
168 F. Y. Zhang, Y. J. Zhang, J. Y. Wang, Q. Wang, H. X. Xu, D. Q. Li, J. T. Feng and X. Duan, *Angew. Chem., Int. Ed.*, 2024, **63**, e202412637.
169 X. Y. Liu, Y. N. Li, J. W. Lee, C. Y. Hong, C. Y. Mou and B. W. L. Jang, *Appl. Catal., A*, 2012, **439**, 8–14.
170 M. Z. Hu, W. J. Yang, S. J. Liu, W. Zhu, Y. Li, B. T. Hu, Z. Chen, R. A. Shen, W. C. Cheong, Y. Wang, K. B. Zhou, Q. Peng, C. Chen and Y. D. Li, *Chem. Sci.*, 2019, **10**, 614–619.
171 Y. Q. Cao, H. Zhang, S. F. Ji, Z. J. Sui, Z. Jiang, D. S. Wang, F. Zaera, X. G. Zhou, X. H. Duan and Y. D. Li, *Angew. Chem., Int. Ed.*, 2020, **59**, 11647–11652.
172 Y. M. Niu, X. Huang, Y. Z. Wang, M. Xu, J. A. Chen, S. L. Xu, M. G. Willinger, W. Zhang, M. Wei and B. S. Zhang, *Nat. Commun.*, 2020, **11**, 3324.
173 Y. Wang, B. Y. Liu, X. C. Lan and T. F. Wang, *ACS Catal.*, 2021, **11**, 10257–10266.
174 J. M. Ma, F. L. Xing, Y. Nakaya, K. I. Shimizu and S. Furukawa, *Angew. Chem., Int. Ed.*, 2022, **61**, e202200889.
175 R. Tsukuda, S. Ohhashi, Y. Xu, C. Nishimura and S. Kameoka, *Mater. Trans.*, 2022, **63**, 343–350.
176 X. H. Ge, Z. H. Ren, Y. Q. Cao, X. Liu, J. Zhang, G. Qian, X. Q. Gong, L. W. Chen, X. G. Zhou, W. K. Yuan and X. Z. Duan, *J. Mater. Chem. A*, 2022, **10**, 19722–19731.
177 X. H. Ge, M. Y. Dou, Y. Q. Cao, L. Xi, Y. W. Qiang, Z. Jing, Q. Gang, X. Q. Gong, X. G. Zhou, L. W. Chen, W. K. Yuan and X. Z. Duan, *Nat. Commun.*, 2022, **13**, 5534.
178 H. R. Zhou, H. G. Fu, B. X. Li, X. Y. Yan, Y. Su, X. L. Pan, Q. H. Tang, X. B. Wang, X. H. Zhao, Y. Liu, Z. X. Yang, Z. S. Lu, X. D. Lou and L. Li, *ACS Sustainable Chem. Eng.*, 2023, **11**, 11052–11066.
179 J. M. Ma, F. L. Xing, K. Shimizu and S. Furukawa, *Chem. Sci.*, 2024, **15**, 4086–4094.
180 Y. L. Liu, C. J. Xu, B. Yang, X. Y. Meng, G. W. Qin and S. Li, *Catal. Sci. Technol.*, 2023, **13**, 5345–5350.
181 S. M. Dong, Y. M. Niu, Y. H. Pu, Y. Z. Wang and B. S. Zhang, *Chin. Chem. Lett.*, 2024, **35**, 109525.
182 T. Komatsu, K. Sou and K. Ozawa, *J. Mol. Catal. A: Chem.*, 2010, **319**, 71–77.
183 R. V. Maligal-Ganesh, Y. C. Pei, C. X. Xiao, M. D. Chen, T. W. Goh, W. J. Sun, J. S. Wu and W. Y. Huang, *ChemCatChem*, 2020, **12**, 3022–3029.
184 D. Zhou, G. H. Zhang, Y. Li, S. Liu, S. B. Han, Y. Zhou and W. J. Shen, *Chem. Eng. J.*, 2023, **472**, 144875.
185 D. Köhler, M. Heise, A. I. Baranov, Y. Luo, D. Geiger, M. Ruck and M. Armbrüster, *Chem. Mater.*, 2012, **24**, 1639–1644.
186 X. C. Lan, Y. Wang, B. Y. Liu, Z. Y. Kang and T. F. Wang, *Chem. Sci.*, 2024, **15**, 1758–1768.
187 M. Armbrüster, K. Kovnir, M. Friedrich, D. Teschner, G. Wowsnick, M. Hahne, P. Gille, L. Szentmiklósi, M. Feuerbacher, M. Heggen, F. Girgsdies, D. Rosenthal, R. Schlögl and Y. Grin, *Nat. Mater.*, 2012, **11**, 690–693.
188 I. G. Aviziotis, T. Duguet, K. Soussi, M. Heggen, M. C. Lafont, F. Morfin, S. Mishra, S. Daniele, A. G. Boudouvis and C. Vahlas, *Phys. Status Solidi A*, 2018, **215**, 1700692.
189 X. H. Ge, J. Q. Ming, Y. D. Jing, N. N. Fei, L. L. Guo, Y. Q. Cao, H. Jiang, J. Zhang, G. Qian, X. G. Zhou and X. Z. Duan, *ACS Catal.*, 2025, **15**, 2282–2291.
190 X. Y. Dai, Z. Chen, T. Yao, L. R. Zheng, Y. Lin, W. Liu, H. X. Ju, J. F. Zhu, X. Hong, S. Q. Wei, Y. E. Wu and Y. D. Li, *Chem. Commun.*, 2017, **53**, 11568–11571.

191 Y. C. Chai, G. J. Wu, X. Y. Liu, Y. J. Ren, W. L. Dai, C. M. Wang, Z. K. Xie, N. J. Guan and L. D. Li, *J. Am. Chem. Soc.*, 2019, **141**, 9920–9927.
192 B. A. Fu, A. J. McCue, Y. A. Liu, S. X. Weng, Y. F. Song, Y. F. He, J. T. Feng and D. Q. Li, *ACS Catal.*, 2022, **12**, 607–615.
193 J. Gu, M. Z. Jian, L. Huang, Z. H. Sun, A. W. Li, Y. Pan, J. Z. Yang, W. Wen, W. Zhou, Y. Lin, H. J. Wang, X. Y. Liu, L. L. Wang, X. X. Shi, X. H. Huang, L. N. Cao, S. Chen, X. S. Zheng, H. B. Pan, J. F. Zhu, S. Q. Wei, W. X. Li and J. L. Lu, *Nat. Nanotechnol.*, 2021, **16**, 1141.
194 C. Q. Sui, H. Ma, F. Huang, M. L. Wang, X. B. Cai, J. Y. Diao, P. J. Ren, X. D. Wen, L. Jin, G. Q. Wang, D. Ma and H. Y. Liu, *ACS Catal.*, 2024, **14**, 14689–14695.
195 F. Huang, Y. C. Deng, Y. L. Chen, X. B. Cai, M. Peng, Z. M. Jia, J. L. Xie, D. Q. Xiao, X. D. Wen, N. Wang, Z. Jiang, H. Y. Liu and D. Ma, *Nat. Commun.*, 2019, **10**, 4431.
196 X. X. Shi, Y. Lin, L. Huang, Z. H. Sun, Y. Yang, X. H. Zhou, E. Vovk, X. Y. Liu, X. H. Huang, M. Sun, S. Q. Wei and J. L. Lu, *ACS Catal.*, 2020, **10**, 3495–3504.
197 F. Huang, M. Peng, Y. L. Chen, Z. R. Gao, X. B. Cai, J. L. Xie, D. Q. Xiao, L. Jin, G. Q. Wang, X. D. Wen, N. Wang, W. Zhou, H. Y. Liu and D. Ma, *ACS Catal.*, 2022, **12**, 48–57.
198 Y. X. Yue, B. L. Wang, C. X. Jin, K. X. Huang, Q. Zhou, R. Q. Chang, S. S. Wang, Z. Y. Pan, J. Zhao and X. N. Li, *ACS Catal.*, 2024, **14**, 3900–3911.
199 Y. R. Li, Y. Q. Cao, X. H. Ge, H. Zhang, K. L. Yan, J. Zhang, G. Qian, Z. Jiang, X. Q. Gong, A. M. Li, X. G. Zhou, W. K. Yuan and X. Z. Duan, *J. Catal.*, 2022, **407**, 290–299.
200 M. S. Sun, F. M. Wang, J. Q. Hu, G. J. Lv and X. B. Zhang, *Chem. Eng. Sci.*, 2022, **247**, 116939.
201 M. S. Sun, F. M. Wang, G. J. Lv and X. B. Zhang, *Appl. Surf. Sci.*, 2022, **589**, 153021.
202 F. Xue, Q. Li, M. X. Lv, Y. F. Song, T. X. Yang, X. G. Wang, T. Y. Li, Y. Ren, K. Ohara, Y. F. He, D. Q. Li, Q. H. Li, X. Chen, K. Lin and X. R. Xing, *J. Am. Chem. Soc.*, 2023, **145**, 26728–26735.
203 C. X. Che, G. L. Gou, H. Wen, Y. L. Liang, W. Han, F. Zhang and X. X. Cai, *Inorg. Nano-Met. Chem.*, 2021, **51**, 70–77.
204 Y. Y. Zhang, W. J. Diao, C. T. Williams and J. R. Monnier, *Appl. Catal., A*, 2014, **469**, 419–426.
205 S. Riyapan, Y. Y. Zhang, A. Wongkaew, B. Pongthawornsakun, J. R. Monnier and J. Panpranot, *Catal. Sci. Technol.*, 2016, **6**, 5608–5617.
206 Q. Fu and Y. Luo, *ACS Catal.*, 2013, **3**, 1245–1252.
207 P. Zhai, D. A. Cullen and K. L. Ding, *Chem. Eng. J.*, 2024, **480**, 145028.
208 J. G. Ma, C. Y. Yang, X. Ye, X. L. Pan, S. Y. Nie, X. Cao, H. A. Li, H. Matsumoto, L. Wu and C. Chen, *Chem. Sci.*, 2024, **15**, 8363–8371.
209 V. D. Stytsenko, D. P. Melnikov, A. P. Glotov and V. A. Vinokurov, *Mol. Catal.*, 2022, **533**, 112750.
210 A. Sárkány, O. Geszti and G. Sáfrán, *Appl. Catal., A*, 2008, **350**, 157–163.
211 P. Zhai, Y. F. Shi, Q. X. Wang, Y. N. Xia and K. L. Ding, *Nanoscale*, 2021, **13**, 18498–18506.
212 C. W. Zhu, W. L. Xu, F. Liu, J. Luo, J. L. Lu and W. X. Li, *Angew. Chem., Int. Ed.*, 2023, **62**, e202300110.
213 K. Abe, R. Tsukuda, N. Fujita and S. Kameoka, *RSC Adv.*, 2021, **11**, 15296–15300.
214 K. Kovnir, J. Osswald, M. Armbrüster, D. Teschner, G. Weinberg, U. Wild, A. Knop-Gericke, T. Ressler, Y. Grin and R. Schlögl, *J. Catal.*, 2009, **264**, 93–103.
215 A. Ota, J. Kröhnert, G. Weinberg, I. Kasatkin, E. L. Kunkes, D. Ferri, F. Girgsdies, N. Hamilton, M. Armbrüster, R. Schlögl and M. Behrens, *ACS Catal.*, 2014, **4**, 2048–2059.
216 F. Meunier, M. Maffre, Y. Schuurman, S. Colussi and A. Trovarelli, *Catal. Commun.*, 2018, **105**, 52–55.
217 Q. Guo, C. Qin, J. P. Guo and P. Chen, *Chem. Commun.*, 2023, **59**, 2259–2262.
218 K. Bader, A. Dorner and P. Gille, *J. Cryst. Growth*, 2020, **532**, 125401.
219 M. C. Hu and X. Q. Wang, *Catal. Today*, 2016, **263**, 98–104.
220 S. M. Hosseini, M. Ghiaci and H. Farrokhpour, *Struct. Chem.*, 2021, **32**, 2087–2097.
221 S. Hock, M. Lucas, E. Kolle-Görgen, M. Mellin, J. P. Hofmann and M. Rose, *ChemCatChem*, 2023, **15**, e202201479.
222 G. Kyriakou, M. B. Boucher, A. D. Jewell, E. A. Lewis, T. J. Lawton, A. E. Baber, H. L. Tierney, M. Flytzani-Stephanopoulos and E. C. H. Sykes, *Science*, 2012, **335**, 1209–1212.
223 L. Z. Jiang, K. L. Liu, S. F. Hung, L. Y. Zhou, R. X. Qin, Q. H. Zhang, P. X. Liu, L. Gu, H. M. Chen, G. Fu and N. F. Zheng, *Nat. Nanotechnol.*, 2020, **15**, 848.
224 G. X. Pei, X. Y. Liu, M. Q. Chai, A. Q. Wang and T. Zhang, *Chin. J. Catal.*, 2017, **38**, 1540–1548.
225 C. Hartwig, K. Schweinar, T. E. Jones, S. Beeg, F. P. Schmidt, R. Schlögl and M. Greiner, *J. Chem. Phys.*, 2021, **154**, 184703.
226 D. L. Molina, M. Muir, M. K. Abdel-Rahman and M. Trenary, *J. Chem. Phys.*, 2021, **154**, 184701.
227 L. Y. Zhang, Y. X. Ding, K. H. Wu, Y. M. Niu, J. J. Luo, X. K. Yang, B. S. Zhang and D. S. Su, *Nanoscale*, 2017, **9**, 14317–14321.
228 Y. N. Liu, F. Z. Fu, A. McCue, W. Jones, D. M. Rao, J. T. Feng, Y. F. He and D. Q. Li, *ACS Catal.*, 2020, **10**, 15048–15059.
229 S. H. Zhou, C. Y. Lu, W. Y. Zhou, Y. Bi, C. L. Zhou, A. N. Zeng, A. J. Wang, L. X. Tan and L. C. Dong, *Chem. Commun.*, 2022, **58**, 11398–11401.
230 C. Y. Lu, S. H. Zhou, W. Y. Zhou, C. L. Zhou, Q. Li, A. A. Zeng, A. J. Wang, L. X. Tan and L. C. Dong, *Chem. Eng. J.*, 2023, **464**, 142609.
231 L. N. Yang, Y. S. Guo, J. Long, L. X. Xia, D. Li, J. P. Xiao and H. Y. Liu, *Chem. Commun.*, 2019, **55**, 14693–14696.
232 Q. Fu, F. Wu, B. X. Wang, Y. X. Bu and C. Draxl, *ACS Appl. Mater. Interfaces*, 2020, **12**, 39352–39361.
233 F. Liu, Y. J. Xia, W. L. Xu, L. N. Cao, Q. Q. Guan, Q. Q. Gu, B. Yang and J. L. Lu, *Angew. Chem., Int. Ed.*, 2021, **60**, 19324–19330.
234 L. B. Ding, H. Yi, W. H. Zhang, R. You, T. Cao, J. L. Yang, J. L. Lu and W. X. Huang, *ACS Catal.*, 2016, **6**, 3700–3707.

235 S. H. Zou, B. H. Lou, K. R. Yang, W. T. Yuan, C. Z. Zhu, Y. H. Zhu, Y. H. Du, L. F. Lu, J. J. Liu, W. X. Huang, B. Yang, Z. M. Gong, Y. Cui, Y. Wang, L. Ma, J. Y. Ma, Z. Jiang, L. P. Xiao and J. Fan, *Nat. Commun.*, 2021, **12**, 5770.
236 A. Sarkany, *React. Kinet. Catal. Lett.*, 2009, **96**, 43–54.
237 H. J. Chen, Z. M. Li, Z. X. Qin, H. J. Kim, H. Abroshan and G. Li, *ACS Appl. Nano Mater.*, 2019, **2**, 2999–3006.
238 T. Fu, T. Wang, H. F. Sun, Y. D. Xu, Z. Dong, X. K. Guo, L. M. Peng, Y. Zhu, Z. X. Chen and W. P. Ding, *Sci. China: Chem.*, 2018, **61**, 1014–1019.
239 Z. J. Yuan, A. Kumar, D. J. Zhou, J. T. Feng, B. Liu and X. M. Sun, *J. Catal.*, 2022, **414**, 374–384.
240 J. Liu, A. Zeng, B. Xu, Y. Wang, Z. Sun, Y. Liu, W. Wang and A. Wang, *Catal. Lett.*, 2024, **154**, 5171–5183.
241 J. C. Rodríguez, A. J. Marchi, A. Borgna and A. Monzón, *J. Catal.*, 1997, **171**, 268–278.
242 A. Aitugan, S. Tanirbergenova, Y. Tileuberdi, O. Yucel, D. Tugelbayeva, Z. Mansurov and Y. Ongarbayev, *React. Kinet., Mech. Catal.*, 2021, **133**, 277–292.
243 S. Hock, C. V. Reichel, A. M. Zieschang, B. Albert and M. Rose, *ACS Sustainable Chem. Eng.*, 2021, **9**, 16570–16576.
244 F. Studt, F. Abild-Pedersen, T. Bligaard, R. Z. Sorensen, C. H. Christensen and J. K. Norskov, *Science*, 2008, **320**, 1320–1322.
245 Y. A. Liu, B. A. Fu, F. Z. Fu, Y. F. He and D. Q. Li, *Chem. Eng. Sci.*, 2022, **260**, 117852.
246 Y. Y. Shu, L. E. Murillo, J. P. Bosco, W. Huang, A. I. Frenkel and J. G. Chen, *Appl. Catal., A*, 2008, **339**, 169–179.
247 E. Kockrick, F. Schmidt, K. Gedrich, M. Rose, T. A. George, T. Freudenberg, R. Kraehnert, R. Skomski, D. J. Sellmyer and S. Kaskel, *Chem. Mater.*, 2010, **22**, 1624–1632.
248 L. C. Jones, Z. Buras and M. J. Gordon, *J. Phys. Chem. C*, 2012, **116**, 12982–12988.
249 L. C. Jones and M. J. Gordon, *J. Phys. Chem. C*, 2012, **116**, 23472–23476.
250 C. S. Spanjers, J. T. Held, M. J. Jones, D. D. Stanley, R. S. Sim, M. J. Janik and R. M. Rioux, *J. Catal.*, 2014, **316**, 164–173.
251 G. L. Zhou, P. G. Wang, Z. X. Jiang, P. L. Ying and C. Li, *Chin. J. Catal.*, 2011, **32**, 27–30.
252 Y. X. Zhao, Ö. Bozkurt, S. F. Kurtoglu-Öztulum, M. S. Yordanli, A. S. Hoffman, J. Y. Hong, J. E. Perez-Aguilar, A. Saltuk, D. Akgül, O. Demircan, T. A. Atesin, V. Aviyente, B. C. Gates, S. R. Bare and A. Uzun, *J. Catal.*, 2024, **429**, 115196.
253 O. B. Ayodele, S. Vinati, E. Barborini, L. Boddapati, K. El Hajraoui, J. Kröhnert, F. L. Deepak, A. Trunschke and Y. V. Kolen'ko, *Catal. Sci. Technol.*, 2020, **10**, 7471–7475.
254 J. Cheng, P. Hu, P. Ellis, S. French, G. Kelly and C. M. Lok, *J. Phys. Chem. C*, 2008, **112**, 1308–1311.
255 C. T. Kuo, Y. B. Lu, L. Kovarik, M. Engelhard and A. M. Karim, *ACS Catal.*, 2019, **9**, 11030–11041.
256 F. Zhang, Q. J. Zhang, Y. C. Chen, L. Y. Xu, Z. L. Li, Q. T. Wang, Q. F. Zhang and X. N. Li, *Appl. Catal., A*, 2023, **667**, 119447.
257 J. Carrasco, G. Vilé, D. Fernández-Torre, R. Pérez, J. Pérez-Ramírez and M. V. Ganduglia-Pirovano, *J. Phys. Chem. C*, 2014, **118**, 5352–5360.
258 A. Primo, F. Neatu, M. Florea, V. Parvulescu and H. Garcia, *Nat. Commun.*, 2014, **5**, 5291.
259 D. Albani, M. Capdevila-Cortada, G. Vilé, S. Mitchell, O. Martin, N. López and J. Pérez-Ramírez, *Angew. Chem., Int. Ed.*, 2017, **56**, 10755–10760.
260 C. Riley, A. De La Riva, S. L. Zhou, Q. Wan, E. Peterson, K. Artyushkova, M. D. Farahani, H. B. Friedrich, L. Burkemper, N. V. Atudorei, S. Lin, H. Guo and A. Datye, *ChemCatChem*, 2019, **11**, 1526–1533.
261 Y. B. Wang, J. Yang, R. T. Gu, L. M. Peng, X. F. Guo, N. H. Xue, Y. Zhu and W. P. Ding, *ACS Catal.*, 2018, **8**, 6419–6425.
262 T. Cao, R. You, Z. R. Li, X. Y. Zhang, D. Li, S. L. Chen, Z. H. Zhang and W. X. Huang, *Appl. Surf. Sci.*, 2020, **501**, 144120.
263 G. L. Gou, C. X. Che, H. Wen, J. H. Qin, X. Cao, W. Han, F. Zhang, Y. Long and J. T. Ma, *J. Catal.*, 2022, **408**, 128–132.
264 Z. R. Li, L. Chen, Z. F. Wu, A. P. Jia, S. C. Shi, H. Zhang, J. Wang, Z. Liu, W. P. Shao, F. Yang, X. P. Wu, X. Q. Gong and W. X. Huang, *ACS Catal.*, 2023, **13**, 5213–5224.
265 I. B. Bychko, A. A. Abakumov, N. V. Lemesh and P. E. Strizhak, *ChemCatChem*, 2017, **9**, 4470–4474.
266 A. A. Abakumov, I. B. Bychko, O. V. Selyshchev, D. R. T. Zahn, X. H. Qi, J. G. Tang and P. E. Strizhak, *Carbon*, 2020, **157**, 277–285.
267 A. A. Abakumov, I. B. Bychko, O. V. Selyshchev, D. R. T. Zahn, M. Chen, J. Tang and P. E. Strizhak, *Materialia*, 2021, **18**, 277–285.
268 C. Riley, S. L. Zhou, D. Kunwar, A. De La Riva, E. Peterson, R. Payne, L. Y. Gao, S. Lin, H. Guo and A. Datye, *J. Am. Chem. Soc.*, 2018, **140**, 12964–12973.
269 M. Tejeda-Serrano, M. Mon, B. Ross, F. Gonell, J. Ferrando-Soria, A. Corma, A. Leyva-Pérez, D. Armentano and E. Pardo, *J. Am. Chem. Soc.*, 2018, **140**, 8827–8832.
270 J. N. Li, M. Pu, C. C. Ma, Y. Tian, J. He and D. G. Evans, *J. Mol. Catal. A: Chem.*, 2012, **359**, 14–20.
271 T. Abdollahi and D. Farmanzadeh, *Appl. Surf. Sci.*, 2018, **433**, 513–529.
272 B. Yang, R. Burch, C. Hardacre, G. Headdock and P. Hu, *J. Catal.*, 2013, **305**, 264–276.
273 M. Crespo-Quesada, S. Yoon, M. S. Jin, A. Prestianni, R. Cortese, F. Cárdenas-Lizana, D. Duca, A. Weidenkaff and L. Kiwi-Minsker, *J. Phys. Chem. C*, 2015, **119**, 1101–1107.
274 B. Yang, R. Burch, C. Hardacre, P. Hu and P. Hughes, *Surf. Sci.*, 2016, **646**, 45–49.
275 P. Tiruppathi, J. J. Low, A. S. Y. Chan, S. R. Bare and R. J. Meyer, *Catal. Today*, 2011, **165**, 106–111.
276 D. Torres, F. Cinquini and P. Sautet, *J. Phys. Chem. C*, 2013, **117**, 11059–11065.
277 B. Yang, R. Burch, C. Hardacre, P. Hu and P. Hughes, *J. Phys. Chem. C*, 2014, **118**, 3664–3671.
278 P. Wang and B. Yang, *Chin. J. Catal.*, 2018, **39**, 1493–1499.
279 J. F. Wang, W. S. Hao, L. J. Ma, J. F. Jia and H. S. Wu, *Comput. Theor. Chem.*, 2019, **1170**, 112636.

280 Y. Y. Wu, W. T. Zhao, Y. Wang, B. J. Wang, M. H. Fan and R. G. Zhang, *ACS Appl. Mater. Interfaces*, 2022, **14**, 56743–56757.
281 W. B. Xie, J. Y. Xu, Y. X. Ding and P. Hu, *ACS Catal.*, 2021, **11**, 4094–4106.
282 W. B. Xie and P. Hu, *Catal. Sci. Technol.*, 2021, **11**, 5212–5222.
283 D. H. Mei, M. Neurock and C. M. Smith, *J. Catal.*, 2009, **268**, 181–195.
284 J. H. Liu, L. D. Meng, C. Q. Lv and G. C. Wang, *RSC Adv.*, 2016, **6**, 14593–14601.
285 Q. Li, Y. C. Qin, D. P. Tan, Y. Xie, M. L. Lv and L. J. Song, *New J. Chem.*, 2018, **42**, 19827–19836.
286 L. D. Meng and G. C. Wang, *Phys. Chem. Chem. Phys.*, 2014, **16**, 17541–17550.
287 X. T. Li, L. Chen, C. Shang and Z. P. Liu, *J. Am. Chem. Soc.*, 2021, **143**, 6281–6292.
288 J. Y. Wang, H. X. Xu, C. X. Che, J. Q. Zhu and D. J. Cheng, *ACS Catal.*, 2023, **13**, 433–444.
289 P. P. Wei, J. Zheng, Q. Li, Y. C. Qin, H. M. Guan, D. P. Tan and L. J. Song, *Inorg. Chem. Front.*, 2022, **9**, 5169–5180.
290 E. Vignola, S. N. Steinmann, B. D. Vandegehuchte, D. Curulla and P. Sautet, *J. Phys. Chem. C*, 2016, **120**, 26320–26327.
291 Z. J. Wang, J. Y. Chen, Y. G. Huang and Z. X. Chen, *Mater. Today Commun.*, 2021, **28**, 102475.
292 R. G. Zhang, M. F. Xue, B. J. Wang, L. X. Ling and M. H. Fan, *J. Phys. Chem. C*, 2019, **123**, 16107–16117.
293 Y. M. Qi, X. X. Shao, B. J. Wang, D. B. Li, L. X. Ling and R. G. Zhang, *Chem. Eng. Sci.*, 2021, **245**, 116786.
294 R. G. Zhang, B. Zhao, L. X. Ling, A. J. Wang, C. K. Russell, B. J. Wang and M. H. Fan, *ChemCatChem*, 2018, **10**, 2424–2432.
295 C. X. Yang, G. Q. Wang, A. M. Liang, Y. Yue, H. Peng and D. J. Cheng, *Catal. Commun.*, 2019, **124**, 41–45.
296 Y. Wang, W. J. Zheng, B. J. Wang, L. X. Ling and R. G. Zhang, *Chem. Eng. Sci.*, 2021, **229**, 116131.
297 W. J. Zheng, L. X. Ma, B. J. Wang, J. G. Wang and R. G. Zhang, *Mol. Catal.*, 2021, **510**, 111660.
298 W. J. Zheng, Y. Wang, B. J. Wang, M. H. Fan, L. X. Ling and R. G. Zhang, *J. Phys. Chem. C*, 2021, **125**, 15251–15261.
299 Y. G. Huang and Z. X. Chen, *Appl. Surf. Sci.*, 2022, **575**, 151513.
300 Y. G. Huang, H. L. Lu and Z. X. Chen, *Phys. Chem. Chem. Phys.*, 2022, **24**, 3182–3190.
301 A. C. Foucher, H. T. Ngan, T. Shirman, A. Filie, K. Duanmu, M. Aizenberg, R. J. Madix, C. M. Friend, J. Aizenberg, P. Sautet and E. A. Stach, *ACS Appl. Nano Mater.*, 2023, **6**, 22927–22938.
302 M. Krajcí and J. Hafner, *J. Catal.*, 2012, **295**, 70–80.
303 J. Prinz, C. A. Pignedoli, Q. S. Stöckl, M. Armbrüster, H. Brune, O. Gröning, R. Widmer and D. Passerone, *J. Am. Chem. Soc.*, 2014, **136**, 11792–11798.
304 M. Krajci and J. Hafner, *J. Catal.*, 2014, **312**, 232–248.
305 M. Krajcí and J. Hafner, *J. Phys. Chem. C*, 2014, **118**, 12285–12301.
306 N. Kumar and P. Ghosh, *J. Phys. Chem. C*, 2016, **120**, 28654–28663.
307 M. Sandoval, P. Bechthold, V. Orazi, E. A. González, A. Juan and P. V. Jasen, *Appl. Surf. Sci.*, 2018, **435**, 568–573.
308 M. Krajcí and J. Hafner, *J. Phys. Chem. C*, 2012, **116**, 6307–6319.
309 J. B. Zhao, S. J. Zha, R. T. Mu, Z. J. Zhao and J. L. Gong, *J. Phys. Chem. C*, 2018, **122**, 6005–6013.
310 Y. Zhao, M. Y. Zhu and L. H. Kang, *Catal. Lett.*, 2018, **148**, 2992–3002.
311 S. F. Yuk, G. Collinge, M. T. Nguyen, M. S. Lee, V. A. Glezakou and R. Rousseau, *J. Chem. Phys.*, 2020, **152**, 154703.
312 S. Zhao, Y. Tang, X. H. Yu and J. Li, *Sci. China: Mater.*, 2023, **66**, 3912–3921.
313 H. Thirumalai and J. R. Kitchin, *Top. Catal.*, 2018, **61**, 462–474.
314 Y. M. Qi, B. J. Wang, M. H. Fan, D. B. Li and R. G. Zhang, *Chem. Eng. Sci.*, 2021, **243**, 116786.
315 D. Liu, *Appl. Surf. Sci.*, 2016, **386**, 125–137.
316 D. L. Molina, M. Muir, M. K. Abdel-Rahman and M. Trenary, *J. Chem. Phys.*, 2021, **154**, 184701.
317 L. L. Ma, C. Q. Lv and G. C. Wang, *Appl. Surf. Sci.*, 2017, **410**, 154–165.
318 R. G. Zhang, J. Zhang, B. Zhao, L. L. He, A. J. Wang and B. J. Wang, *J. Phys. Chem. C*, 2017, **121**, 27936–27949.
319 R. G. Zhang, M. F. Xue, B. J. Wang and L. X. Ling, *Appl. Surf. Sci.*, 2019, **481**, 421–432.
320 M. Jorgensen and H. Grönbeck, *J. Am. Chem. Soc.*, 2019, **141**, 8541–8549.
321 B. Zhao, R. G. Zhang, Z. X. Huang and B. J. Wang, *Appl. Catal., A*, 2017, **546**, 111–121.
322 T. Abdollahi and D. Farmanzadeh, *J. Alloys Compd.*, 2018, **735**, 117–130.
323 Y. Wang, Y. Wu, X. Guo, B. Wang, M. Fan and R. Zhang, *ACS Appl. Mater. Interfaces*, 2022, **14**, 41896–41911.
324 Y. Wang, B. J. Wang, M. H. Fan, L. X. Ling and R. G. Zhang, *Chem. Eng. Sci.*, 2022, **251**, 117494.
325 T. Abdollahi and D. Farmanzadeh, *C. R. Chim*, 2018, **21**, 484–493.
326 P. Yin, Y. Jie, X. J. Zhao, Y. L. Feng, T. Sun, D. M. Rao, M. Pu and H. Yan, *Phys. Chem. Chem. Phys.*, 2021, **23**, 27340–27347.
327 Z. S. Wang, A. Garg, L. X. Wang, H. R. He, A. Dasgupta, D. Zanchet, M. J. Janik, R. M. Rioux and Y. Román-Leshkov, *ACS Catal.*, 2020, **10**, 6763–6770.
328 C. Jimenez-Orozco, A. A. Koverga, E. Florez and J. A. Rodriguez, *Surf. Sci.*, 2023, **728**, 122197.
329 K. R. Yang and B. Yang, *Faraday Discuss.*, 2021, **229**, 50–61.
330 Z. F. Wu, F. Wang, G. H. Sun, F. Xiong, B. T. Teng and W. X. Huang, *J. Phys. Chem. Lett.*, 2022, **13**, 7667–7672.
331 L. Wang, B. J. Wang, M. H. Fan, L. X. Ling and R. G. Zhang, *Fuel*, 2023, **336**, 127131.
332 J. Y. Li, Z. H. Yao, J. Y. Zhao, S. W. Deng, S. B. Wang and J. G. Wang, *Mol. Catal.*, 2023, **535**, 112845.
333 K. H. Sun, R. Zou, C. Y. Shen and C. J. Liu, *Catal. Sci. Technol.*, 2024, **14**, 3041–3049.

334 R. G. Zhang, J. Zhang, Z. Jiang, B. J. Wang and M. H. Fan, *Chem. Eng. J.*, 2018, **351**, 732–746.
335 R. G. Zhang, B. Zhao, L. L. He, A. J. Wang and B. J. Wang, *Phys. Chem. Chem. Phys.*, 2018, **20**, 17487–17496.
336 B. Yang, R. Burch, C. Hardacre, G. Headdock and P. Hu, *ACS Catal.*, 2012, **2**, 1027–1032.
337 L. Wang, B. J. Wang, M. H. Fan, L. X. Ling and R. G. Zhang, *Fuel*, 2022, **321**, 124118.
338 D. M. Rao, S. T. Zhang, C. M. Li, Y. D. Chen, M. Pu, H. Yan and M. Wei, *Dalton Trans.*, 2018, **47**, 4198–4208.
339 Y. J. Song and S. Laursen, *J. Catal.*, 2019, **372**, 151–162.
340 D. M. Rao, T. Sun, Y. S. Yang, P. Yin, M. Pu, H. Yan and M. Wei, *Phys. Chem. Chem. Phys.*, 2019, **21**, 1384–1392.
341 Z. Almisbaa, H. A. Aljama, K. Almajnouni, L. Cavallo and P. Sautet, *ACS Catal.*, 2023, **13**, 7358–7370.
342 M. Krajcí and J. Hafner, *Philos. Mag.*, 2011, **91**, 2904–2912.
343 M. Krajcí and J. Hafner, *J. Catal.*, 2011, **278**, 200–207.
344 D. Kandaskalov, V. Fournée, J. Ledieu and E. Gaudry, *J. Phys. Chem. C*, 2017, **121**, 18738–18745.
345 M. Meier, J. Ledieu, V. Fournée and É. Gaudry, *J. Phys. Chem. C*, 2017, **121**, 4958–4969.
346 L. Wang, B. J. Wang, M. H. Fan, L. X. Ling and R. G. Zhang, *J. Catal.*, 2022, **416**, 112–128.
347 Y. Wang and L. H. Kang, *Catalysts*, 2020, **10**, 115.
348 Y. Wang and L. H. Kang, *Chem. Phys. Lett.*, 2020, **757**, 137871.
349 H. Y. Zhuo, X. H. Yu, Q. Yu, H. Xiao, X. Zhang and J. Li, *Sci. China: Mater.*, 2020, **63**, 1741–1749.
350 M. Z. Jian, J. X. Liu and W. X. Li, *Chem. Sci.*, 2021, **12**, 10290–10298.
351 H. Y. Ma and G. C. Wang, *ACS Catal.*, 2020, **10**, 4922–4928.
352 D. L. Gao, D. Yi, F. Lu, S. Li, L. Pan, Y. Xu and X. Wang, *Chem. Eng. Sci.*, 2021, **240**, 116664.
353 X. X. Shao, B. J. Wang, M. H. Fan, L. X. Ling and R. G. Zhang, *Appl. Surf. Sci.*, 2023, **611**, 155720.
354 Z. Q. Huang, L. P. Liu, S. T. Qi, S. Zhang, Y. Q. Qu and C. R. Chang, *ACS Catal.*, 2018, **8**, 546–554.
355 M. C. Padole, B. P. Gangwar, A. Pandey, A. Singhal, S. Sharma and P. A. Deshpande, *Phys. Chem. Chem. Phys.*, 2017, **19**, 14148–14159.
356 S. L. Zhou, L. Y. Gao, F. F. Wei, S. Lin and H. Guo, *J. Catal.*, 2019, **375**, 410–418.
357 S. L. Zhou, Q. Wan, S. Lin and H. Guo, *Phys. Chem. Chem. Phys.*, 2022, **24**, 11295–11304.
358 X. Y. Guo, H. J. Han, B. J. Wang, L. X. Ling, M. H. Fan and R. G. Zhang, *Chem. Eng. Sci.*, 2024, **296**, 120263.
359 Q. Wan, Y. Chen, S. L. Zhou, J. Lin and S. Lin, *J. Mater. Chem. A*, 2021, **9**, 14064–14073.
360 K. W. Romero, F. Polo-Garzon, Z. L. Wu, A. Savara and D. E. Jiang, *ACS Catal.*, 2023, **13**, 9213–9221.
361 Q. Wan, J. Li, R. Jiang and S. Lin, *Phys. Chem. Chem. Phys.*, 2021, **23**, 24349–24356.
362 Á. Molnár, A. Sárkány and M. Varga, *J. Mol. Catal. A: Chem.*, 2001, **173**, 185–221.
363 Q. Li, L. J. Song, L. H. Pan, X. L. Zhuang, M. L. Ling and L. H. Duan, *Phys. Chem. Chem. Phys.*, 2013, **15**, 20345–20353.
364 X. J. Xie, X. L. Song, W. Y. Dong, Z. H. Liang, C. M. Fan and P. D. Han, *Chin. J. Chem.*, 2014, **32**, 631–636.
365 I. Horiuti and M. Polanyi, *Trans. Faraday Soc.*, 1934, **30**, 1164–1172.
366 Y. Y. Wu, X. Y. Guo, X. F. Shi, B. J. Wang, M. H. Fan and R. G. Zhang, *Appl. Surf. Sci.*, 2023, **637**, 157906.
367 C. Amatore and A. Jutand, *J. Organomet. Chem.*, 1999, **576**, 254–278.
368 S. Kozuch and S. Shaik, *Acc. Chem. Res.*, 2011, **44**, 101–110.
369 S. Komhom, O. Mekasuwandumrong, P. Praserthdam and J. Panpranot, *Catal. Commun.*, 2008, **10**, 86–91.
370 S. Komeili, M. T. Ravanchi and A. Taeb, *Appl. Catal., A*, 2015, **502**, 287–296.
371 H. L. Zhang, J. L. Cao, B. J. Wu, W. Dai, Z. H. Chen and M. J. Ma, *RSC Adv.*, 2016, **6**, S7174–S7182.
372 S. Wang, G. F. Zhao, Y. Liu and Y. Lu, *Ind. Eng. Chem. Res.*, 2019, **58**, 16431–16441.
373 L. Y. Xu, S. Y. Hua, J. Zhou, Y. Q. Xu, C. S. Lu, F. Feng, J. Zhao, X. L. Xu, Q. T. Wang, Q. F. Zhang and X. N. Li, *Appl. Catal., A*, 2022, **642**, 118690.
374 Z. R. Yang, Y. Li, Y. Q. Cao, X. Q. Zhao, W. Y. Chen, J. Zhang, G. Qian, C. Peng, X. Q. Gong and X. Z. Duan, *Chem. Eng. J.*, 2022, **445**, 136681.
375 T. Sangkhum, O. Mekasuwandumrong, P. Praserthdam and J. Panpranot, *React. Kinet. Catal. Lett.*, 2009, **97**, 115–123.
376 L. B. Sun, L. Jiang, X. Y. Hua, Y. H. Zheng, X. Sun, M. Zhang, H. J. Su and C. X. Qi, *J. Alloys Compd.*, 2019, **811**, 152052.
377 H. Chen, B. Yang, Y. F. Zhang, C. X. Che, F. Zhang, W. Han, H. Wen, A. Q. Wang and T. Zhang, *ChemCatChem*, 2024, **16**, e202400566.
378 J. T. Feng, X. Y. Ma, D. G. Evans and D. Q. Li, *Ind. Eng. Chem. Res.*, 2011, **50**, 1947–1954.
379 Y. F. He, J. X. Fan, J. T. Feng, C. Y. Luo, P. F. Yang and D. Q. Li, *J. Catal.*, 2015, **331**, 118–127.
380 X. Sun, F. F. Li, J. J. Shi, Y. H. Zheng, H. J. Su, L. B. Sun, S. Peng and C. X. Qi, *Appl. Surf. Sci.*, 2019, **487**, 625–633.
381 H. Dai, X. Xiao, L. H. Huang, C. J. Zhou and J. Deng, *Appl. Clay Sci.*, 2021, **211**, 106173.
382 Z. J. Yuan, L. Liu, W. Ru, D. J. Zhou, Y. Kuang, J. T. Feng, B. Liu and X. M. Sun, *Nano Res.*, 2022, **15**, 6010–6018.
383 Z. W. Li, G. Lin, Y. X. Chen, Q. Q. Xue, K. Feng and B. H. Yan, *Catal. Today*, 2023, **423**, 114253.
384 F. Z. Fu, Y. A. Liu, Y. W. Li, B. A. Fu, L. R. Zheng, J. T. Feng and D. Q. Li, *ACS Catal.*, 2021, **11**, 11117–11128.
385 E. V. Ilyina, D. V. Yurpalova, D. A. Shlyapin, G. B. Veselov, D. M. Shivtsov, V. O. Stoyanovskii, A. V. Bukhtiyarov and A. A. Vedyagin, *Mol. Catal.*, 2024, **560**, 114151.
386 E. Kim, E. W. Shin, C. W. Bark, I. Chang, W. J. Yoon and W. J. Kim, *Appl. Catal., A*, 2014, **471**, 80–83.
387 J. E. Um, W. J. Yoon, H. W. Choi and W. J. Kim, *J. Ind. Eng. Chem.*, 2014, **20**, 4183–4187.
388 Y. N. Liu, J. T. Feng, Y. F. He, J. H. Sun and D. Q. Li, *Catal. Sci. Technol.*, 2015, **5**, 1231–1240.
389 Y. N. Liu, J. Y. Zhao, Y. F. He, J. T. Feng, T. Wu and D. Q. Li, *J. Catal.*, 2017, **348**, 135–145.

390 T. Gong, Y. Huang, L. J. Qin, W. L. Zhang, J. G. Li, L. F. Hui and H. Feng, *Appl. Surf. Sci.*, 2019, **495**, 143495.
391 K. J. Wang, Y. Y. Chen, X. S. Li and H. X. Ding, *Catal. Lett.*, 2009, **127**, 392–399.
392 W. Huang, A. Li, R. F. Lobo and J. G. Chen, *Catal. Lett.*, 2009, **130**, 380–385.
393 Y. K. Gulyaeva, V. V. Kaichev, V. I. Zaikovskii, A. P. Suknev and B. S. Bal'zhinimaev, *Appl. Catal., A*, 2015, **506**, 197–205.
394 D. Melnikov, M. Reshetina, A. Novikov, K. Cherednichenko, A. Stavitskaya, V. Stytsenko, V. Vinokurov, W. Huang and A. Glotov, *Appl. Clay Sci.*, 2023, **232**, 106763.
395 S. Peng, X. Sun, L. B. Sun, M. Zhang, Y. H. Zheng, H. J. Su and C. X. Qi, *Catal. Lett.*, 2019, **149**, 465–472.
396 Y. N. Liu, A. J. McCue, P. F. Yang, Y. F. He, L. R. Zheng, X. Z. Cao, Y. Man, J. T. Feng, J. A. Anderson and D. Q. Li, *Chem. Sci.*, 2019, **10**, 3556–3566.
397 Z. W. Li, J. J. Zhang, J. M. Tian, K. Feng, Y. X. Chen, X. Li, Z. H. Zhang, S. R. Qian, B. Yang, D. Su, K. H. Luo and B. H. Yan, *ACS Catal.*, 2024, **14**, 1514–1524.
398 Z. H. Tao, L. Y. Pan, H. D. Yao, L. Chao, L. W. Cui, C. P. Du, Y. X. Wang, Y. S. Xi, D. Li and W. H. Li, *Surf. Interfaces*, 2024, **52**, 104923.
399 A. D. Benavidez, P. D. Burton, J. L. Nogales, A. R. Jenkins, S. A. Ivanov, J. T. Miller, A. M. Karim and A. K. Datye, *Appl. Catal., A*, 2014, **482**, 108–115.
400 H. M. Lu, B. L. Xu, X. Z. Wang, Z. Hu and Y. N. Fan, *Catal. Lett.*, 2014, **144**, 2198–2203.
401 Y. Q. Cao, W. Z. Fu, Z. H. Ren, Z. J. Sui, J. H. Zhou, J. Luo, X. Z. Duan and X. G. Zhou, *AIChE J.*, 2020, **66**, e16857.
402 Q. T. Wang, J. Y. Zhao, L. Y. Xu, L. Yu, Z. H. Yao, G. J. Lan, L. L. Guo, J. Zhao, C. S. Lu, Z. Y. Pan, J. G. Wang, Q. F. Zhang and X. N. A. Li, *Appl. Surf. Sci.*, 2021, **562**, 150141.
403 A. Khannanov, I. Il'yasov, A. Kiiamov, I. Vakhitov, A. Kirgizov, A. Lamberov and A. M. Dimiev, *New J. Chem.*, 2019, **43**, 19035–19043.
404 S. Hwang, Y. B. Hwang, H. W. Hwang, D. Kim, J. Y. Lee, J. Hwang, E. D. Park and S. K. Kim, *Adv. Energy Sustainability Res.*, 2025, DOI: **10.1002/aesr.202400341**.
405 M. Z. Hu, S. Zhao, S. J. Liu, C. Chen, W. X. Chen, W. Zhu, C. Liang, W. C. Cheong, Y. Wang, Y. Yu, Q. Peng, K. B. Zhou, J. Li and Y. D. Li, *Adv. Mater.*, 2018, **30**, e201801878.
406 S. Wang, Z. J. Zhao, X. Chang, J. B. Zhao, H. Tian, C. S. Yang, M. R. Li, Q. Fu, R. T. Mu and J. L. Gong, *Angew. Chem., Int. Ed.*, 2019, **58**, 7668–7672.
407 Z. L. Guo, Y. F. Liu, Y. Liu and W. Chu, *Appl. Surf. Sci.*, 2018, **442**, 736–741.
408 R. R. Li, Y. X. Yue, Y. K. Li, X. L. Chen, R. Q. Chang, J. X. Zhang, B. Zhao, X. Ying, Z. J. Wang, J. Zhao and X. N. Li, *Inorg. Chem. Front.*, 2022, **9**, 5969–5981.
409 Q. L. Wu, C. Y. Shen and C. J. Liu, *Mol. Catal.*, 2024, **569**, 114529.
410 M. T. Ravanchi, S. Fadaeerayeni and M. R. Fard, *Res. Chem. Intermed.*, 2016, **42**, 4797–4811.
411 M. T. Ravanchi, S. Sahebdelfar and M. R. Fard, *Int. J. Chem. React. Eng.*, 2016, **14**, 1035–1046.
412 K. Ravindran, G. Madhu, V. R. Renjith and S. Rugmini, *React. Kinet., Mech. Catal.*, 2021, **134**, 867–882.
413 K. Ravindran, G. Madhu, V. R. Renjith and S. Rugmini, *J. Indian Chem. Soc.*, 2023, **100**, 867–882.
414 S. Asplund, *J. Catal.*, 1996, **158**, 267–278.
415 C. X. Che, B. K. Wang, C. F. Shan, H. Chen, W. S. Liu and Y. Tang, *Catal. Lett.*, 2017, **147**, 483–490.
416 X. Y. Ma, Y. Y. Chai, D. G. Evans, D. Q. Li and J. T. Feng, *J. Phys. Chem. C*, 2011, **115**, 8693–8701.
417 S. Chinayon, O. Mekasuwandumrong, P. Praserthdam and J. Panpranot, *Catal. Commun.*, 2008, **9**, 2297–2302.
418 X. P. Gao, Y. A. Zhou, F. L. Jing, J. J. Luo, Q. S. Huang and W. Chu, *Chin. J. Chem.*, 2017, **35**, 1009–1015.
419 S. Komeili, M. T. Ravanchi and A. Taeb, *Res. Chem. Intermed.*, 2018, **44**, 1335–1349.
420 C. L. Miao, L. Y. Cai, Y. F. Wang, X. J. Xu, J. R. Yang, Y. F. He, D. Q. Li and J. T. Feng, *Ind. Eng. Chem. Res.*, 2021, **60**, 8362–8374.
421 D. R. Aireddy, H. R. Yu, D. A. Cullen and K. L. Ding, *ACS Appl. Mater. Interfaces*, 2022, **14**, 24290–24298.
422 S. Riyapan, Y. Boonyongmaneerat, O. Mekasuwandumrong, P. Praserthdam and J. Panpranot, *Catal. Today*, 2015, **245**, 134–138.
423 X. P. Gao, Z. L. Guo, Y. N. Zhou, F. L. Jing and W. Chu, *Acta Phys.-Chim. Sin.*, 2017, **33**, 602.
424 Y. P. Yang, J. R. Yang, S. C. Shi, Y. H. Luo, X. J. Xu, Y. A. Liu, D. Q. Li and J. T. Feng, *AIChE J.*, 2023, **69**, e18078.
425 Z. L. Guo, Q. S. Huang, S. Z. Luo and W. Chu, *Top. Catal.*, 2017, **60**, 1009–1015.
426 W. J. Kim, I. Y. Ahn, J. H. Lee and S. H. Moon, *Catal. Commun.*, 2012, **24**, 52–55.
427 W. J. Kim and S. H. Moon, *Catal. Today*, 2012, **185**, 2–16.
428 W. F. Simanullang, J. M. Ma, K. Shimizu and S. Furukawa, *Catal. Sci. Technol.*, 2021, **11**, 4016–4020.
429 Z. W. Liu, Q. F. Zhu, N. Hou, Y. Fu, L. X. Wen and J. F. Chen, *Catal. Today*, 2013, **216**, 205–210.
430 Y. K. Gulyaeva, V. V. Kaichev, V. I. Zaikovskii, E. V. Kovalyov, A. P. Suknev and B. S. Bal'zhinimaev, *Catal. Today*, 2015, **245**, 139–146.
431 L. H. Kang, B. Z. Cheng and M. Y. Zhu, *R. Soc. Open Sci.*, 2019, **6**, 191155.
432 M. Q. Chai, Y. Tan, G. X. Pei, L. Li, L. L. Zhang, X. Y. Liu, A. Q. Wang and T. Zhang, *J. Phys. Chem. C*, 2017, **121**, 19727–19734.
433 W. G. Augustyn, R. I. McCrindle and N. J. Coville, *Appl. Catal., A*, 2010, **388**, 1–6.
434 H. Bazzazzadegan, M. Kazemeini and A. M. Rashidi, *Appl. Catal., A*, 2011, **399**, 184–190.
435 V. V. Chesnokov, O. Y. Podyacheva and R. M. Richards, *Mater. Res. Bull.*, 2017, **88**, 78–84.
436 X. L. Chen, Q. Q. Xu, B. Zhao, S. B. Ren, Z. H. Wu, J. P. Wu, Y. X. Yue, D. M. Han and R. R. Li, *Catal. Lett.*, 2021, **151**, 3372–3380.
437 F. Dodangeh, A. Rashidi, H. Aghaie and K. Zare, *J. Phys. Chem. Solids*, 2021, **158**, 110219.

438 H. R. Zhou, B. X. Li, H. G. Fu, X. H. Zhao, M. M. Zhang, X. B. Wang, Y. Liu, Z. X. Yang and X. D. Lou, *ACS Sustainable Chem. Eng.*, 2022, **10**, 4849–4861.
439 Q. S. Luo, H. Wang, L. Wang and F. S. Xiao, *ACS Mater. Au*, 2022, **2**, 313–320.
440 J. Yang, F. J. Zhang, H. Y. Lu, X. Hong, H. L. Jiang, Y. Wu and Y. D. Li, *Angew. Chem., Int. Ed.*, 2015, **54**, 10889–10893.
441 L. R. Redfern, Z. Y. Li, X. Zhang and O. K. Farha, *ACS Appl. Nano Mater.*, 2018, **1**, 4413–4417.
442 M. R. Mian, L. R. Redfern, S. M. Pratik, D. Ray, J. Liu, K. B. Idrees, T. Islamoglu, L. Gagliardi and O. K. Farha, *Chem. Mater.*, 2020, **32**, 3078–3086.
443 J. J. Wang, H. T. Xu, C. C. Ao, X. B. Pan, X. K. Luo, S. J. Wei, Z. Li, L. D. Zhang, Z. L. Xu and Y. D. Li, *iScience*, 2020, **23**, 101233.
444 J. Q. Zhang, G. Y. Zhang, L. He, Y. Z. Shi, R. R. Miao, Y. Z. Zhu and Q. Q. Guan, *Appl. Surf. Sci.*, 2021, **570**, 150881.
445 N. López, B. Bridier and J. Pérez-Ramírez, *J. Phys. Chem. C*, 2008, **112**, 9346–9350.
446 X. X. Shao, X. Y. Guo, X. F. Shi, B. J. Wang, M. H. Fan and R. G. Zhang, *Fuel*, 2024, **358**, 130053.
447 D. L. Trimm, I. O. Y. Liu and N. W. Cant, *J. Mol. Catal. A: Chem.*, 2009, **307**, 13–20.
448 D. L. Trimm, I. O. Y. Liu and N. W. Cant, *Appl. Catal., A*, 2010, **374**, 58–64.
449 A. J. McCue, A. Guerrero-Ruiz, I. Rodríguez-Ramos and J. A. Anderson, *J. Catal.*, 2016, **340**, 10–16.
450 D. Albani, M. Shahrokhi, Z. P. Chen, S. Mitchell, R. Hauert, N. López and J. Pérez-Ramírez, *Nat. Commun.*, 2018, **9**, 2634.
451 Y. N. Liu, A. J. McCue, J. T. Feng, S. L. Guan, D. Q. Li and J. A. Anderson, *J. Catal.*, 2018, **364**, 204–215.
452 L. Wang, B. Zhao, C. K. Russell, M. H. Fan, B. J. Wang, L. X. Ling and R. G. Zhang, *Chem. Eng. Sci.*, 2021, **246**, 116984.
453 Y. Wang, Y. Zhang, B. J. Wang, M. H. Fan, L. X. Ling and R. G. Zhang, *Fuel*, 2022, **315**, 123180.
454 X. X. Shao, B. J. Wang, M. H. Fan, L. X. Ling and R. G. Zhang, *Chem. Eng. Sci.*, 2023, **270**, 118494.
455 Y. Y. Wu, B. J. Wang, M. H. Fan, L. X. Ling and R. G. Zhang, *Fuel*, 2023, **331**, 125661.
456 M. Ruta, G. Laurenczy, P. J. Dyson and L. Kiwi-Minsker, *J. Phys. Chem. C*, 2008, **112**, 17814–17819.
457 T. Herrmann, L. Rössmann, M. Lucas and P. Claus, *Chem. Commun.*, 2011, **47**, 12310–12312.
458 T. Zhou, K. Jang and B. W. L. Jang, *Catal. Today*, 2013, **211**, 147–155.
459 Y. C. Chen, Q. J. Zhang, F. Zhang, Z. L. Li, Y. K. Zhou, Y. X. Qin, L. Y. Xu, F. Feng, Q. T. Wang, Q. F. Zhang and X. N. Li, *Appl. Catal., A*, 2024, **681**, 11977.
460 Q. F. Zhang, Y. Q. Xu, Q. T. Wang, W. M. Huang, J. Zhou, Y. S. Jiang, H. Xu, L. L. Guo, P. Z. Zhang, J. Zhao, F. Feng and X. N. Li, *Chem. Commun.*, 2019, **55**, 14910–14913.
461 Q. T. Wang, Y. Q. Xu, J. Zhou, L. Y. Xu, L. Yu, D. H. Jiang, C. S. Lu, Z. Y. Pan, Q. F. Zhang and X. N. Li, *J. Ind. Eng. Chem.*, 2021, **93**, 448–460.
462 R. J. Hou, X. C. Lan and T. F. Wang, *Catal. Today*, 2015, **251**, 47–52.
463 Y. Q. Xu, Y. S. Jiang, H. Xu, Q. T. Wang, W. M. Huang, H. H. He, Y. Y. Zhai, S. X. Di, L. L. Guo, X. L. Xu, J. Zhao, F. Feng, Q. F. Zhang and X. N. Li, *Appl. Catal., A*, 2018, **567**, 12–19.
464 Y. Kim, T. Kim, K. H. Kang and I. Ro, *ChemCatChem*, 2023, **15**, e202201428.
465 F. M. McKenna and J. A. Anderson, *J. Catal.*, 2011, **281**, 231–240.
466 F. M. McKenna, R. P. K. Wells and J. A. Anderson, *Chem. Commun.*, 2011, **47**, 2351–2353.
467 F. M. McKenna, L. Mantarosie, R. P. K. Wells, C. Hardacre and J. A. Anderson, *Catal. Sci. Technol.*, 2012, **2**, 632–638.
468 A. J. McCue, F. M. McKenna and J. A. Anderson, *Catal. Sci. Technol.*, 2015, **5**, 2449–2459.
469 L. Altmann, X. D. Wang, J. Stöver, M. Klink, V. Zielasek, K. Thiel, J. Kolny-Olesiak, K. Al-Shamery, H. Borchert, J. Parisi and M. Bäumer, *ChemCatChem*, 2013, **5**, 1803–1810.
470 G. Tiwari, G. Sharma, R. Verma, P. Gakhad, A. K. Singh, V. Polshettiwar and B. R. Jagirdar, *Chem. – Eur. J.*, 2023, **29**, e202301932.
471 Q. L. Wu, C. Y. Shen and C. J. Liu, *Appl. Surf. Sci.*, 2023, **607**, 154976.
472 E. Wasim, N. U. Din, D. Le, X. M. Zhou, G. E. Sterbinsky, M. S. Pape, T. S. Rahman and S. L. Tait, *J. Catal.*, 2022, **413**, 81–92.
473 T. Liu, J. Q. Xiong, Q. Luo, S. J. Mao and Y. Wang, *ACS Catal.*, 2024, **14**, 5838–5846.
474 S. Lee, S. J. Shin, H. Baek, Y. Choi, K. Hyun, M. Seo, K. Kim, D. Y. Koh, H. Kim and M. Choi, *Sci. Adv.*, 2020, **6**, eabb7369.
475 K. Hyun, Y. Park, S. Lee, J. Lee, Y. Choi, S. J. Shin, H. Kim and M. Choi, *Angew. Chem., Int. Ed.*, 2021, **60**, 12482–12489.
476 Y. Park, S. Lee, K. Hyun, J. Lee, J. Y. Park, R. Ryoo and M. Choi, *J. Catal.*, 2021, **404**, 716–725.
477 K. Hyun, Y. Park and M. Choi, *J. Catal.*, 2022, **416**, 267–276.
478 K. Hyun, S. H. Yun and M. Choi, *ACS Catal.*, 2024, **14**, 2938–2948.
479 Y. Park, K. Hyun, S. Yun and M. Choi, *ChemCatChem*, 2024, **16**, e202301378.
480 R. K. Edvinsson, A. M. Holmgren and S. Irandoust, *Ind. Eng. Chem. Res.*, 1995, **34**, 94–100.
481 N. B. Shitova, D. A. Shlyapin, T. N. Afonasenko, E. N. Kudrya, P. G. Tsyrul'nikov and V. A. Likholobov, *Kinet. Catal.*, 2011, **52**, 251–257.
482 R. J. Hou, T. F. Wang and X. C. Lan, *Ind. Eng. Chem. Res.*, 2013, **52**, 13305–13312.
483 B. B. Huang, T. Wang, C. Lei, W. Q. Chen, G. M. Zeng and F. Maran, *J. Catal.*, 2016, **339**, 14–20.
484 H. Shariff and M. H. Al-Dahhan, *Ind. Eng. Chem. Res.*, 2024, **63**, 8899–8905.
485 Z. Kang, Y. Wang, B. Liu, Z. Huang, X. Lan and T. Wang, *Chem. Eng. J.*, 2024, **491**, 151755.
486 D. V. Glyzdova, N. S. Smirnova, N. N. Leont'eva, E. Y. Gerasimov, I. P. Prosvirin, V. I. Vershinin, D. A. Shlyapin and P. G. Tsyrul'nikov, *Kinet. Catal.*, 2017, **58**, 140–146.

487 T. N. Afonasenko, V. L. Temerev, D. A. Shlyapin and P. G. Tsyrul'nikov, *Russ. J. Appl. Chem.*, 2019, **92**, 128–134.
488 T. N. Afonasenko, V. L. Temerev, D. V. Glyzdova, N. N. Leont'eva, M. V. Trenikhin, I. P. Prosvirin and D. A. Shlyapin, *Mater. Lett.*, 2021, **305**, 130843.
489 B. B. Huang, T. Wang, Z. Yang, W. T. Qian, J. M. Long, G. M. Zeng and C. Lei, *ACS Sustainable Chem. Eng.*, 2017, **5**, 1668–1674.
490 D. V. Glyzdova, N. S. Smirnova, V. L. Temerev, E. V. Khramov, T. I. Gulyaeva, M. V. Trenikhin, D. A. Shlyapin and P. G. Tsyrul'nikov, *Russ. J. Appl. Chem.*, 2017, **90**, 1908–1917.
491 D. V. Glyzdova, T. N. Afonasenko, E. Khramov, M. Trenikhin, I. P. Prosvirin and D. A. Shlyapin, *ChemCatChem*, 2022, **14**, e202200893.
492 D. V. Glyzdova, T. N. Afonasenko, E. V. Khramov, N. N. Leont'eva, I. P. Prosvirin, A. V. Bukhtiyarov and D. A. Shlyapin, *Appl. Catal., A*, 2020, **600**, 117627.
493 D. V. Glyzdova, A. A. Vedyagin, A. M. Tsapina, V. V. Kaichev, A. L. Trigub, M. V. Trenikhin, D. A. Shlyapin, P. G. Tsyrulnikov and A. V. Lavrenov, *Appl. Catal., A*, 2018, **563**, 18–27.
494 J. D. Krooswyk, I. Waluyo and M. Trenary, *ACS Catal.*, 2015, **5**, 4725–4733.
495 C. S. Spanjers, R. S. Sim, N. P. Sturgis, B. Kabius and R. M. Rioux, *ACS Catal.*, 2015, **5**, 3304–3315.
496 O. B. Ayodele and G. Jacobs, *Chem. Eng. J.*, 2024, **498**, 155168.
497 A. L. Bugaev, A. A. Guda, A. Lazzarini, K. A. Lomachenko, E. Groppo, R. Pellegrini, A. Piovano, H. Emerich, A. V. Soldatov, L. A. Bugaev, V. P. Dmitriev, J. A. van Bokhoven and C. Lamberti, *Catal. Today*, 2017, **283**, 119–126.
498 A. L. Bugaev, O. A. Usoltsev, A. A. Guda, K. A. Lomachenko, I. A. Pankin, Y. V. Rusalev, H. Emerich, E. Groppo, R. Pellegrini, A. V. Soldatov, J. A. van Bokhoven and C. Lamberti, *J. Phys. Chem. C*, 2018, **122**, 12029–12037.
499 Y. M. Niu, B. S. Zhang, J. J. Luo, L. Y. Zhang, C. M. Chen and D. S. Su, *ChemCatChem*, 2017, **9**, 3435–3439.
500 K. Kovnir, M. Armbrüster, D. Teschner, T. V. Venkov, L. Szentmiklósi, F. C. Jentoft, A. Knop-Gericke, Y. Grin and R. Schlögl, *Surf. Sci.*, 2009, **603**, 1784–1792.
501 T. Cao, R. You, X. Y. Zhang, S. L. Chen, D. Li, Z. H. Zhang and W. X. Huang, *Phys. Chem. Chem. Phys.*, 2018, **20**, 9659–9670.
502 J. Moon, Y. Q. Cheng, L. L. Daemen, M. J. Li, F. Polo-Garzon, A. J. Ramirez-Cuesta and Z. L. Wu, *ACS Catal.*, 2020, **10**, 5278–5287.
503 C. S. Wondergem, J. J. G. Kromwijk, M. Slagter, W. L. Vrijburg, E. J. M. Hensen, M. Monai, C. Vogt and B. M. Weckhuysen, *ChemPhysChem*, 2020, **21**, 625–632.
504 X.-T. Li, L. Chen, G.-F. Wei, C. Shang and Z.-P. Liu, *ACS Catal.*, 2020, **10**, 9694–9705.
505 L. Chen, X. T. Li, S. C. Ma, Y. F. Hu, C. Shang and Z. P. Liu, *ACS Catal.*, 2022, **12**, 14872–14881.
506 H. S. Feng, H. Ding, S. Wang, Y. J. Liang, Y. Deng, Y. S. Yang, M. Wei and X. Zhang, *ACS Appl. Mater. Interfaces*, 2022, **14**, 25288–25296.
507 R. B. Fang, Q. J. Zhang, C. Yao, H. J. Wu, S. K. Xie, X. H. Zhang, Q. T. Wang, J. Lyu, F. Feng, C. S. Lu, Q. F. Zhang and X. N. Li, *Appl. Catal., A*, 2024, **687**, 119969.
508 X. H. Ge, J. Yin, Z. H. Ren, K. L. Yan, Y. D. Jing, Y. Q. Cao, N. N. Fei, X. Liu, X. N. Wang, X. G. Zhou, L. W. Chen, W. K. Yuan and X. Z. Duan, *J. Am. Chem. Soc.*, 2024, **146**, 4993–5004.
509 K. Yang, X. Chen, J. Qi, Z. Bai, L. Zhang and C. Liang, *J. Catal.*, 2019, **369**, 363–371.
510 Z. Guo, R. Wang, Y. Guo, J. Jiang, Z. Wang, W. Li and M. Zhang, *ACS Catal.*, 2022, **12**, 15193–15206.
511 H. Yang, H. Chen, J. Chen, O. Omotoso and Z. Ring, *J. Catal.*, 2006, **243**, 36–42.
512 X. Zhang, Y. Zhou, G. Li, L. Zhang, C. Yin, Y. Yang, H. Wang, F. Feng, L. Wei, Q. Zhang, F. Yang, L. Lin, C. Lu and X. Li, *Appl. Catal., B*, 2022, **315**, 121566.
513 L. Lin, S. Yao, R. Gao, X. Liang, Q. Yu, Y. Deng, J. Liu, M. Peng, Z. Jiang, S. Li, Y.-W. Li, X.-D. Wen, W. Zhou and D. Ma, *Nat. Nanotechnol.*, 2019, **14**, 354–361.
514 Z. Wang, C. Dong, X. Tang, X. Qin, X. Liu, M. Peng, Y. Xu, C. Song, J. Zhang, X. Liang, S. Dai and D. Ma, *Nat. Commun.*, 2022, **13**, 4404.
515 I. Y. Ahn, J. H. Lee, S. K. Kim and S. H. Moon, *Appl. Catal., A*, 2009, **360**, 38–42.
516 M. T. Ravanchi and S. Sahebdelfar, *Appl. Catal., A*, 2016, **525**, 197–203.
517 R. J. Liu, P. A. Crozier, C. M. Smith, D. A. Hucul, J. Blackson and G. Salaita, *Appl. Catal., A*, 2005, **282**, 111–121.
518 A. A. Lamberov, S. R. Egorova, I. R. Il'yasov, K. K. Gil'manov, S. V. Trifonov, V. M. Shatilov and A. S. Ziyatdinov, *Kinet. Catal.*, 2007, **48**, 136–142.
519 A. Pachulski, R. Schödel and P. Claus, *Appl. Catal., A*, 2011, **400**, 14–24.
520 H.-X. Su, Y. Jiao, J.-G. Shi, Z.-W. Yuan, D. Zhang, X.-P. Wang, J. Ren, D. Liu, J.-Z. Gui, H.-Y. Gao and X.-L. Xu, *Pet. Sci.*, 2024, **21**, 1405–1414.
521 M. R. Rahimpour, O. Dehghani, M. R. Gholipour, M. S. Shokrollahi Yancheshmeh, S. Seifzadeh Haghighi and A. Shariati, *Chem. Eng. J.*, 2012, **198–199**, 491–502.
522 M. Mosafer, A. Hafizi, M. R. Rahimpour and A. Bolhasani, *J. Nat. Gas Sci. Eng.*, 2016, **34**, 1382–1391.
523 T. R. Bilalov, F. M. Gumerov, F. R. Gabitov, K. E. Kharlampidi, G. I. Fedorov, A. A. Sagdeev, R. S. Yarullin and I. A. Yakushev, *Russ. J. Phys. Chem. B*, 2009, **3**, 1093–1105.
524 B. T. Burganov, K. E. Kharlampidi, F. M. Gumerov and V. F. Khairutdinov, *Russ. J. Phys. Chem. B*, 2016, **10**, 1147–1152.
525 Y. Liu, Y. Li, J. A. Anderson, J. Feng, A. Guerrero-Ruiz, I. Rodríguez-Ramos, A. J. McCue and D. Li, *J. Catal.*, 2020, **383**, 51–59.
526 S. A. Nikolaev, N. Z. Leonid, V. V. Smirnov, A. A. Vyacheslav and K. L. Zanaveskin, *Russ. Chem. Rev.*, 2009, **78**, 231.
527 M. R. Wang, Y. Wang, X. L. Mou, R. H. Lin and Y. J. Ding, *Chin. J. Catal.*, 2022, **43**, 1017–1041.
528 A. J. McCue, A. Gibson and J. A. Anderson, *Chem. Eng. J.*, 2016, **285**, 384–391.

529 Z. Q. Wang, L. Yang, R. Zhang, L. Li, Z. M. Cheng and Z. M. Zhou, *Catal. Today*, 2016, **264**, 37–43.
530 Z. S. Wang, C. L. Yang, S. L. Xu, H. Nan, S. C. Shen and H. W. Liang, *Inorg. Chem.*, 2020, **59**, 5694–5701.
531 Z. X. Li, M. L. Hu, B. W. Liu, J. H. Liu, P. Wang, J. S. Yao, X. Zhang, M. He and W. Y. Song, *ChemCatChem*, 2021, **13**, 868–873.
532 G. Wowsnick, D. Teschner, M. Armbrüster, I. Kasatkin, F. Girgsdies, Y. Grin, R. Schlögl and M. Behrens, *J. Catal.*, 2014, **309**, 221–230.
533 K. L. Yan, X. H. Ge, W. H. Li, Y. J. Liang, W. J. Xiong, J. Zhang, G. Qian, D. Chen, Y. Q. Cao, X. G. Zhou and X. Z. Duan, *J. Mater. Chem. A*, 2024, **12**, 16482–16490.
534 J. H. Xi, K. L. Yan, N. C. Zhu, X. H. Ge, Y. W. Qiang, M. M. Chen, H. Jiang, Y. Q. Cao, X. G. Zhou and X. Z. Duan, *AIChE J.*, 2024, **70**, e18416.
535 M. K. Abdel-Rahman and M. Trenary, *ACS Catal.*, 2020, **10**, 9716–9724.
536 Q. Yuwen, K. L. Yan, X. H. Ge, G. Qian, J. Zhang, Y. Q. Cao, X. G. Zhou and X. Z. Duan, *Ind. Eng. Chem. Res.*, 2023, **62**, 16280–16290.
537 L. M. Zhao, X. T. Qin, X. R. Zhang, X. B. Cai, F. Huang, Z. M. Jia, J. Y. Diao, D. Q. Xiao, Z. Jiang, R. F. Lu, N. Wang, H. Y. Liu and D. Ma, *Adv. Mater.*, 2022, **34**, e202110455.
538 S. C. Wang, T. Liu, Y. A. Zhu, X. K. Liu, Q. Q. Luo, M. Z. Zhu, T. Ding and T. Yao, *J. Phys. Chem. C*, 2023, **127**, 5911–5919.
539 H. H. Ibrahim, T. Weckman, D. Y. Murzin and K. Honkala, *J. Catal.*, 2024, **434**, 115523.
540 Q. C. Yang, R. J. Hou and K. N. Sun, *J. Catal.*, 2019, **374**, 12–23.
541 H. W. Ma, X. P. Xu, H. X. Xu, H. X. Feng, Y. Xie and D. J. Cheng, *Catal. Commun.*, 2021, **149**, 106255.
542 O. E. B. Corstius, H. L. Nolten, G. F. Tierney, Z. Xu, E. J. Doskocil, J. E. S. van der Hoeven and P. E. de Jongh, *Catal. Today*, 2024, **441**, 114877.
543 Z. B. Chen, X. T. Chen, Y. L. Lv, X. L. Mou, J. H. Fan, J. W. Li, L. Yan, R. H. Lin and Y. J. Ding, *Chin. J. Catal.*, 2024, **60**, 304–315.
544 Z. B. Chen, Y. L. Lv, X. T. Chen, X. L. Mou, J. W. Li, L. Yan, R. H.
Lin and Y. J. Ding, *Catal. Sci. Technol.*, 2024, **14**, 137–144.
545 Y. X. Feng, L. S. Zhou, Q. Wan, S. Lin and H. Guo, *Chem. Sci.*, 2018, **9**, 5890–5896.
546 H. Yan, H. F. Lv, H. Yi, W. Liu, Y. J. Xia, X. H. Huang, W. X. Huang, S. Q. Wei, X. J. Wu and J. L. Lu, *J. Catal.*, 2018, **366**, 70–79.
547 Z. Yan, L. X. Cui, Z. Pang, K. Shi, M. Y. Zhang, J. W. Guo, R. Gao and H. G. Hao, *Appl. Surf. Sci.*, 2023, **617**, 156585.
548 M. R. Hossain and M. Trenary, *J. Phys. Chem. C*, 2024, **128**, 19204–19209.
549 B. B. Huang, C. Durante, A. A. Isse and A. Gennaro, *Electrochem. Commun.*, 2013, **34**, 90–93.
550 Z. Liu, L. Zhang, Z. Ren and J. Zhang, *Chem. – Eur. J.*, 2023, **29**, e202202979.
551 F. Arcudi, L. Dordevic, N. Schweitzer, S. I. Stupp and E. A. Weiss, *Nat. Chem.*, 2022, **14**, 1007.
552 A. Stone, L. Dordevic, S. I. Stupp, E. A. Weiss, F. Arcudi and J. T. Hupp, *ACS Energy Lett.*, 2023, **8**, 4684–4693.
553 A. Stone, A. Fortunato, X. J. Wang, E. Saggioro, R. Q. Snurr, J. T. Hupp, F. Arcudi and L. Dordevic, *Adv. Mater.*, 2025, **37**, e202408658.
554 B.-H. Zhao, F. Chen, M. Wang, C. Cheng, Y. Wu, C. Liu, Y. Yu and B. Zhang, *Nat. Sustainability*, 2023, **6**, 827–837.
555 L. D. Burke, F. A. Lewis and C. Kemball, *Trans. Faraday Soc.*, 1964, **60**, 919–929.
556 M. Bełtowska-Brzezinska, T. Łuczak, M. Mączka, H. Baltruschat and U. Müller, *J. Electroanal. Chem.*, 2002, **519**, 101–110.
557 L. Zhang, Z. Chen, Z. P. Liu, J. Bu, W. X. Ma, C. Yan, R. Bai, J. Lin, Q. Y. Zhang, J. Z. Liu, T. Wang and J. Zhang, *Nat. Commun.*, 2021, **12**, 6574.
558 Z. Chen, C. Cai and T. Wang, *J. Phys. Chem. C*, 2022, **126**, 3037–3042.
559 J. Bu, Z. P. Liu, W. X. Ma, L. Zhang, T. Wang, H. P. Zhang, Q. Y. Zhang, X. L. Feng and J. Zhang, *Nat. Catal.*, 2021, **4**, 557–564.
560 Z. P. Wang, L. Shang, H. Z. Yang, Y. X. Zhao, G. I. N. Waterhouse, D. Li, R. Shi and T. R. Zhang, *Adv. Mater.*, 2023, **35**, e202400122.
561 X. L. Jiang, L. Tang, L. Dong, X. D. Sheng, W. F. Zhang, Z. Liu, J. H. Shen, H. L. Jiang and C. Z. Li, *Angew. Chem., Int. Ed.*, 2023, **62**, e202307848.
562 W. Q. Xue, X. Y. Liu, C. X. Liu, X. Y. Zhang, J. W. Li, Z. W. Yang, P. X. Cui, H. J. Peng, Q. Jiang, H. L. Li, P. P. Xu, T. T. Zheng, C. Xia and J. Zeng, *Nat. Commun.*, 2023, **14**, 2137.
563 X. Gao, D. S. Wang, R. Bai, D. Lin, J. Zhang, Z. J. Li, Y. Hou, L. C. Lei and B. Yang, *Adv. Funct. Mater.*, 2025, **35**, e202415384.
564 Z. P. Wang, C. Y. Li, G. Peng, R. Shi, L. Shang and T. R. Zhang, *Angew. Chem., Int. Ed.*, 2024, **63**, e202400122.
565 X. H. Lv, H. Huang, L. T. Cui, Z. Y. Zhou, W. K. Wu, Y. C. Wang and S. G. Sun, *ACS Appl. Mater. Interfaces*, 2024, **16**, 8668–8678.
566 C. Dou, Y. M. Huang, B. H. Zhao, W. W. Lei, B. Zhang and Y. F. Yu, *Angew. Chem., Int. Ed.*, 2025, **64**, e202423381.
567 B. Miao, F. Chen, C. Cheng, M. Tao, B.-H. Zhao and B. Zhang, *Angew. Chem., Int. Ed.*, 2025, **64**, e202502757.
568 Z. P. Liu, Z. Chen, J. Bu, W. X. Ma, L. Zhang, H. Zhong, L. Cheng, S. M. Li, T. Wang and J. Zhang, *Chem. Eng. J.*, 2022, **431**, 134129.
569 W. X. Ma, Z. Chen, J. Bu, Z. P. Liu, J. J. Li, C. Yan, L. Cheng, L. Zhang, H. P. Zhang, J. C. Zhang, T. Wang and J. Zhang, *J. Mater. Chem. A*, 2022, **10**, 6122–6128.
570 M. Yuan, H. Jiang, R. Jiang, Z. Wang, Z.-H. Zhao, B.-L. Su and J. Zhang, *ACS Catal.*, 2024, **14**, 18385–18396.
571 L. Zhang, R. Bai, J. Lin, J. Bu, Z. P. Liu, S. Y. An, Z. H. Wei and J. Zhang, *Nat. Chem.*, 2024, **16**, 893–900.
572 L. Bai, Y. Wang, Z. Han, J. B. Bai, K. Y. Leng, L. R. Zheng, Y. T. Qu and Y. Wu, *Nat. Commun.*, 2023, **14**, 8384.
573 L. S. Huang, D. Y. Bao, Y. L. Jiang, Y. Zheng and S. Z. Qiao, *Angew. Chem., Int. Ed.*, 2024, **63**, e202405943.

